

# 3

## CHAPTER 3 EARTHQUAKE CATALOG

---

This chapter describes the development of the earthquake catalog for the CEUS SSC Project. The catalog development consists of four major steps: catalog compilation, assessment of a uniform size measure to apply to each earthquake, identification of dependent earthquakes (catalog declustering), and an assessment of the completeness of the catalog as a function of location, time, and earthquake size. Each of these steps is described in detail in the chapter. The result is an earthquake catalog covering the entire study region defined in Chapter 1 for the time period of 1568 through the end of 2008. Earthquake size is defined in terms of the moment magnitude scale (Hanks and Kanamori, 1979), consistent with the magnitude scale used in modern ground motion prediction equations for CEUS earthquakes.

### 3.1 Goals for the Earthquake Catalog Development

The catalog of past earthquakes that have occurred in a region is an important source of information for the quantification of future seismic hazards. This is particularly true in stable continental regions such as the CEUS where the causative mechanisms and structures for the occurrence of damaging earthquakes are generally poorly understood, and the rates of crustal deformation are low such that surface and near-surface indications of the buildup and release of crustal stresses are difficult to identify. Because the earthquake catalog will be used to characterize the occurrence of future earthquakes in the CEUS, developing an updated earthquake catalog for the study region was an important focus of the CEUS SSC Project. The specific goals for earthquake catalog development are described in the following sections.

#### 3.1.1 Completeness

The goal of compiling an earthquake catalog is to record the occurrence of all known earthquakes in the magnitude range considered important to the characterization of future earthquake hazards. It is recognized that there have been extensive past efforts put forward toward this goal. In the United States, the work performed in the EPRI-SOG project (EPRI, 1988), subsequently revised by Seeber and Armbruster (1991), ultimately led to the catalog used by the U.S. Geological Survey (USGS) for seismic hazard mapping (Mueller et al., 1997; Petersen et al., 2008). Similarly, work by the Geological Survey of Canada (GSC) to develop an earthquake catalog for seismic hazard analysis (Adams and Halchuk, 2003) provides an equally important source catalog for earthquakes in the northern portion of the study region. The CEUS SSC Project relied on the work underlying the USGS and GSC catalogs to form the backbone of the updated project earthquake catalog.

The USGS and GSC catalogs each represent a synthesis of catalog information from many sources into simple one-line catalog entries of date, time, location, and selected estimate(s) of

earthquake size. In that process, some information important to the use of the earthquake catalog for this project may not have been retained. Therefore, an extensive review of original catalog sources was performed as part of the catalog compilation, among them Stover and Coffman (1993); Smith (1962, 1966); the Southeastern United States Network (SUSN) catalog; and the USGS/National Earthquake Information Center (NEIC) Preliminary Determination of Epicenters (PDE) catalog. In addition, numerous special studies of individual earthquakes, earthquake sequences, and specific geographic areas were reviewed and the information compiled as part of the catalog development. The use of these studies is described in subsequent sections of this chapter. A number of these studies included information on important parameters (e.g., moment magnitudes) that is not included in the more regional catalogs.

It is also recognized that the process of catalog compilation from many sources may lead to inclusion of duplicate entries for some earthquakes and inclusion of nontectonic events that have been excluded from other catalogs. To address this issue, catalogs of identified nontectonic events and false entries were also examined and a list of identified nontectonic events was compiled. This list forms one product of the CEUS SSC Project (see Appendix B). The catalog was also reviewed line by line to identify potential duplicate entries not readily identified by automatic means.

### **3.1.2 Uniformity of Catalog Processing**

An important goal of catalog compilation was to use an earthquake size measure that is consistent with the ground motion models that will be used to compute seismic hazards. Most recent ground motion models applicable to the CEUS use the moment magnitude scale,  $M$ , as the earthquake size measure, and it is expected that the next generation of ground motion models being developed in the near future will continue to use the moment magnitude scale.

Unfortunately, however, this is not the magnitude scale that has been used for routine earthquake monitoring and catalog compilation. The current practice for many hazard analyses in the CEUS is to estimate earthquake occurrence rates in terms of the catalog magnitude (commonly, body-wave magnitude, or  $m_b$ ) and then use conversion relationships from this magnitude scale to  $M$  as part of the ground motion estimation. This introduces an additional source of uncertainty, particularly since many of the catalog magnitude entries are themselves converted from other size measures, such as shaking intensity for pre-instrumental earthquakes.

The EPRI-SOG project (EPRI, 1988, Vol. 1) developed techniques to produce a catalog with a uniform size measure that is appropriate for unbiased estimation of earthquake occurrence rates for use in seismic hazard assessment. These techniques were used in the EPRI-SOG study to develop a uniform catalog of  $m_b$  magnitudes. A goal of the catalog development efforts in this project is to use the same techniques to produce a uniform catalog of moment magnitude values that have properly accounted for the uncertainty in size estimation as part of development of earthquake occurrence rates. This will eliminate the need for magnitude conversion as part of the hazard calculation and avoid propagation of unnecessary uncertainty through the hazard analysis. To achieve this goal, updated conversions were developed from a variety of earthquake size measures to moment magnitude.

An equally important task was to obtain the original size measures for catalog entries in order to use a direct conversion to moment magnitude rather than introduce additional uncertainty by converting previously converted size estimates. One example is that a number of the magnitudes

listed in the GSC catalog are designated local magnitude,  $M_L$ . Yet many of these earthquakes occurred in the pre-instrumental period. Examination of the magnitude entries suggests that they were in fact converted from maximum intensity,  $I_0$ , using the Gutenberg and Richter (1956) relationship. Therefore, the original source for the catalog of intensity data was obtained (Smith, 1962, 1966) and the  $I_0$  values for these earthquakes were entered into the catalog in order to make a direct conversion from  $I_0$  to  $M$ .

### 3.1.3 Catalog Review

Development of earthquake catalogs is a complex and a tedious process in which there are many sources of uncertainty and opportunities for either missing important sources of information or adding unwanted or fictitious information. Therefore, an important part of the catalog development process was reviewed by seismologists with extensive knowledge and experience in catalog compilation. The first draft of the catalog was reviewed by Dr. Charles Mueller and Margaret Hopper from the USGS, Dr. John Ebel from Boston College, Dr. Martin Chapman from Virginia Tech, Dr. Pradeep Talwani from the University of South Carolina, Dr. Donald Stevenson from Savannah River Nuclear Solutions, and James Marrone from Bechtel. The following summarizes the main review comments and the actions taken to implement the reviewers' recommendations in the development of the final project catalog.

#### *Use Original Sources*

Several reviewers made the comment that original source catalogs should be used as much as possible instead of relying on the compilation catalogs. To address this issue, the entries in the project catalog were traced back to their original sources to the extent possible. For example, the USGS catalog (Mueller et al., 1997; Petersen et al., 2008) considers all earthquake magnitudes as  $m_b$ . However, the USGS catalog also lists the source of the magnitude estimate for many earthquakes. These sources were used to identify the proper magnitude type (e.g.,  $m_{bLg}$  versus  $M_N$ ). The primary source for the USGS catalog is the NCEER-91 catalog (Seeber and Armbruster, 1991, 1993), which updates the EPRI-SOG (EPRI, 1988) catalog. In the case of instrumentally recorded earthquakes, the preferred magnitude listed in the NCEER-91 catalog is typically the largest among the various magnitude types available in the EPRI-SOG (EPRI, 1988) catalog (e.g., the largest value among magnitude types  $m_b$ ,  $m_{bLg}$ ,  $M_N$ ,  $M_{CB}$ ,  $M_D$ , or  $M_L$ ). Each of these magnitude types, if present for a particular earthquake, was entered into the project catalog. In addition, to the extent possible, the magnitude entries included the original source of the magnitude estimate (e.g., Weston Observatory; Lamont-Doherty Earth Observatory; the 1983 Nuttli catalog; Dewey and Gordon, 1984).

The NCEER-91 catalog also contained a field in which a flag indicated whether the preferred magnitude was based on instrumental magnitudes (type 1), felt area (type 2), or maximum intensity (type 3). These flags were used to identify those reported magnitudes that were in fact based on shaking intensity measures so that the original size measure, intensity, rather than an estimated magnitude from intensity was used to provide an estimate of moment magnitude. In a similar manner, the Southeastern United States Seismic Network (SEUSSN) catalog (Virginia Tech) provided codes that indicated the source and type of body-wave magnitude reported for each earthquake. These were entered into the project catalog to indicate the type of magnitude and to identify earthquakes whose magnitudes were derived from macroseismic data.

A number of original sources of data suggested by the reviewers were reviewed and added to the project catalog. For example, the Dewey and Gordon (1984) catalog was digitized and included in the project catalog. Felt areas listed in the published paper version of Stover and Coffman (1993) were also digitized and added to the project catalog. The additional catalogs that were reviewed are described in Section 3.2.3.

### ***Examine Individual Magnitude Types***

Several reviewers suggested that potential differences in body-wave magnitude types may exist due to differences in the approaches used by various agencies to calculate magnitude. To address this issue, body-wave magnitudes reported by various agencies for the same set of earthquakes were examined for systematic differences. The results of this examination led to inclusion of regional and time-dependent effects in the correlation between various magnitude scales and  $M$ , as described in Section 3.3. Examination of  $M_L$  magnitudes reported in the catalog obtained from the GSC indicated that many of the reported values were actually based on maximum intensity converted to  $M_L$  using the relationship given in Gutenberg and Richter (1956). Moment magnitudes for these catalog entries were estimated using correlations with maximum intensity instead of with instrumental  $M_L$ .

### ***Provide Recommendations for Specific Catalog Entries***

Individual reviewers provided specific recommendations for a number of catalog entries. For example, Dr. Ebel provided suggestions for the catalog entries in the time period 1500–1700 and the larger earthquakes post-1700 in the northeastern portion of the study region. Dr. Talwani and Dr. Stevenson reviewed the catalog entries in the vicinity of the 1886 Charleston, South Carolina, earthquake. The suggestions made by the reviewers included indications of possible false, duplicate, or erroneous catalog entries, and changes to earthquake locations and times. These suggestions were implemented in the project catalog with indications of the source of the catalog update. Dr. Mueller recommended specific catalog sources and in particular catalog entries from the International Seismological Centre (ISC) for the study region. Review of the project catalog, however, indicated that a number of catalog entries with ISC magnitude values of about 3 were derived from local catalogs that contained either much smaller magnitude entries for the earthquake or no entry at all. Therefore, the ISC catalog was not used as a source in developing the final catalog.

### ***Create a Catalog of Nontectonic Events***

A number of reviewers suggested that a separate catalog be created listing nontectonic events identified as part of the catalog compilation. Appendix B contains a listing of the nontectonic events (e.g., explosions, mine collapses, false entries) identified during the course of the catalog development and includes the reference for the event classification.

## **3.2 Catalog Compilation**

The process used for catalog compilation was to provide each entry in a source catalog with a unique ID number specific to that catalog. The catalogs were merged by sorting all records in chronological order based on the calculated Julian date of each earthquake. After merging, each earthquake was assigned a project ID number that is common to multiple entries from different catalogs (duplicates). As an example, the 1897/5/31 Giles County earthquake is reported by eight catalogs: USGS (record number 1065); NCEER (record number 1079); Ohio Geological Survey

(record number 61); SEUSSN (record number 1743); Hopper (record number 97); USHIS (record number 101); EPRI (record number 840); and Reinbold and Johnston (1987; record number 39). Each of these catalog entries receives the same project ID number (TMP02921) indicating that each of the eight records is a duplicate entry for the Giles County earthquake. In the following sections the major sources of catalog data are described.

### 3.2.1 Continental-Scale Catalogs

The catalogs developed by the USGS and the GSC were the primary sources for earthquake entries. The primary earthquake listing that forms the basis for the USGS catalog was obtained from Dr. Charles Mueller, and the primary earthquake listing that forms the basis for the GSC catalog was obtained from Dr. Steven Halchuk. Figure 3.2-1 shows the areal coverage of these two catalogs. The region outlined by the blue box in the figure indicates the portion of each catalog that was used to develop the project catalog. The USGS catalog was updated through the end of 2008 using the NEIC PDE catalog website, and the GSC catalog was updated through the end of 2008 using data from the National Earthquake Database (NEDB) of Canada.

The USGS catalog is itself a compilation based on a number of other sources including the catalogs of Stover and Coffman (1993); Stover et al. (1984); EPRI (1988) as updated by Seeber and Armbruster (1991) and Armbruster (2002); NEIC PDE; U.S. Advanced National Seismic System (ANSS), and the Centennial Catalog (Engdahl and Villasenor, 2002). The purpose of including all these additional sources in the compilation of the CEUS SSC catalog was to obtain as much information as possible on size measures for the earthquakes. A principal example is obtaining shaking intensity values for pre-instrumental earthquakes that are not given in the primary sources. In some cases, the printed copies of catalogs were used to make hand entries of size measures into the database. For example, the felt area data listed in Stover and Coffman (1993) was entered into the database. As described above in Section 3.1.3, the magnitude type for the entries in the USGS catalog was identified using the source designation provided in the USGS catalog. The source for most of the entries in the USGS catalog was the NCEER-91 catalog (Seeber and Armbruster, 1991), and the NCEER-91 catalog entries were included in the combined earthquake compilation, along with the primary source for the NCEER-91 catalog, the EPRI-SOG catalog (EPRI, 1988). The NCEER-91 catalog contains entries for multiple magnitude types based on the entries in the EPRI-SOG catalog. These entries were used to identify the magnitude type reported in the USGS catalog. For example, if the source of a USGS record is an NCEER record obtained from the EPRI-SOG catalog, and the source used in EPRI-SOG is Dewey and Gordon (1984), all the records (EPRI, NCEER, and USGS) were modified to reflect that the magnitude type is  $m_{bLg}$  and the magnitude source is Dewey and Gordon (1984).

The GSC catalog entries consist primarily of two magnitude types,  $M_L$  and  $M_N$ . The source of the pre-1900  $M_L$  values is most likely intensity. Figure 3.2-2 shows a histogram of  $M_L$  magnitudes from the GSC catalog for the time period 1660–1899 for the region east of longitude  $-105^\circ$  and south of latitude  $53^\circ$ . The dashed vertical lines indicate magnitudes computed using the Gutenberg and Richter (1956) relationship  $M_L = \frac{2}{3}I_0 + 1$ . The magnitudes clearly line up on values computed from specific modified Mercalli intensity scale (MMI)  $I_0$  values spaced at  $\frac{1}{2}$  intensity units. Figure 3.2-3 shows the data for the period 1900–1930. With the exception of a few entries, the magnitudes again line up with specific  $I_0$  values. Figure 3.2-4 shows the data for the period 1930–1979, and Figure 3.2-5 shows the data for the period 1980–2007. These plots indicate that after 1980, most  $M_L$  values are probably instrumental, but during the period 1930–

1980, the GSC catalog likely contains a mixture of intensity-based and instrumental  $M_L$  magnitudes.

To sort out intensity-based  $M_L$  magnitudes in the GSC catalog, the catalogs of Smith (1962, 1966) were used to identify those earthquakes where instrumental  $M_L$  values were reported. In addition, the SUSN and EPRI/NCEER catalogs were used to separate instrumental from  $I_0$  based magnitudes. Where no primary source catalog provided an indication that an instrumental magnitude was recorded, the reported  $M_L$  values that are consistent with  $M_L = \frac{2}{3}I_0 + 1$  for the  $I_0$  value in the catalog in the time period after 1928 (the earliest reported  $M_L$  in the Smith catalogs) were considered to be computed from  $I_0$ . If not, the values were considered to be instrumental  $M_L$  magnitudes. Figure 3.2-6 shows the histogram of what are interpreted to be instrumental  $M_L$  magnitudes in the GSC catalog for the time period 1928–1979. For the most part, the values appear to indicate an exponential distribution, although some  $I_0$  based magnitudes may remain in the catalog.

An additional source of shaking intensity data for recent earthquakes is the USGS “Did You Feel It?” (DYFI) program (<http://earthquake.usgs.gov/earthquakes/dyfi/>; Wald et al., 1999). Two types of data are available from the DYFI website: (1) the archives, which list date, time, location, magnitude, and intensity of each earthquake; and (2) the reports, which contain the number of responses, average MMI for a specific zip code (not rounded), and distance for each zip code. The epicentral intensity reported in the DYFI data for an earthquake is the maximum intensity observed, independent of the distance and/or the number of observations. For some earthquakes, felt reports are prepared using geocoding, a technique that assigns latitude and longitude to street addresses, but this kind of report is available only for a limited number of earthquakes because observers often do not disclose their address. While reports based on zip code were used in this project, it should be noted that they do not describe how the distance from the epicenter to each observation is determined. If the distance is calculated from the center of the zip code, it may introduce a bias if the zip code covers a very large area.

The DYFI archives were downloaded and compared to the corresponding earthquake records in the CEUS SSC catalog. It was found that all the earthquakes occurred within the study region listed in the DYFI archives were already in the catalog. In more than half of the cases, the  $I_0$  level in the catalog corresponds to the intensity from the DYFI archives. In one-third of the cases, the intensity from the DYFI archive was higher (typically by one level) than the  $I_0$  value in the catalog. In a few cases (2001/6/3 Lake Erie, OH; 2004/7/20 South Carolina; 2005/2/23 Maryland), the difference between the DYFI intensity and the  $I_0$  in the catalog (from NEIC) was as high as three levels. To find an explanation for this difference, the felt reports of these three earthquakes were downloaded and analyzed. In all cases, the intensity assigned by DYFI is reported by few observers (in some cases just one) at great distance from the epicenter (100 km, or 62 mi., or more). The  $I_0$  obtained from NEIC for the same earthquakes approximates the largest intensity observed at short distance.

Approximately 20 earthquakes with  $I_0 \geq 4$  MMI in the DYFI archives did not have a corresponding intensity value in the CEUS SSC catalog. Because the same intensity is assigned to the entire zip code, maps of the earthquake effects from DYFI are very different from isoseismal maps, and the appropriate intensity level for the earthquake may not be immediately visible. Therefore, the felt reports for the earthquakes that do not have an intensity measure in the CEUS SSC catalog were carefully analyzed. Intensities obtained from just a few responses at

very great distances were disregarded. In almost all cases, it was found that the estimated maximum intensity needed to be adjusted to reflect the responses at close distance to the epicenter and to take into account the number of responses. This is consistent with the approach followed by Stover and Coffman (1993), who select  $I_0$  as the maximum intensity observed, and it can be argued from their isoseismal maps that it is typically very close to the epicenter.

If there are no observations within 20–30 km (12–18.5 mi.) of the epicenter,  $I_0$  is calculated adding one level to the average observed MMI at the closest distance. This accounts for a decay of about one degree in 30 km, consistent with the Atkinson and Wald (2007) MMI attenuation relation assuming a  $M 4 \pm 0.5$ , which is an appropriate value for the earthquakes analyzed. In four cases, the responses were too sparse and/or too distant and a value of  $I_0$  was not assigned.

### **3.2.2 Regional Catalogs**

The following regional catalogs were included in the compilation:

- Center for Earthquake Research and Information (CERI) catalog
- Saint Louis University (Nuttli, microearthquake, and moment magnitude catalogs)
- Lamont-Doherty Cooperative Seismographic Network catalog (LDO)
- Weston Observatory catalog (WES)
- Ohio Seismic Network catalog
- Department of Conservation and Natural Resources of Pennsylvania catalog
- Reinbold and Johnston (1987)
- Oklahoma Geological Survey catalog (OKO)
- South Carolina Seismic Network (SCSN) catalog
- Southeastern United States (SUSN) catalog (Virginia Tech)

These catalogs were used to obtain additional information on the size measures for earthquakes and to identify the magnitude types reported for each earthquake. For example, the Nuttli catalog from Saint Louis University indicates when the reported  $m_b$  values are instrumental and when they are based on shaking intensity data. The SUSN catalog contains both earthquakes recorded by SEUSSN and data taken from Stover et al. (1984). Included in the SUSN catalog is information on the type and source of individual magnitude values that was incorporated into the project catalog. Based on the recommendation of Dr. John Ebel (e-mail comm., January 13, 2011), magnitudes reported in the Weston Observatory catalog were classified as  $M_N$  for years prior to 1995 and as  $m_{Lg}(f)$  based on the use of the Ebel (1994) formula for 1995 and later years.

### **3.2.3 Catalogs from Special Studies**

A number of published studies contain information on specific earthquakes in limited geographical areas, often providing seismic moment or moment magnitude values and revised locations and/or depths, or indicating events of nontectonic origin. Information from the following studies was included in the catalog development: Adams and Simmons (1991); Atkinson et al. (2008); Basham et al. (1979); Bent (1992, 1995, 1996a, 1996b, 2009); Bent and

Hasegawa (1992); Bent and Perry (2002); Bent et al. (2002, 2003); Boatwright (1994); Brown and Ebel (1985); Dineva et al. (2004); Du et al. (2003); Ebel (1996, 2000, 2006a); Ebel et al. (1986); Faust et al. (1997); Fujita and Sleep (1991); Kim et al. (2006); Lamontagne and Ranalli (1997); Lamontagne et al. (2004); Larson (2002); Leblanc (1981); Ma and Atkinson (2006); Ma and Eaton (2007); Ma et al. (2008); Macherides (2002); Nabelek and Suarez (1989); Nicholson et al. (1988); Pomeroy et al. (1976); Reagor et al. (1980); Ruff et al. (1994); Scharnberger (1990); Seeber and Armbruster (1993); Seeber et al. (1998); Shedlock (1987); Shumway (2008); Stevenson and McColluh (2001); Street and Turcotte (1977); Street et al. (1975, 2002); and Sykes et al. (2008).

For the most part, the authors of these studies indicate the specific magnitude type reported, and this information was included in the project catalog. For example, Jones et al. (1977) and Street and Turcotte (1977) provide  $m_{bLg}$  values. Bollinger (1979) uses Nuttli's (1973) formula to determine  $m_{bLg}$  for 17 earthquakes in the southeastern United States, using World-Wide Standardized Seismograph Network (WWSSN) records. His study indicates that Nuttli's (1973) formula is applicable to earthquakes in this region, provided that epicentral distance is less than 2,000 km (1,243 mi.). However, Dr. Ebel (e-mail comm., January 13, 2011) pointed out that Nuttli's formula should only be applied to Lg waves with periods ranging between 0.7 and 1.3 sec. In Table 2 of Bollinger (1979) the period of the Lg wave used in some stations is smaller than the specified range; therefore, these magnitudes are considered in the CEUS catalog as  $M_N$  rather than  $m_{bLg}$ . The catalog by Basham et al. (1979) is a mix of different magnitudes ( $mI_0$ ,  $mFA$ ,  $ML$ ,  $m_b$ ,  $m_{bLg}$ ,  $M_N$ ), all assumed to be equal. Since in most cases it was impossible to determine what kind of magnitude was indicated, the CEUS catalog does not specify any kind of magnitude for the events that originate in the Basham et al. (1979) catalog. Instead, the magnitudes were cross-checked against other sources to identify the magnitude type.

In addition to the above, catalogs from three studies addressing historical earthquakes were included in the composite catalog. The first was the catalog of earthquakes in New Brunswick identified from historical records by Burke (2009). The second was the catalog developed by Metzger et al. (2000) covering the region around New Madrid. The third was the catalog developed by Munsey (2006) from newspaper archives for the region of Kentucky and Tennessee and adjoining areas. These studies provide either felt area or maximum intensity measures of earthquake size.

### **3.2.4 Focal Depth Data**

The compiled catalog contains a variety of depth estimates from different agencies and authors. Depths are routinely determined by the software used to locate the earthquakes (e.g., HYPO71, HYPOELLIPSE, etc.) and may have an associated flag that ranks the quality of the solution, and/or a flag that identifies depths fixed or assigned by a geophysicist. Depths of this kind are found in most regional (e.g., CERl, Saint Louis University, SUSN, LDO) and national (e.g., NEIC, NEDB, GSC) catalogs and in studies such as Brown and Ebel (1985); Dineva et al. (2003); Shedlock (1987); and Shumway et al. (2009). In addition, a number of studies (i.e., Atkinson, 2008; Bent, 1992, 1995, 1996a, 1996b; Bent and Hasegawa, 1992; Bent and Perry, 2002; Bent et al., 2002; Du et al., 2003; Ebel, 1986; Ma and Atkinson, 2006; Ma and Eaton, 2007; Ma et al., 2008; Nabelek and Suarez, 1989) calculate earthquake depths from regional depth phases or moment tensor analysis.

Depths were added to the catalog from studies published in the literature. Studies by Chapman and Bollinger (1984); Chapman et al. (1997); Dunn et al. (2010); Johnston et al. (1985); Pulli and Guenette (1981); Rhea (1987); Shoemaker et al. (2009); Talwani (1982); Teague et al. (1986); and Vlahovic et al. (1998) calculate earthquake depth while relocating earthquakes and microearthquakes. However, only the depths obtained by Chapman and Bollinger (1984); Chapman et al. (1997); Johnston et al. (1985); Shoemaker et al. (2009); and Stepp (2008) have been added to the project catalog because the other studies either do not provide tables with data, or focus on microearthquakes that are not included in the project catalog because of their very small magnitude.

The depth flags in the project catalog were standardized as follows: depths assigned to historical events are flagged by the letter H; fixed depths by F; depths obtained from regional depth phases or moment tensor analysis by D; and unreliable or questionable depths by a question mark (?). The latter include all the depths calculated by inversion software with quality of solution D, which according to Johnston et al. (1985) are unreliable.

Histograms of the earthquakes depth distribution for the events that are not flagged as fixed, historical, or unreliable show clear peaks at 5, 10, 18, and 33 km (3, 6, 11, and 20.5 mi.). These depths correspond to the typical fixed depth values adopted by Ohio, Oklahoma, and Pennsylvania catalogs (5 km), NEIC and other U.S. regional catalogs (10 km [6 mi.] for shallow and 33 km [20.5 mi.] for deep events), and Canadian catalogs (18 km, or 11 mi.). This indicates that a number of fixed depths have not been flagged in the original catalogs and consequently in the project catalog. Only a small number of these depths are calculated depths that have been rounded to the nearest integer. For example, Shedlock (1987) calculated a depth of 10.11 km (6.28 mi.) for the 1978/09/07 earthquake at coordinates 33.063°N, -80.209°E. This earthquake is contained in the NCEER catalog but the depth was rounded to a value of 10 km (6 mi.).

### **3.2.5 Nontectonic Events**

Nontectonic and erroneous earthquake entries were identified using lists compiled by ANSS, ISC, NEDB, and the NEIC Mining Catalog (<http://earthquake.usgs.gov/earthquakes/eqarchives/mineblast/>), and using information given in the SEUSSN bulletins and in a number of the studies listed in Section 3.2.3 (e.g., Seeber and Armbruster, 1993, 2002; Fujita and Sleep, 1991; Scharnberger, 1991a, 1991b; Street et al, 2002; Ma et al., 2008; Sykes et al., 2008; Burke, 2009; Ebel, 1996, 2010). In addition, Dr. Charles Mueller at the USGS shared a personal working file containing a list of nontectonic earthquakes; this has been checked against the information already in the catalog. Comments from Dr. John Ebel, Dr. Pradeep Talwani, and Dr. Donald Stevenson were used to identify many false events, particularly in the historical portion of the catalog. Earthquakes of nontectonic origin include mining-related activity (quarry blasts, collapses); reservoir-induced events; explosions; cryoseism; and other disturbances (sonic booms, storms, etc.). If the nontectonic origin of an earthquake is suspected but not confirmed, the classification is considered “probable.” A separate catalog of events of nontectonic (or probable nontectonic) origin is contained in Appendix B.

### **3.2.6 Identification of Unique Earthquake Entries**

The compiled master catalog listing containing all entries from multiple sources is retained in the CEUS SSC Project database. This listing is described in Appendix B. The final stage of catalog

compilation was the identification of duplicate entries for individual earthquakes within the master listing.

Duplicates were first identified by an algorithm that flags all events that occurred within a narrow time window. The time window is specified as difference in Julian date and it is larger for older events and smaller for newer events. The time windows were determined by running tests on different portions of the catalog.

An initial check of the catalog of duplicates identified indicated that many more duplicates still needed to be removed. The main issue appeared to be the difference between local and universal time. In order to identify these events, each line of the catalog was manually checked to confirm or modify the results of the algorithm. Information contained in some of the studies listed in Section 3.2.3 (e.g., Sykes et al., 2008; Fujita and Sleep, 1991; Bent, 2009) and reviewers' comments were used to identify and flag earthquake records with errors in date or time. In all cases, the date and time listed in the original record was retained but the record was considered a duplicate of the correct catalog entry, and a short explanation was added in the "Comment" field of the master catalog listing.

The master listing was then searched for earthquakes identified by only a single source. These earthquake sources were then rechecked to verify the master listing entries. For example, a number of entries have as a single source the SUSN catalog. A list of these events was submitted to Dr. Martin Chapman at Virginia Tech who provided references for all of them. Another source of information that was useful in verifying the correctness of several records was the USGS's online Earthquake History by State (<http://earthquake.usgs.gov/earthquakes/states/>).

Upon completion of these reviews, the master catalog listing was then re-examined line by line to verify the assignment of individual entries to unique earthquake identification numbers. Earthquake entries from different catalogs with similar origin times, locations, and sizes were typically assigned the same identification number unless visual examination indicated multiple earthquakes from one of the source catalogs. Comments were added to the "Comment" field of the master catalog listing to indicate interpretations of duplicate entries.

The next step in catalog processing was to select a preferred entry for each unique earthquake number while retaining the relevant information on various size measures for use in assigning a uniform magnitude and identification of a nontectonic entry. The following order of preference was used for selection of the preferred time and location for each catalog entry. If the earthquake was included in one of the special studies listed in Section 3.2.3, then that entry was used as the preferred entry. Otherwise, if the earthquake was contained in one of the two national catalogs used for seismic hazard mapping, the USGS catalog for earthquakes south of the U.S.-Canada border and the GSC/NEDB catalogs north of the border, then that catalog's entry was selected as the preferred entry. This choice was based on the assumption that these two catalogs have already undergone considerable review within each agency. If the earthquake was not contained in one of these two catalogs, then the local regional catalog entry was selected as the preferred entry (e.g., SUSN, CERL, Weston, Saint Louis University, Lamont-Doherty, the Oklahoma Geological Survey).

Finally, if the earthquake was listed only in other compilations, such as ANSS or Stover and Coffman (1993), then that entry was used as the preferred entry. Entries for earthquakes within the study region that only appear in the ISC catalog were not retained in the final catalog. This

decision was based on the observation that if the ISC reported magnitudes for these entries were of sufficient size (typically magnitude 3 or larger), then the earthquakes should have been contained in one or more regional catalogs. Questions about ISC catalog entries were raised by Dr. Charles Mueller of the USGS during the review of the draft catalog.

The multiple entries of earthquake size were used for assessing the uniform magnitude for each earthquake. Different values reported for the same magnitude scale by different source catalogs were not resolved, as this would require obtaining the original records and reassessing the magnitudes, a task well beyond the scope of the present study. Instead, these different magnitudes were retained and factored into the uncertainty in the assigned uniform magnitude measure for each earthquake.

The final project catalog contains 3,298 individual earthquakes of uniform moment magnitude  $E[M]$  2.9 and larger (the development of the uniform moment magnitude estimate  $E[M]$  is described in Section 3.3). Most of these earthquakes (2,642) are also contained in the USGS seismic hazard mapping catalog (Petersen et al., 2008). Table 3.2-1 summarizes the number of additional earthquakes as a function of time period, and Table 3.2-2 summarizes the sources of the added earthquakes. Figure 3.2-7 shows a map of the final CEUS SSC Project. The locations of the earthquakes added to the USGS catalog are denoted by the colored symbols with the catalog source indicated by the color code in the legend. The largest group added to the USGS catalog (319) are smaller-magnitude earthquakes that occurred in the time period 1960–2006 and are contained in multiple other catalog sources. The second largest group of added earthquakes (190) occurred in the period 1800–1899. Many of these earthquakes were identified in the studies of historical documents conducted by Burke (2009), Metzger et al. (2000), and Munsey (2006).

### **3.3 Development of a Uniform Moment Magnitude Earthquake Catalog**

As stated in Section 3.1.2, an important goal is to provide an earthquake catalog that can be used to develop unbiased estimates of the recurrence of earthquakes as a function of magnitude using a magnitude scale that is consistent with modern ground motion prediction equations for the CEUS: the moment magnitude scale defined by Hanks and Kanamori (1979). Because the size measures available for most of the earthquakes in the project catalog are different from this scale, a process for converting from a variety of magnitude and shaking intensity measures to moment magnitude is needed. In addition, it has been shown by Veneziano and Van Dyck (1985) and Tinti and Mulargia (1985) that uncertainty in the magnitudes reported in an earthquake catalog can lead to bias in the estimation of earthquake recurrence rates unless appropriate adjustments are applied. The EPRI-SOG project (EPRI, 1988) developed an approach for assigning a uniform magnitude measure to earthquakes in an earthquake catalog and producing unbiased recurrence parameters from that catalog. The EPRI-SOG approach was updated for application in the CEUS SSC Project.

#### **3.3.1 Approach for Uniform Magnitude and Unbiased Recurrence Estimation**

The magnitudes for all earthquakes reported in an earthquake catalog contain some amount of uncertainty. This uncertainty arises from the estimation process as magnitude is typically assigned as a statistical average of measurements obtained by a number of seismograph stations. In addition, the process of conversion from one magnitude scale to another introduces additional

uncertainty. If the reported magnitudes are used to estimate earthquake recurrence parameters using standard techniques, such as the Weichert (1980) maximum likelihood approach using earthquake counts in magnitude bins, then the uncertainty in the magnitudes leads to a bias in the estimated recurrence rate. This bias arises because of the underlying exponential distribution of earthquake magnitudes in a large source region. Considering the number of earthquakes in magnitude bin  $m_i$ , the exponential distribution in magnitude means that there are more earthquakes in the next smaller magnitude bin,  $m_{i-1}$  and fewer earthquakes in the next larger magnitude bin,  $m_{i+1}$ . The unequal numbers of earthquakes in adjacent magnitude bins means that more earthquakes are shifted from magnitude bin  $m_{i-1}$  to  $m_i$  due to statistical magnitude uncertainty than are shifted from magnitude bin  $m_i$  to bin  $m_{i+1}$ . A similar and consistent bias in the shifted earthquake counts occurs between magnitude bins  $m_i$  and  $m_{i+1}$ .

The effect of uncertainty on recurrence parameter estimation is readily illustrated through simulation. The process used is to simulate a catalog of 10,000 earthquakes from a truncated exponential distribution in the magnitude range of  $\mathbf{M}$  3 to  $\mathbf{M}$  7 with a recurrence rate of 100 earthquakes per year of  $\mathbf{M}$  3 and larger and a  $b$ -value of 1.0. A catalog of observed magnitudes,  $\hat{\mathbf{M}}$ , is simulated by adding a normally distributed random error to each earthquake magnitude with a standard deviation of 0.2 magnitude units. The resulting catalogs of  $\mathbf{M}$  and  $\hat{\mathbf{M}}$  are then used to compute recurrence parameters for magnitudes of  $\mathbf{M}$  4 and larger using the Weichert (1980) method with a magnitude bin width of 0.5 units. The purpose of using magnitudes of 4 and larger is to eliminate the truncation effects at the lower end of the magnitude range that result from starting the magnitude simulation at magnitude 3. The process was repeated for 500 simulations. The following table lists the average earthquake counts in each magnitude bin and the resulting average values of  $N(\mathbf{M} \geq 4)$  and  $b$ -value. The table also contains results for the adjusted magnitude  $\mathbf{M}^*$  that is described below.

Average Results from 500 Simulated Catalogs of True  $\mathbf{M}$ ,  $\hat{\mathbf{M}}$ , and  $\mathbf{M}^*$

Parameter	True $\mathbf{M}$	$\hat{\mathbf{M}}$	$\mathbf{M}^*$
Number $4.0 \leq \mathbf{M} < 4.5$	685	762	685
Number $4.5 \leq \mathbf{M} < 5.0$	216	241	217
Number $5.0 \leq \mathbf{M} < 5.5$	68	76	69
Number $5.5 \leq \mathbf{M} < 6.0$	21	24	21
Number $6.0 \leq \mathbf{M} < 6.5$	7	7	7
Number $6.5 \leq \mathbf{M} < 7.0$	2	2	2
$N(\mathbf{M} \geq 4)$	10.00	11.13	10.01
$b$ -value	1.004	1.003	1.005

As indicated by these results, the counts of  $\hat{\mathbf{M}}$  in each magnitude bin are larger than those for the true magnitudes, and the resulting estimate of  $N(\mathbf{M} \geq 4)$  is biased, although the  $b$ -value estimate is unbiased.

Tinti and Mulargia (1985) explored this bias, finding that the estimated  $b$ -value is unaffected by the magnitude uncertainty (as long as the same uncertainty applies to all magnitudes). They introduced a correction to the recurrence rate estimated from  $\hat{\mathbf{M}}$  given by

$$N(\mathbf{M}_{True}) = N(\hat{\mathbf{M}}) \exp\{-\gamma^2\} \quad (3.3.1-1)$$

with

$$\gamma^2 = \frac{\beta^2 \sigma^2[\mathbf{M}|\hat{\mathbf{M}}]}{2} \quad (3.3.1-2)$$

Parameter  $\beta$  is equal to the  $b$ -value in natural log units ( $\beta = b \ln\{10\}$ ) and  $\sigma[\mathbf{M}|\hat{\mathbf{M}}]$  is the standard deviation of the normally distributed error in the observed magnitudes. Using the fitted  $b$ -value of 1.0 and  $\sigma[\mathbf{M}|\hat{\mathbf{M}}] = 0.2$  yields  $\gamma^2$  equal to 0.106. Applying Equation 3.3.1-1 to the value of  $N(\mathbf{M} \geq 4)$  estimated from  $\hat{\mathbf{M}}$  in the table above yields a value of 10.01, very close to the correct value of 10.00 obtained from the true  $\mathbf{M}$  catalog.

The EPRI-SOG project (EPRI, 1988, Vol. 1) developed an alternative approach for obtaining unbiased recurrence parameter estimates.<sup>1</sup> An adjusted magnitude,  $\mathbf{M}^*$ , was introduced defined by the expression:

$$\mathbf{M}^* = \hat{\mathbf{M}} - \beta \sigma^2[\mathbf{M}|\hat{\mathbf{M}}] / 2 \quad (3.3.1-3)$$

Recurrence parameters estimated using the adjusted magnitudes were shown to be unbiased. The simulations described above were repeated to include the calculation of  $\mathbf{M}^*$  for each earthquake in each simulated catalog using Equation 3.3.1-3. The right-hand column of the above table shows the resulting average counts by magnitude bin and the resulting recurrence parameters. The values are very close to those obtained using the true  $\mathbf{M}$  values. These results are to be expected as the adjustment defined by Equations 3.3.1-1 and 3.3.1-2 is equivalent to the adjustment defined by Equation 3.3.1-3 as the value of  $\gamma^2 = \beta \times (\hat{\mathbf{M}} - \mathbf{M}^*) = \beta^2 \sigma^2[\mathbf{M}|\hat{\mathbf{M}}] / 2$ .

Figure 3.3-1 shows this equivalence graphically.

The EPRI-SOG project (EPRI, 1988, Vol. 1) extended the adjustment defined by Equation 3.3.1-3 to the case where the magnitudes  $\mathbf{M}$  are estimated from a vector of other size measures  $\mathbf{X}$ , such as other magnitude scales or shaking intensity measures. In this case, the adjusted magnitude  $\mathbf{M}^*$  is given by

$$\mathbf{M}^* = E[\mathbf{M}|\mathbf{X}] + \beta \sigma^2[\mathbf{M}|\mathbf{X}] / 2 \quad (3.3.1-4)$$

The change in sign of the adjustment occurs because, as also shown by EPRI (1988), the expected value of the true magnitude,  $E[\mathbf{M}]$ , given uncertainty  $\sigma[\mathbf{M}|\hat{\mathbf{M}}]$  and an underlying exponential distribution in magnitude is given by

$$E[\mathbf{M}] = \hat{\mathbf{M}} - \beta \sigma^2[\mathbf{M}|\hat{\mathbf{M}}] \quad (3.3.1-5)$$

---

<sup>1</sup> The EPRI-SOG project used  $m_b$  as the uniform magnitude scale. However, the relationships developed there for obtaining unbiased recurrence estimates and uniform magnitudes are not dependent on the chosen magnitude scale.

Applying Equation 3.3.1-5 to Equation 3.3.1-3 yields

$$\mathbf{M}^* = E[\mathbf{M}] + \beta\sigma^2[\mathbf{M}|\hat{\mathbf{M}}]/2 \quad (3.3.1-6)$$

Thus, the adjustments from  $E[\mathbf{M}]$  to  $\mathbf{M}^*$  are the same regardless of whether  $E[\mathbf{M}]$  is estimated from other size measures  $\mathbf{X}$  or from the observed magnitudes  $\hat{\mathbf{M}}$ .

The process of using Equation 3.3.1-4 to correct for bias when  $\mathbf{M}$  is estimated from  $\mathbf{X}$  was also tested using simulation. The simulation steps consisted of the following:

1. Simulate a catalog of true values of  $\mathbf{M}$  from a truncated exponential distribution in the magnitude range of 3 to 8 with a  $b$ -value of one.
2. Add a normally distributed random error to  $\mathbf{M}$  to produce observed magnitudes  $\hat{\mathbf{M}}$ .
3. Simulate associated values of  $m_b$  using the relationship  $m_b = \mathbf{M} + 0.3$ . Include a normally distributed random error with standard deviation 0.3 to simulate randomness in the relationship between  $\mathbf{M}$  and  $m_b$  from earthquake to earthquake. (Note that inclusion of measurement error in  $m_b$  in effect just adds to the random difference between  $\mathbf{M}$  and  $m_b$  and it is unimportant to separate this component from the total random difference between the two magnitude scales).
4. Regress  $\hat{\mathbf{M}}$  against  $m_b$  and obtain the values of  $E[\mathbf{M}|m_b]$  and  $\sigma[\hat{\mathbf{M}}|m_b]$  for each simulated  $m_b$ . This is performed by first trimming the catalog to  $m_b \geq 4$  to remove the truncation effect at the low end resulting from the initial limit of  $\mathbf{M}$  to  $\geq 3$ .
5. Use Equation 3.3.1-4 to obtain a catalog of  $\mathbf{M}^*$ . Trim off the events below  $\mathbf{M}^* 4$  to remove the edge effect and estimate the seismicity parameters  $N(\mathbf{M} \geq 4)$  and  $b$ -value from the counts of  $\mathbf{M}^*$ .
6. Estimate the recurrence parameters for the simulated catalogs using the true  $\mathbf{M}$  values, the  $E[\mathbf{M}]$  values, and the  $\mathbf{M}^*$  values.

The following table presents the results averaged over 500 simulations.

Average Results from 500 Simulated Catalogs of True  $\mathbf{M}$ ,  $\hat{\mathbf{M}}$ ,  $m_b$ , and  $\mathbf{M}^*$

Parameter	True $\mathbf{M}$	$E[\mathbf{M}]$	$\mathbf{M}^*$	$\mathbf{M}^*_{adjusted}$
$N(\mathbf{M} \geq 4)$	10.00	8.02	10.68	10.06
$b$ -value	1.000	1.001	1.001	1.001

Use of the catalog of  $E[\mathbf{M}]$  values results in an underestimate of the true recurrence rate. Use of the catalog of adjusted magnitudes  $\mathbf{M}^*$  produces a close but slight overestimate of the true rate. Examination of Equation 3.3.1-4 indicates that the source of the difference is that the adjusted magnitudes should be based on the value of  $\sigma[\mathbf{M}|m_b]$ , the variability in true  $\mathbf{M}$  given  $m_b$ , while the results of the regression between the observed values of the two magnitude scales produces  $\sigma[\hat{\mathbf{M}}|m_b]$ . The latter value is inflated over  $\sigma[\mathbf{M}|m_b]$  due to the random error in the observed

values of  $\hat{\mathbf{M}}$  used in the regression. This suggests that a modified value of  $\mathbf{M}^*$  be computed using the relationship

$$\mathbf{M}^*_{adjusted} = E[\mathbf{M}|\mathbf{X}] + \beta(\sigma^2[\hat{\mathbf{M}}|\mathbf{X}] - \sigma^2[\mathbf{M}|\hat{\mathbf{M}}])/2 \quad (3.3.1-7)$$

using the assumption that

$$\sigma^2[\mathbf{M}|\mathbf{X}] = \sigma^2[\hat{\mathbf{M}}|\mathbf{X}] - \sigma^2[\mathbf{M}|\hat{\mathbf{M}}] \quad (3.3.1-8)$$

where  $\sigma^2[\mathbf{M}|\hat{\mathbf{M}}]$  is the variance in the observed values  $\hat{\mathbf{M}}$  used in the regression of  $\mathbf{X}$  versus  $\hat{\mathbf{M}}$ .

The right-hand column of the above table shows that the use of Equation 3.3.1-7 to compute  $\mathbf{M}^*$  results in predicted recurrence parameters very close to those obtained using the simulated true  $\mathbf{M}$  values.

As part of the simulation testing, the average value of  $(\text{true } \mathbf{M} - E[\mathbf{M}|m_b])$  was found to be less than 0.01, indicating that the regression of  $m_b$  against  $\hat{\mathbf{M}}$  produces  $E[\mathbf{M}]$ .

The advantage of the  $\mathbf{M}^*$  approach is that it allows inclusion of the variability in the values of  $\sigma[\mathbf{M}|\hat{\mathbf{M}}]$  and  $\sigma[\mathbf{M}|X]$  from earthquake to earthquake. EPRI (1988) provided the following relationships for the case where  $E[\mathbf{M}]$  is estimated from a vector  $\hat{\mathbf{X}}$  of  $R$  observed size measures:

$$E[\mathbf{M}|\hat{\mathbf{X}}] = \left\{ \sum_i \frac{\sigma^2[\mathbf{M}|\hat{\mathbf{X}}_i]}{\sigma^2[\mathbf{M}|\hat{\mathbf{X}}_i]} \cdot E[\mathbf{M}|\hat{\mathbf{X}}_i] \right\} + (R-1)\beta\sigma^2[\mathbf{M}|\hat{\mathbf{X}}] \quad (3.3.1-9)$$

and

$$\sigma^2[\mathbf{M}|\hat{\mathbf{X}}] = \left\{ \sum_i \frac{1}{\sigma^2[\mathbf{M}|\hat{\mathbf{X}}_i]} \right\}^{-1} \quad (3.3.1-10)$$

where  $\hat{\mathbf{X}}_i$  is a single member of  $\hat{\mathbf{X}}$ . The individual values of  $\sigma[\mathbf{M}|\hat{\mathbf{X}}_i]$  should include the adjustment given by Equation 3.3.1-8. Use of Equation 3.3.1-9 represents a variance weighted estimate of  $E[\mathbf{M}]$ . The final term of Equation 3.3.1-9 is needed to adjust for bias introduced by the underlying exponential distribution in magnitude. Simulation testing using multiple size measures showed that Equation 3.3.1-9 produced the correct value of  $E[\mathbf{M}]$  and the use of Equation 3.3.1-7 to compute  $\mathbf{M}^*$  with the variance given by Equation 3.3.1-10 resulted in unbiased recurrence parameters.

The procedure developed by Tinti and Mulargia (1985) can also be applied to the case of  $E[\mathbf{M}]$  estimated from  $\hat{\mathbf{X}}$ . The parameter  $\gamma^2$  is computed using the variance defined by Equation 3.3.1-10. However, in this case the adjustment to the computed recurrence rate is given by

$$N(\mathbf{M}_{True}) = N(E[\mathbf{M}]) \exp\{+\gamma^2\} \quad (3.3.1-11)$$

The change in sign is due to the true rate being underestimated from the  $E[\mathbf{M}]$  magnitudes and is a direct result of relationship between  $\hat{\mathbf{M}}$  and  $E[\mathbf{M}]$  defined by Equation 3.3.1-5.

The above results were obtained using earthquake catalogs that had the same level of completeness at all magnitude levels; that is, the catalogs contain all earthquakes that occurred during the time period used for the simulation. The process was repeated using simulation of partially complete catalogs in which the completeness of reporting for smaller magnitudes is less than for the larger magnitude, the typical case encountered in practice. These tests showed that the use of the  $\mathbf{M}^*$  correction did not lead to unbiased estimates of the earthquake recurrence parameters; in general, the values of  $N(\mathbf{M} \geq 4)$  and  $b$ -value were biased low. The source of this bias can be envisioned by comparing the EPRI (1988) and Tinti and Mulargia (1985) bias adjustments. If one considers the magnitude interval  $m_i$  (e.g., magnitudes  $4.5 \leq \mathbf{M} < 5$ ), the true rate of earthquakes in that interval,  $\lambda_i$ , is equal to  $n_i^C / T_i^C$ , where  $n_i^C$  is the count of true  $\mathbf{M}$  in the catalog completeness period for that magnitude interval  $T_i^C$ .

In the case where the catalog contains the observed magnitudes  $\hat{\mathbf{M}}$ , the results of Tinti and Mulargia (1985) show that the counts of  $\hat{\mathbf{M}}$  are too large by the factor  $\exp\{\gamma^2\}$  and the true rate can be obtained by multiplying the observed counts by the factor  $\exp\{-\gamma^2\}$ . The  $\mathbf{M}^*$  approach of EPRI (1988) is to shift the observed magnitudes down by the factor  $\gamma^2 / \beta = \beta \sigma^2[\mathbf{M} | \hat{\mathbf{M}}]$  such that the counts in the interval  $m_i$  are effectively reduced by the same factor  $\exp\{-\gamma^2\}$ . If the catalog instead consists of the expected magnitudes  $E[\mathbf{M}]$ , then the adjustment is in the opposite direction. The counts of  $E[\mathbf{M}]$  are too low by the factor  $\exp\{+\gamma^2\}$  and one can either adjust the rate using Equation 3.3.1-11 or shift the magnitudes using Equation 3.3.1-7 to effectively increase the counts by the same factor. Where the problem lies is that when the completeness for earthquakes in the next lowest magnitude interval is less than for magnitudes in the interval in question ( $T_{i-1}^C < T_i^C$ ), then insufficient earthquakes are shifted from magnitude interval  $m_{i-1}$  to  $m_i$  using the  $\mathbf{M}$  and the true rate remains underestimated.

The solution to this problem is to use the approach of Tinti and Mulargia (1985) to adjust the earthquake counts in each magnitude interval rather than use the EPRI (1996) adjusted magnitudes  $\mathbf{M}^*$ . However, to maintain the EPRI (1988) ability to account for differences in magnitude uncertainty for individual earthquakes, the adjustment is applied individually, earthquake by earthquake, rather than globally to the total earthquake counts in a magnitude interval. The earthquake catalog is processed to obtain values of  $E[\mathbf{M}]$  and  $\sigma[\mathbf{M}]$  for each earthquake as described above. Each earthquake is then assigned an equivalent count  $N^*$  defined as

$$N^* = \exp\left\{\beta^2 \sigma^2 [|\mathbf{M}|\hat{\mathbf{M}}]/2\right\}$$

or

$$N^* = \exp\left\{\beta^2 \sigma^2 [|\mathbf{M}|\mathbf{X}]/2\right\} \tag{3.3.1-12}$$

The rate of earthquakes in the magnitude interval  $m_i$  is then obtained by summing the values of  $N^*$  for earthquakes with values of  $E[\mathbf{M}]$  in the magnitude interval and dividing by period of completeness for the magnitude interval. Earthquake recurrence parameters are thus computed using standard approaches, such as maximum likelihood, and the effective counts  $N^*$  rather than the observed counts.

The performance of the use of the  $N^*$  approach compared to the  $\mathbf{M}^*$  approach was tested on simulated catalogs. The simulation steps were as follows:

1. Simulate a catalog of true values of  $\mathbf{M}$  from a truncated exponential distribution in the magnitude range  $3 \leq \mathbf{M} \leq 8$  with a recurrence rate of  $25 \mathbf{M} \geq 3$  earthquakes per year and a 300-year complete catalog.
2. Add random error to each value of  $\mathbf{M}$  to produce a catalog of observed magnitudes.
3. Simulate an estimate of size measure  $\mathbf{X}$  for each  $\mathbf{M}$  with random variability in the relationship between  $\mathbf{X}$  and  $\mathbf{M}$ .
4. Regress against  $\mathbf{X}$  to obtain the values of  $E[\mathbf{M}|\mathbf{X}]$  and  $\sigma[\mathbf{M}|\mathbf{X}]$ .
5. Use Equation 3.3.1-7 to obtain a catalog of  $\mathbf{M}^*$ .
6. Use Equation 3.3.1-12 to obtain  $N^*$  for each earthquake.
7. Assign to each earthquake a probability of being observed based on its size and specified relative values of equivalent periods of completeness as a function of magnitude.
8. Reduce the simulated catalog to the observed one in the periods of completeness for each magnitude.
9. Trim off the events below  $\mathbf{M}^* 4$  to remove the edge effect and estimate the seismicity parameters  $N(\mathbf{M} \geq 4)$  and  $b$ -value from the counts of  $\mathbf{M}^*$ .
10. Trim off the events below  $E[\mathbf{M}] = 4$  to remove the edge effect and estimate the seismicity parameters  $N(\mathbf{M} \geq 4)$  and  $b$ -value from the counts of  $N^*$ .
11. Repeat the process for 500 simulations and compute the average difference between the values of  $N(\mathbf{M} \geq 4)$  and  $b$ -value obtained by steps 9 and 10 from the values computed from the full catalog of simulated true values of  $\mathbf{M}$ .

Simulations were performed for three cases:  $m_b$  was computed from  $\mathbf{M}$  using the expression  $m_b = \mathbf{M} + 0.3$ ;  $I_0$  was computed from  $\mathbf{M}$  using the expression  $I_0 = 3(\mathbf{M}-1)/2$ ; and a mixture of the two. Three levels of catalog completeness were used as listed in the table below. The partial completeness cases consist of  $T^C_i$  for magnitude 4 being about two-thirds of the catalog length (“Two-thirds” case) and  $T^C_i$  for magnitude 4 being half of the catalog length (“Half” case).

Completeness Cases Used in Simulations

Completeness Case	Equivalent Period of Completeness (years) for Magnitude Interval:									
	3–3.5	3.5–4	4–4.5	4.5–5	5–5.5	5.5–6	6–6.5	6.5–7	7–7.5	7.5–8
Full	300	300	300	300	300	300	300	300	300	300
Two-thirds	200	210	220	230	240	250	260	280	300	300
Half	100	125	150	175	200	225	250	275	300	300

The results of the simulations are listed in the following table. Shown for each case are the average percent errors between the values of  $N(\mathbf{M} \geq 4)$  and  $b$ -value obtained using the  $\mathbf{M}^*$  and  $N^*$  approaches and the values obtained using the simulated true values of  $\mathbf{M}$ . The  $X$  cases labeled “Mixture” consist of the use of  $I_0$  for the first 200 years and  $m_b$  for the last 100 years, consistent with the general mix of size measures in the CEUS SSC Project catalog. For the case of full completeness, either method works as well as the other. However, as the relative completeness in the lower magnitudes becomes smaller, the bias in the  $\mathbf{M}^*$  estimates increases while the results obtained using the  $N^*$  approach remain close to those obtained using the true simulated values of  $\mathbf{M}$ . These results indicate that the  $N^*$  approach performs better than the  $\mathbf{M}^*$  approach for earthquake catalogs with variable levels of completeness as a function of magnitude. As this is the case for the CEUS SSC Project catalog, the  $N^*$  approach was used to obtain unbiased estimates of earthquake recurrence parameters. Consistent with this approach, the uniform magnitude measure adopted for the CEUS SSC Project catalog is  $E[\mathbf{M}]$ , the expected value of moment magnitude for each earthquake given the uncertainty in estimating its size.

Results of Simulation Testing of  $\mathbf{M}^*$  and  $N^*$  Approaches for Partially Complete Catalogs

$X$ Case	Completeness Case	Percent Error In Parameters Obtained by:			
		Estimation Using $\mathbf{M}^*$		Estimation Using $N^*$	
		$N(\mathbf{M} \geq 4)$	$b$ -value	$N(\mathbf{M} \geq 4)$	$b$ -value
$I_0$	Full	2.29%	0.56%	1.79%	-0.14%
$I_0$	Two-thirds	-25.00%	-2.37%	1.11%	0.96%
$I_0$	Half	-48.42%	-11.28%	1.19%	0.36%
$m_b$	Full	0.10%	0.04%	0.14%	0.21%
$m_b$	Two-thirds	-26.02%	-3.87%	-0.52%	0.09%
$m_b$	Half	-48.09%	-12.01%	-1.34%	0.00%
Mixture	Full	1.49%	0.48%	1.25%	0.17%
Mixture	Two-thirds	-25.32%	-3.29%	1.05%	0.20%
Mixture	Half	-49.59%	-12.52%	-0.83%	-0.69%

### 3.3.2 Estimation of $E[M]$ for the CEUS SSC Project Catalog

This section summarizes the relationships used to develop the uniform moment magnitude estimate  $E[M]$  for earthquakes in the CEUS SSC Project catalog. Two general types of data are available for the estimation of  $E[M]$ , either direct observation of moment magnitudes,  $\hat{M}$ , or observations of other size measures  $X$  that require development of scaling relationships from  $X$  to  $E[M]$ . The majority of earthquakes in the project catalog that occurred after about 1930 have reported values of instrumental magnitude in one or more of the magnitude scales  $m_b$ ,  $m_{bLg}$ ,  $M_N$ ,  $M_S$ ,  $M_L$ ,  $M_C$ , or  $M_D$ . The data in the project catalog were used to develop scaling relationships between these magnitude scales and moment magnitude. The final relationships are listed in Table 3.3-1.

Before presenting these relationships, the issue of the effect of rounding off in reported magnitudes will be addressed.

#### 3.3.2.1 Effect of Magnitude Rounding on Statistical Tests

As part of the development of scaling relationships from various magnitude scales to moment magnitudes, statistical tests were performed to identify potential differences in scaling between different catalog sources. Most of the magnitudes are reported in various catalogs to the first decimal place. The issue of the effect of rounding in reported magnitudes has been examined by Felzer (2008) with regard to the effect on seismicity rates, with emphasis on the effect of rounding to the nearest 0.5 magnitude units. For the CEUS SSC Project, the issue is the potential impact of rounding of data to the first decimal place on results of  $t$ -tests for nonzero values of the difference between magnitudes reported by source A and by source B (e.g., the difference between  $M_N$  reported by the GSC and that reported by Weston for a set of common earthquakes).

The impact of rounding to the nearest 0.1 magnitude unit was examined by simulating hypothetical data sets for Source A and Source B with specified average differences in magnitude and specified random variability in the magnitude differences. A  $t$ -test is performed comparing the mean difference between the magnitudes from Source A and Source B to see if a nonzero difference is statistically significant at the 5 percent level ( $p$ -value = 0.05). This corresponds to the absolute value of the mean difference divided by the standard deviation of mean differences being greater than 2.13. The simulated magnitudes from the two sources are then rounded to the nearest 0.1 magnitude units and the  $t$ -test is repeated. Differences in the test results for the unrounded and rounded simulated samples would indicate that rounding potentially affects the ability to properly detect differences in reported magnitudes. The selected 5 percent significance level means that even if the true average difference in magnitude reported by the two agencies is zero, one would expect to see a statistically significant difference in 5 percent of random samples.

The following table reports the results of simulation tests performed for magnitude sample sizes of 50 and 100. For each case, a mean difference in magnitude was specified along with the standard deviation for the random variability in magnitudes reported by the two agencies. Then 10,000 simulations of each data set were performed. The percentage of simulated samples that indicated a statistically significant difference is given in the table below. For the cases with specified mean difference of zero, approximately 5 percent of the simulated samples show a statistically significant difference, consistent with expectation. Comparison of the results in the last two columns indicates that nearly the same percentages are obtained for the unrounded and

rounded samples. The results indicate that the rounding to 0.1 magnitude units does not cause a significant disruption in *t*-test results for identifying mean differences in magnitudes between two magnitude sources, and its effect can be ignored.

Simulation of *t*-Test Results for Differences in Magnitudes

Sample Size	Specified Mean Difference	Specified Standard Deviation of Difference of Individual Magnitudes	Percentage with <i>p</i> -value $\leq 0.05$ for unrounded sample	Percentage with <i>p</i> -value $\leq 0.05$ for rounded sample
100	0	0.1	5.1	5.1
100	0	0.2	5.2	5.0
100	0	0.3	5.1	5.1
100	0.1	0.1	100	100
100	0.1	0.2	99.9	99.9
100	0.1	0.3	91.4	91.1
100	0.2	0.3	100	100
100	0.2	0.4	99.8	99.8
50	0	0.1	4.9	5.2
50	0	0.2	5.3	5.2
50	0	0.3	5.0	5.0
50	0.1	0.1	100	100
50	0.1	0.2	93.4	92.9
50	0.1	0.3	63.8	63.6
50	0.2	0.3	99.6	99.6
50	0.2	0.4	93.6	93.4

### 3.3.2.2 Moment Magnitude Data

Moment magnitude data for earthquakes in the project catalog provide both a direct assessment of  $E[\mathbf{M}]$  and the necessary data for the development relationships between moment magnitude and other size measures. Two types of moment magnitude data were used. The first are published moment magnitudes for specific earthquakes that are assumed to be based on a reliable assessment of seismic moment from inversions of either long-period waveforms or surface-wave spectra. Table B-2 in Appendix B lists the 272 earthquakes with reported values of  $\mathbf{M}$  that were used for both observed values of  $\mathbf{M}$  for specific earthquakes and for developing the magnitude conversions.

As discussed in Section 3.3.1, the reported values of moment magnitude represent  $\hat{\mathbf{M}}$ , magnitude measured with uncertainty. These magnitude values are adjusted to  $E[\mathbf{M}]$  using Equation 3.3.1-5. The values of  $\sigma[\mathbf{M}|\hat{\mathbf{M}}]$  are taken from the source of the reported magnitude estimate, if available. If an uncertainty was not reported, then the following average values for

moment magnitude estimation as a function of time were used. The average of the values of uncertainty in moment magnitude estimates presented by Johnston (1996a, Table B2) gives 0.28 for the period prior to 1960, 0.15 for earthquakes in the time period 1960–1974, and 0.13 for the period 1975–1990. The average uncertainty in  $M$  for the seven CEUS earthquakes in the Harvard Centroid Moment Tensor catalog in the period 1978–1984 is 0.12 and for the eight earthquakes in the period 1985–present is 0.10. Using this information, the following nominal uncertainty values were assigned to instrumental moment magnitudes when data for a specific earthquake was not available.

Assigned Values of  $\sigma[M|\hat{M}]$

Time Period	Nominal $\sigma[M \hat{M}]$
1920–1959	0.30
1960–1975	0.15
1975–1984	0.125
1985–2008	0.10

The second type of moment magnitude estimates are those obtained by approximate means in the studies of Atkinson (2004a, 2004b), Boatwright (1994), and Moulis (2002). These approximate moment magnitudes were corrected for minor biases as described below before using them to augment the  $M$  data set.

***Atkinson (2004) Study***

Atkinson (2004a, 2004b) developed estimates of moment magnitudes for eastern Canada earthquakes based on analysis of Fourier spectra. Figure 3.3-2 compares her estimates of  $M$  with moment magnitudes listed in Table B-2 in Appendix B for earthquakes in common. The moment magnitude values obtained by Atkinson (2004a, 2004b) are close to reported moment magnitudes for values of  $M$  above magnitude 4, but they overestimate  $M$  by about 0.2 units for smaller values. The one exception is the estimate for the 1989 Ungava, Quebec, foreshock. Atkinson (pers. comm., 2011) indicates that her estimate for this event is unreliable given the great distances between the earthquake and the stations she used. Ignoring this one event, a locally weighted least-squares fit to the data shown on Figure 3.3-2 was used to adjust the values of moment magnitudes reported in Atkinson (2004b) to values of  $M$  used in this study.

***Boatwright (1994) Study***

Boatwright (1994) inverted vertical recordings from the Eastern Canada Telemetered Network (ECTN) to obtain estimates of earthquake source spectra, including seismic moment. Figure 3.3-3 compares Boatwright’s (1994) estimates of moment magnitude with moment magnitudes listed in Table B-2 in Appendix B for earthquakes in common. The moment magnitude values obtained by Boatwright (1994) are close to reported moment magnitudes for values of  $M$  below 3.5 and tend to slightly underestimate the value of  $M$  at larger values. A locally weighted least-squares (Loess) fit to the data shown on Figure 3.3-3 was used to adjust the moment magnitudes reported in Boatwright (1994) to values of  $M$  used in this study.

### ***Moulis (2002) Study***

Moulis (2002) developed estimates of moment magnitudes for northeastern United States earthquakes using a coda wave technique. Figure 3.3-4 compares her estimates of moment magnitude with moment magnitudes listed in Table B-2 in Appendix B for earthquakes in common. The moment magnitude values obtained by Moulis (2002) are close to reported moment magnitudes, albeit with more scatter than shown by the Atkinson (2004a, 2004b) and Boatwright (1994) estimates. A least-squares fit to the data shown on Figure 3.3-4 was used to adjust the moment magnitudes reported in Moulis (2002) to values of  $\mathbf{M}$  used in this study.

### ***Combined Estimates***

The relationships shown on Figures 3.3-2, 3.3-3, and 3.3-4 were used to compute  $E[\mathbf{M}]$  for each earthquake with an approximate moment magnitude estimate from the three studies described above. Where multiple estimates are available from two or three of the studies, they were combined using the variance weighing approach defined by Equations 3.3.1-9 and 3.3.1-10. Table B-3 in Appendix B lists the resulting approximate moment magnitudes.

#### **3.3.2.3 Estimation of $E[\mathbf{M}]$ from Body-Wave Magnitudes**

Two types of body-wave magnitudes are contained in the catalog data, magnitudes computed from the amplitude of compression waves, and  $m_{bLg}$  magnitudes computed from amplitude of Lg waves. The latter are sometimes denoted as  $M_N$  or Nuttli magnitudes, referring to Nuttli (1973), who originally proposed the relationship for defining the  $m_{bLg}$  scale. The distinction between  $m_{bLg}$  and  $M_N$  is maintained in the project catalog as not all agencies compute Lg magnitudes in exactly the same way. Herrmann and Kijko (1983) discuss this issue and suggest the magnitude scale  $m_{Lg(f)}$  to indicate what frequencies were used to compute the magnitude. This scale is currently being used by the Weston Observatory (see below). Catalog data were examined to assess the potential for regional/time/network differences in the conversion from various body-wave magnitude scales to  $\mathbf{M}$ .

#### ***Comparison of Body-Wave Magnitudes Reported by Various Agencies***

The largest differences found in comparing magnitudes reported by different agencies were in comparison of  $M_N$  magnitudes for earthquakes in the northeastern United States and southeastern Canada reported by the GSC and Weston Observatory. Figure 3.3-5 shows the difference in reported magnitudes for the same earthquake as a function of time. John Ebel (pers. comm., 2011) indicates that the history of magnitude calculations reported in the Weston Observatory catalog consists of four periods:

- 1938–1962:  $M_N$  computed from the original Weston Observatory Benioff system (Ebel, 1987)
- 1962–1975:  $M_N$  computed from the Weston Observatory WWSSN system (Ebel, 1987)
- 1975–1994:  $M_N$  computed from the Weston Observatory Develocorder system or early digital system (NEUSSN bulletins and the Weston Observatory earthquake catalog)
- 1994–present:  $m_{Lg(f)}$  computed from the evolving seismometer and digital systems at Weston Observatory

The  $M_N$  magnitudes reported in the GSC and National Earthquake Database (NEDB) for Canada are computed using Nuttli's formula but with a broader frequency range than originally defined by Nuttli (1973) without making a specific frequency correction (J. Adams, pers. comm., 2011).

The data on Figure 3.3-5 show clearly that there are time periods where the two magnitude scales cannot be considered equivalent: 1938–1975, and after about 1997. The time periods of differences in magnitude reporting generally coincide with changes in magnitude calculation methods used by Weston Observatory, as indicated by the color coding on Figure 3.3-5.

The SUSN catalog also contained a number of earthquakes in the northeastern United States. The catalog indicated that the magnitude data were obtained from the Earth Physics Branch (EPB) of Canada. Tests of these magnitudes against  $M_N$  magnitudes reported in the GSC/NEDB catalog indicate that the mean difference is small ( $\sim 0.03$  units) and is only statistically significant when using a combination of  $m_b$  and  $m_{bLg}$  magnitudes reported by EPB. Therefore, the SUSN magnitudes reported with a sited source of EPB were considered equivalent to GSC  $M_N$  magnitudes.

The other major seismic network in the northeastern United States is the Lamont-Doherty network. Earthquake magnitudes in the catalog obtained from the Lamont-Doherty catalog have the source designation LDO or PAL (Palisades), or are based on work by Sykes et al. (2008). Testing of the difference between magnitudes reported by Lamont and magnitudes reported by Weston Observatory indicate a small ( $-0.08$  magnitude unit) difference that is statistically significant.

For the remaining portions of the study region, the magnitudes come from a variety of sources. The SUSN catalog lists the following sources for magnitudes in the CEUS:

- B—Bollinger (1975), Southeastern U.S. Catalog 1754–1974
- E—Earth Physics Branch (EPB), Canadian catalog
- G—USGS State Seismicity Maps (Stover et al., 1984)
- I—EPRI-SOG Catalog (EPRI, 1988)
- M—Sibol et al. (1987)
- N—Nielsen (1982)—Stanford Data Base
- O—Nuttli (1974)
- R—Barstow et al. (1981) (Rondout Associates), NUREG/CR-1577
- S—Street and Turcotte (1977)
- T—Reinbold and Johnston (1987)
- U—Earthquake History of the U.S./U.S. Earthquakes (Stover and Coffman, 1993)
- V—SEUSSN Bulletins (Virginia Tech Publication)
- W—Nuttli et al. (1979)

The separation of magnitude source and type was achieved using the following earthquake catalog sources.

- Although all earthquakes in the USGS seismic hazard mapping catalog are considered to be  $m_b$  magnitude, the catalog does provide references for the assigned magnitude. These were used to indicate the magnitude type according to the magnitude source. The major source was NCEER and the NCEER magnitude (last column of the NCEER-91 catalog) was used as the assigned magnitude.
- For those events where the magnitude source was “NCEER,” the NCEER-91 catalog was used to determine which of the several magnitude types was used to define the “NCEER Magnitude.” In the case of instrumental magnitudes, this was typically the magnitude type with the largest reported magnitude, which in a number of cases is  $M_L$  or  $M_C$ . The USGS magnitude type was corrected to correspond to the specified type used in NCEER, and the NCEER source was indicated in the catalog where possible, based on comparisons of the magnitude with those reported by other sources. The SUSN catalog was particularly useful in inferring the source of many of the NCEER/EPRI magnitudes.
- The Nuttli (1983) catalog from Saint Louis University was also reviewed to change those magnitudes with source NUT that were determined from macroseismic data from  $m_b$  to  $m_{10}$  or  $m_{FA}$ , as appropriate.
- The Dewey and Gordon (1984) catalog was reviewed to include those earthquakes for which Dewey and Gordon (1984) calculated the  $m_{bLg}$  magnitude and for these the magnitude source was indicated as D&G.

Comparisons of magnitudes among these different sources indicated differences in some cases of 0.1 to 0.2 units (e.g., comparing D&G  $m_{bLg}$  with  $m_b$  from other sources) or differences of less than 0.1 (e.g., comparing D&G  $m_{bLg}$  with  $m_{bLg}$  from other sources), although these comparisons were often for small samples.

### ***Analysis of Regional/Network Differences in Body-Wave Magnitude to Moment Magnitude Scaling***

The comparisons among body-wave magnitudes reported from various sources indicated that there may be regional/catalog source differences in scaling from body-wave magnitudes to moment magnitude. The next step was to test the scaling from body-wave magnitudes to moment magnitude. The largest differences appeared to be in the northeastern portion of the study region (northeastern United States and southeastern Canada). Therefore, separate investigations were performed for this portion of the study region and for the remaining portion of the study region.

#### **Scaling from $m_b$ to $M$ in the Midcontinent Portion of the Study Region**

The first phase was testing for magnitude differences among sources in the main portion of the study region, excluding the northeastern United States and southeastern Canada. Figure 3.3-6 shows the spatial distribution of earthquakes with reported body-wave and  $M$  magnitudes (112 earthquakes) color-coded by magnitude source. The primary sources for the  $M$  magnitude for these earthquakes were Street et al. (1975) and Dr. Robert Herrmann at Saint Louis University ([http://www.eas.slu.edu/eqc/eqc\\_mt/MECH.NA/](http://www.eas.slu.edu/eqc/eqc_mt/MECH.NA/)).

Figure 3.3-7 shows the  $m_b$ - $\mathbf{M}$  data set for these earthquakes, together with three published relationships that have been used in the past for conversion from  $m_b$  to  $\mathbf{M}$  for hazard calculations. After eliminating the data for  $m_b < 3$  to remove truncation effects, a linear relationship was fit to the data, resulting in a slope of  $0.96 \pm 0.03$ . The linear fit included all specified values for body-wave magnitude for each earthquake, with equal weights assigned to each value. Testing of the linear fit versus an offset model,  $\mathbf{M} = m_b + C$ , indicated that the linear model did not have greater predictive power as measured by the Akaike (1974) information criterion (AIC). The AIC is often used to select between models, in this case between a linear model with two parameters and an offset model with a single parameter. In selecting among models, the one with the lower AIC value is typically preferred. The test results indicate that the slope parameter difference from 1.0 is not statistically significant, and the offset model provides a satisfactory fit to the data. The resulting constant is  $-0.28 \pm 0.02$ , and the offset line is shown on Figure 3.3-7. It is recognized that at larger magnitudes, there is a tendency for saturation of the  $m_b$  scale with increasing moment magnitude (e.g., Boore and Atkinson, 1987). However, the focus in catalog development is in estimating  $\mathbf{M}$  from instrumentally derived  $m_b$  magnitudes in the magnitude range of 3 to 6. All the larger earthquakes in the CEUS SSC catalog have been subjected to special studies, and more robust estimates of  $\mathbf{M}$  have been developed from these efforts.

Testing of inclusion of the  $m_b$  source as a predictor showed no statistical significance for any source differences. Testing of magnitude type indicated no statistical difference between  $m_b$  and  $m_{bLg}$  and a weak difference for  $M_n$ , which is based on only 9 earthquakes. Thus it is concluded that in the midcontinent portion of the study region, the various reported magnitudes  $m_b$ ,  $m_{bLg}$ , and the few  $M_N$  values can be considered equivalent for purposes of estimating  $E[\mathbf{M}]$ .

Figure 3.3-8 shows a plot of the residual for the offset model (Figure 3.3-7) against earthquake year. There is an apparent shift in the residuals after about 1995 such that the average  $m_b$ - $\mathbf{M}$  difference becomes about 0.1 magnitude units. There are 26 earthquakes in the post-1995 data set scattered throughout the region, and the difference shown on Figure 3.3-8 appears to be statistically significant, although it does not correspond to a known change in network configuration. Because the difference is small and has not been independently reported, it was not factored into the magnitude scaling used for the CEUS SSC Project catalog.

#### Scaling from $m_b$ to $\mathbf{M}$ in the Northeastern Portion of the Study Region

The data for the northeastern United States and southeastern Canada come from two principal sources, the GSC and the Weston Observatory. Figure 3.3-9 shows the spatial distribution of earthquakes with both body-wave and  $\mathbf{M}$  magnitudes (580 earthquakes), color coded by magnitude source.

Figure 3.3-10 shows the  $m_b$ - $\mathbf{M}$  data. There are two types of  $\mathbf{M}$  magnitudes for these earthquakes. The points shown as solid circles were determined mostly from waveform modeling by various researchers. The open circles indicate the data where approximate methods were used to estimate the seismic moment. These represent the work of Atkinson (2004a, 2004b), Boatwright (1994), and Moulis (2002). Also shown on the figure are the three scaling relationships shown on Figure 3.3-7 plus the Sonley and Atkinson (2005) relationship between  $M_N$  and  $\mathbf{M}$ .

To examine the correlation between the magnitude scales, the data were again limited to the magnitude range of primary interest ( $m_b \geq 3.5$ ). The very limited data for  $m_b > 6$  were also

removed to eliminate the effects of  $m_b$  saturation. Testing again showed that a linear fit has a slope near 1 ( $0.97 \pm 0.02$ ) and an offset model produces a lower AIC value. However, for this data set, there are marginally significant differences among the sources, with the largest difference between the GSC and other sources. A statistically significant difference among the body-wave magnitude types in this data set was found, principally between  $m_b$  and other magnitude types.

Figure 3.3-11 shows a plot of the residuals from the fit shown on Figure 3.3-10 versus time. The red points indicate the  $m_b$  magnitude types. Time-dependent changes in residuals may be at least partly an effect of magnitude type. Testing of the effect of magnitude type for data prior to 1980 indicates that type becomes much less significant. Exploring further, Figures 3.3-12 and 3.3-13 show the residuals from Figure 3.3-10 versus year for only the GSC and Weston (WES) data, respectively. These two data sets show shifts in scaling that occur at different times: at about 1995 for the GSC data and about 1980 for the WES data. Both offsets appear statistically significant. The difference in  $M_N$  to  $M$  scaling in the GSC data has been noted previously by Bent (2010). The difference in  $M_N$  to  $M$  scaling in the WES data corresponds to about the time of a change in magnitude processing and also to the period where the  $M_N$  magnitudes are most similar between the GSC and WES data (Figure 3.3-5). These results indicate that time dependent scaling of  $m_b$  to  $M$  should be included in converting the GSC and WES body-wave magnitudes.

Figure 3.3-14 shows the residuals from the fit shown on Figure 3.3-10 versus year for the other catalog sources. A similar time trend to that shown by the WES data can be seen. The sources for most of the data shown on the figure are EPRI and SRA (Stover et al., 1984). Both of these are compilations of other catalog sources and the data are following the trends seen in the primary regional catalogs. As the EPRI and SRA source catalogs are compilations, the assignment of magnitudes to a specific network was made by assuming that if that network source (e.g., GSC or WES) reports the same magnitude value as in the compilation, then that region catalog is the likely source of the EPRI or SRA magnitude. In this manner, most of the magnitudes listed in these two catalogs could be assigned to either the GSC or WES source.

The other important magnitude source in the region is the Lamont-Doherty Earth Observatory (LDO) catalog. There are only three earthquakes in the catalog with both body-wave magnitudes attributed to LDO and moment magnitudes so the scaling cannot be tested for this catalog source. Comparison of body-wave magnitudes from LDO to those from other sources is also inconclusive. Figure 3.3-15 shows a plot of the difference between body-wave magnitudes attributed to LDO and those from other sources. The results do not suggest any difference as the time period when most of the earthquakes were recorded corresponds to the period when the GSC and WES magnitudes are essentially equivalent (Figure 3.3-5).

Figure 3.3-16 shows the spatial distribution of earthquakes with reported GSC body-wave magnitudes and moment magnitudes. Figure 3.3-17 shows the  $M$ - $m_b$  ( $M_N$ ) difference as a function of time for the data with both reported magnitudes. There is a suggestion that the  $m_b$ - $M$  scaling is different in the midcontinent region (southwest of the dashed line on Figure 3.3-16), but this may be due to the GSC reporting magnitudes determined by other sources.

Another source of body-wave magnitudes is the Oklahoma Geological Survey Leonard Geophysical Observatory (OKO) catalog, which reports both  $m_{bLg}$  and  $m(3Hz)$  magnitudes. Figure 3.3-18 shows the difference between  $m_{bLg}$  and  $m(3Hz)$  in that catalog as a function of

$m_{bLg}$ . For magnitudes in the range of interest to this study ( $m_{bLg} > 3$ ) there is no statistically significant difference between the two magnitudes and  $m(3\text{Hz})$  was considered equivalent to  $m_{bLg}$  for purposes of estimating  $E[\mathbf{M}]$ .

### **Model for Scaling from $m_b$ to $E[\mathbf{M}]$**

Based on the analyses presented above, the a model for scaling body magnitudes to  $E[\mathbf{M}]$  was developed as follows. A data set of  $m_b$ - $\mathbf{M}$  pairs was created for study region using the following criteria:

- Magnitudes from composite catalogs (e.g., SRA, EPRI, LLL) were assigned a source from one of the primary source catalogs (e.g., WES, GSC) when the reported magnitude was the same.
- Magnitudes with source GSC in the midcontinent area were discarded unless they represent the only reported magnitude for an earthquake.
- Magnitude types  $m_b$ ,  $m_{bLg}$ ,  $M_N$ ,  $m_{Lg(f)}$ , and  $m(3\text{Hz})$  are considered equivalent. However, catalog source designations are retained.

Figure 3.3-19 shows the resulting data set. It was found that if the data below magnitude about  $m_b$  3.5 were removed, then an offset model,  $\mathbf{M} = m_b + C$ , has a better (lower) AIC value; that is, the difference from a slope of unity is not statistically significant. A change in slope can be seen in the data for lower magnitudes. This change may be due to the effects of data truncation or actual changes in the scaling relationships between the two magnitude scales. However, the lower magnitudes are not of primary interest in developing earthquake recurrence relationships for assessing seismic hazard. At the upper end of the magnitude range there is the issue of saturation of the  $m_b$  scale, which has been shown from numerical modeling (e.g., Boore and Atkinson, 1987). Truncation of the data set to remove magnitudes above  $m_b$  6 resulted in little change to the value of  $C$  or the statistical significance of a departure from a slope of unity.

The data from the GSC were then analyzed to identify the best year for the transition in scaling, which was found to be 1997. A similar analysis was performed to identify the best year for a transition in scaling in the WES data, which was found to be 1982. Differences in scaling between the earthquakes in the midcontinent region and the GSC catalog and earthquakes in the midcontinent and the WES catalog (post-1982) were both found to be statistically significant with a difference of about 0.1 magnitude units. The difference in scaling between GSC and WES data after 1982 and before 1997 was found to be only 0.02 units and is not statistically different from zero. It is difficult to determine if the difference between scaling in the northeastern United States applies only to the WES catalog or to both WES and LDO, but the limited data that can be attributed to LDO show no clear difference from the WES catalog (Figure 3.3-15), and the LDO magnitudes were assumed to be equivalent to the WES. The resulting form of the scaling relationship is

$$E[\mathbf{M}] = m_b - 0.316 - 0.118Z_{NE} - 0.192Z_{1997GSC} + 0.280Z_{1982NE}$$

$$\sigma_{M|mb} = 0.24$$

where  $Z_{NE}$  is 1 for earthquakes located in the northeast (northeast of the dashed line on Figure 3.3-16 including GSC data) and 0 otherwise;

$Z_{1997GSC}$  is 1 for earthquakes occurring after 1997 recorded by the GSC and 0 otherwise;  
and

$Z_{1982NE}$  is 1 for earthquakes occurring in the Northeast prior to 1982 recorded by other than the GSC and 0 otherwise.

The value of  $\sigma_{M|mb} = 0.24$  reflects the value of 0.29 obtained from regression reduced by the average value of  $\sigma[\mathbf{M}|\hat{\mathbf{M}}] = 0.16$  for the earthquakes used in the regression (Equation 3.3.1-8).

A test of the model that accounts for a difference between the long-period spectral estimates of  $\mathbf{M}$  and the corrected approximate values of  $\mathbf{M}$  found a statistically insignificant difference of 0.02 magnitude units.

Examination of the residuals indicated that there is more scatter (larger variance) for the data prior to 1980 than for the data after 1980. The ratio of the variances, 1.6, is statistically significant using an F-test. However, use of variance weighted regression produces only about 0.01 unit magnitude differences in the scaling relationships and even less in the  $N^*$  corrections. Therefore, the variance weighted results were not used.

#### 3.3.2.4 Estimation of $E[\mathbf{M}]$ from $M_L$ Magnitudes

Local magnitudes,  $M_L$ , are reported by a number of agencies. These magnitudes were calibrated by the various agencies to correspond to the original local magnitude definition given by Richter (1935). Figure 3.3-20 shows the spatial distribution of earthquakes with reported instrumental  $M_L$  magnitude of 3 and larger in the project catalog. There are a number of earthquakes in the region offshore of Canada. These are  $M_{L(Sb)}$  magnitudes (J. Adams, pers. comm., 2011) that may need different conversion relationships than the onshore  $M_L$  data. However, they occur primarily outside of the CEUS SSC model study region and are not analyzed further. Figure 3.3-21 shows the spatial distribution of earthquakes that have both  $M_L$  and  $\mathbf{M}$  magnitudes in the project catalog. The spatial distribution of the  $M_L$ - $\mathbf{M}$  pairs is limited and is insufficient to examine regional or catalog differences in  $M_L$  to  $\mathbf{M}$  scaling in the CEUS directly.

Figure 3.3-22 shows the  $M_L$ - $\mathbf{M}$  data set. The data for the two offshore Canada earthquakes fall within the distribution of the other data. The data for the two earthquakes in the western part of the study region also lie within the distribution of the other data. Shown on the figure are the relationships developed by Johnston (1996a) and Miao and Langston (2007). The trend of the data on Figure 3.3-22 displays the typical flattening of slope at the lower magnitudes. To minimize the influence of this flattening on the estimation of  $\mathbf{M}$  in the range of interest, the data below  $M_L$  3.5 were not used in fitting the model. The presence of a few outlying data points suggests the use of robust regression and the resulting fitted linear model is shown.

The data shown on Figure 3.3-22 suggest that for the larger  $M_L$  values, the slope of the  $M_L$ - $\mathbf{M}$  relationship may approach 1. Herrmann and Nuttli (1982) report that  $M_L$  and  $m_{bLg}$  values are nearly equal in the western United States. Kim (1998) found that  $M_L$  and  $m_{bLg}$  were nearly equal for earthquakes in eastern North America. This suggests that the better defined  $m_b$  to  $\mathbf{M}$  scaling might be used for the  $M_L$  data.

Figure 3.3-23 compares  $M_N$  and  $M_L$  magnitudes reported by the GSC. For  $M_N \geq 3$ , the data are well fit by the relationship  $M_L = M_N + 0.21$ , with a standard error of 0.30. Robust regression was used because the observed scatter suggests possible outliers in the data. However, ordinary least squares produced only a 0.02 magnitude unit difference in the offset factor and a small increase in the standard error to 0.34. Also shown on Figure 3.3-23 is the relationship developed by Kim (1998). The difference between the results shown for the GSC data and the Kim (1998) relationship may be due to the fact that Kim (1998) used PDE  $m_{bLg}$  magnitudes and computed  $M_L$ , while the data shown on Figure 3.3-23 are based on the reported GSC magnitudes from the project catalog. The data shown on Figure 3.3-23 indicate that the GSC  $M_L$  magnitudes can be converted to  $E[M]$  by subtracting 0.21 magnitude units and then using the  $M_N$  to  $M$  conversion, with an increase in standard error to account for the additional step. This would bring the standard error to a value of 0.42, similar to that for the fitted relationship shown on Figure 3.3-22.

The  $M_L$  data from the remaining portion of the study region require variable treatment. Figure 3.3-24 shows the data for earthquakes in the northeastern portion of the study region with reported  $M_L$  magnitudes and either  $M_C$  or  $M_D$  magnitudes from catalog sources other than the GSC. There are two  $M_D$  values reported by CERI in this region, the largest being for the 1983/10/07 earthquake. Analysis of the data above  $M_C$  or  $M_D$  values of 2.5 indicates that on the average  $M_L$  is equivalent to  $M_C$  or  $M_D$ , although with considerable scatter. As will be shown in Section 3.3.2.6, there is a large sample with which to estimate the  $M_C$  to  $M$  scaling. Figure 3.3-25 shows the data for earthquakes in the northeastern portion of the study region with  $M$  magnitudes a  $M_L$  magnitude from sources other than the GSC. Shown on the figure is the relationship developed in Section 3.3.2.6 for converting  $M_C$  to  $M$ . Testing of the difference between the observed values of  $M$  and those predicted assuming  $M_L$  equivalent to  $M_C$  showed no statistically significant difference. For  $M_L \geq 2.5$ , the mean offset (using robust estimation) is  $0.11 \pm 0.06$  and for  $M_L \geq 3$  the mean offset is  $-0.06 \pm 0.08$ . Therefore, in the northeastern portion of the study region,  $M_L$  magnitudes were converted using the  $M_C$  conversion relationship, with an increased standard error of 0.46 to account for the larger scatter in the data compared to that for the  $M_C$ - $M$  data.

As shown on Figure 3.3-20, only a few earthquakes outside of the northeastern portion of the study region have reported  $M_L$  and  $M$  magnitudes. Therefore, scaling relationships for  $M_L$  magnitudes in this portion of the study region were based on correlation of  $M_L$  with other magnitude scales. The two principal examples are as follows:

- The  $M_L$  magnitudes reported by SCSN are equivalent to the  $M_C$  magnitudes reported by SCSN.
- The  $M_L$  magnitudes reported by ANSS in the vicinity of New Madrid are equivalent (with minor exception) to the  $M_D$  magnitudes reported by CERI for  $M_D \geq 3$ .

### 3.3.2.5 Estimation of $E[M]$ from $M_S$ Magnitudes

Surface wave magnitudes,  $M_S$ , are computed from the amplitude of low frequency ( $< 0.1$  Hz) surface waves. Figure 3.3-26 shows the spatial distribution of earthquakes with  $M_S$  magnitude of 3 and larger in the project catalog. Figure 3.3-27 shows the  $M_S$ - $M$  data set. Also shown on Figure 3.3-27 is the quadratic relationship developed by Johnston (1996a). This relationship was developed using larger magnitudes and does not extrapolate well into the magnitude range of the

CEUS SSC data set. A quadratic polynomial was fit to the data. Figure 3.3-27 shows the fitted model, the 90% confidence interval of the mean, and the 90% prediction interval. At  $M_S > 5$ , the fitted model is very similar to the Johnston (1996a) global model. The resulting conversion relationship is

$$E[\mathbf{M}] = 2.654 + 0.334M_S + 0.040M_S^2$$

$$\sigma_{\mathbf{M}|M_S} = 0.20$$

The value of  $\sigma_{\mathbf{M}|M_S} = 0.20$  reflects the value of 0.24 obtained from regression reduced by the average value of  $\sigma[\mathbf{M}|\hat{\mathbf{M}}] = 0.13$  for the earthquakes used in the regression (Equation 3.3.1-8).

### 3.3.2.6 Estimation of $E[\mathbf{M}]$ from $M_C$ and $M_D$ Magnitudes

The coda magnitude scale,  $M_C$ , and the duration magnitude scale,  $M_D$ , are based on correlations of the length of the seismic signal and earthquake size measured in other magnitude scales, typically  $m_b$  or  $M_L$ . They are typically applied to smaller magnitude earthquakes. The spatial distribution of earthquakes with  $M_C$  magnitudes  $\geq 2.5$  in the project catalog is shown on Figure 3.3-28. These include many earthquakes with magnitude type labeled “UNK” in the LDO catalog that appear to be  $M_C$  magnitudes based on values reported by other agencies. The major sources of data are the WES, LDO, and Southeastern United States (SEUS) networks. The spatial distribution of earthquakes with  $M_C$  magnitudes  $\geq 2.5$  and  $\mathbf{M}$  magnitudes are shown on Figure 3.3-29. The data are only sufficient for estimating the scaling of  $M_C$  to  $\mathbf{M}$  in the northeastern portion of the study region, predominantly magnitudes reported by WES and LDO.

Figure 3.3-30 shows the spatial distribution of earthquakes with  $M_D$  magnitude of 3 and larger in the project catalog. The major sources of data are the CERI, SEUS, OKO, and SNM (Sanford et al., 2002) networks. The spatial distribution of earthquakes with both  $M_D$  and  $\mathbf{M}$  magnitudes is shown on Figure 3.3-31. These data indicate that direct comparisons between  $M_D$  and  $\mathbf{M}$  magnitudes are limited primarily to data from CERI in the midcontinent portion of the study region and to data from WES and LDO in the northeastern portion of the study region.

#### *Scaling to $E[\mathbf{M}]$ for the Northeastern Portion of the Study Region*

Figure 3.3-32 shows the  $M_C$ - $\mathbf{M}$  data set. Testing for differences in scaling between the WES and LDO sources found no statistically significant differences. This was true both assuming that the LDO “UNK” magnitudes are  $M_C$  from that source and using only the magnitudes actually labeled  $M_C$ . The green symbols indicate the few  $M_D$  magnitudes that differ from the reported  $M_C$  magnitudes for the same event. These data points fall well within the mass of the data, consistent with assuming that  $M_C$  and  $M_D$  magnitudes can be considered equivalent in the northeastern portion of the study region. Testing indicated that a linear fit to the data with slope less than 1 provided a better fit than an offset model. Tests for outliers gave conflicting results that suggest that one may be present. However, a robust regression fit to the data produced nearly the same regression coefficients. Therefore, the ordinary least-squares result was used. The resulting model is

$$E[\mathbf{M}] = 0.633 + 0.806M_C$$

$$\sigma_{\mathbf{M}|M_C} = 0.27$$

The value of  $\sigma_{M|MC} = 0.27$  reflects the value of 0.31 obtained from regression reduced by the average value of  $\sigma[M|\hat{M}] = 0.15$  for the earthquakes used in the regression (Equation 3.3.1-8).

### ***Scaling in Midcontinent East of Longitude 100°W***

As indicated on Figures 3.3-29 and 3.3-31, the spatial distribution of  $M_C$ - $M$  magnitude pairs and  $M_D$ - $M$  magnitude pairs is limited. The possibility of combining the two magnitude measures was examined by comparing  $M_C$  and  $M_D$  magnitudes across the study region. Figure 3.3-33 shows the spatial distributions of the data sets investigated.

Figures 3.3-34, 3.3-35, 3.3-36, 3.3-37, and 3.3-38 compare the  $M_C$  and  $M_D$  magnitudes for each data set shown on Figure 3.3-33. Figure 3.3-34 compares  $M_C$  and  $M_D$  magnitudes for earthquakes with magnitude values coming from either the WES or LDO catalog. The data indicates that these two scales can be considered equivalent in the northeastern portion of the study region.

Figure 3.3-35 shows that the  $M_C$  or  $M_D$  magnitudes reported in the OKO catalog are essentially equivalent to values of  $M_C$  or  $M_D$  reported in other catalogs. Figures 3.3-36 and 3.3-37 show similar comparisons for the CERI and SCSN catalogs, respectively. Figure 3.3-38 shows the comparison for other catalog sources. In all cases,  $M_C$  and  $M_D$  can be considered essentially equivalent for magnitudes above about 2.5. Note that there is only one earthquake west of longitude 100°W that can be used to compare magnitudes.

Figure 3.3-39 shows the data set for  $M_D$  and  $M$  magnitudes for the midcontinent portion of the study region. Also shown on the figure are the limited data for  $M_C$ - $M$  and  $M_L$ - $M$  pairs for the same region. These data are generally consistent with the  $M_D$ - $M$  data. In addition, the relationship developed by Miao and Langston (2007) between  $M_L$  and  $M$  is plotted. The Miao and Langston relationship is also consistent with the data. A linear regression was performed of data larger than magnitude 2.9, resulting in the relationship shown by the red curves on Figure 3.3-39. Inclusion of differences between  $M_C$ ,  $M_D$ , and  $M_L$  did not produce a statistically significant improvement in the fit. The resulting relationship is

$$E[M] = 0.869 + 0.762 (M_C, M_D, \text{ or } M_L)$$

$$\sigma_{M|MC} = 0.25$$

The value of  $\sigma_{M|MD} = 0.25$  reflects the value of 0.28 obtained from regression reduced by the average value of  $\sigma[M|\hat{M}] = 0.11$  for the earthquakes used in the regression (Equation 3.3.1-8).

### ***Scaling in the Region Between Longitudes 105°W and 100°W***

The portion of the study region between longitudes 105°W and 100°W has very few earthquakes with reported moment magnitudes. Figures 3.3-40, 3.3-41, and 3.3-42 compare the various magnitude scales for earthquakes in this region contained in the CEUS SSC Project catalog. These comparisons indicate that  $m_b$  correlates fairly well with the other magnitude scales, except for  $M_L$  prior to 1970 (the events on Figure 3.3-41 prior to 1970 occurred after 1960). Therefore, the  $m_b$ - $M$  scaling relationship was applied to scale those events in the region of longitude 105°W to 100°W when only  $M_C$ ,  $M_D$ , or  $M_L$  magnitudes were available.

### 3.3.2.7 Estimation of E[**M**] from the Logarithm of Felt Area

Figure 3.3-43 shows the spatial distribution of earthquakes in the project catalog with reported values of  $\ln(\text{FA})$ , where FA is felt area measured in  $\text{km}^2$ . The red symbols denote those earthquakes that also have a reported value of **M**. The point located offshore Newfoundland is the 1929 Grand Banks earthquake.

Figure 3.3-44 shows the  $\ln(\text{FA})$ -**M** data from the project catalog. The form of the relationship used to fit the data was that proposed by Frankel (1994) based on theoretical grounds. This form was used by Johnston (1996b) to fit data from a worldwide database of SCR earthquakes. The Johnston (1996b) relationship, shown on Figure 48, is generally consistent with the data from the project catalog.

The data were trimmed below  $\ln(\text{FA}) = 8.5$  to limit the effects of sample truncation at low magnitude values. The resulting relationship is shown by the red curves on Figure 3.3-44. Trimming the data at larger values of  $\ln(\text{FA})$  produced greater differences between the fitted model and the Johnston (1996b) relationship.

The data set used to develop the model included the  $\ln(\text{FA})$  value for the 1929 Grand Banks earthquake. The fact that this earthquake occurred offshore increases the uncertainty in estimation of the felt area. Removal of the earthquake from the data set produced a small reduction in the predicted magnitudes for large felt area of about 0.2 magnitude units, less than one standard deviation in the prediction for a single earthquake. The data from this earthquake were used by Johnston (1996b) and are used to develop the model for used for the CEUS SSC Project. The fitted model is

$$E[\mathbf{M}] = 1.41 + 0.218 \times \ln(\text{FA}) + 0.00087\sqrt{\text{FA}}$$

$$\sigma_{\mathbf{M}|\ln(\text{FA})} = 0.22$$

The value of  $\sigma_{\mathbf{M}|\ln(\text{FA})} = 0.22$  reflects the value of 0.29 obtained from regression reduced by the average value of  $\sigma[\mathbf{M}|\hat{\mathbf{M}}] = 0.185$  for the earthquakes used in the regression (Equation 3.3.1-8).

Note that the standard error is comparable to the estimation of **M** from  $m_b$ .

A *t*-test of the difference between the project data and the Johnston (1996b) predictions for  $\ln(\text{FA}) \geq 10$  (the region where Johnston's data lie) showed a statistically significant difference from zero, indicating that the above relationship provides a better fit to the CEUS project data than the Johnston (1996b) relationship.

### 3.3.2.8 Estimation of E[**M**] from the Maximum Intensity, $I_0$

The size measure available for most pre-instrumental earthquakes is maximum shaking intensity,  $I_0$ , predominately reported in the MMI scale. Figure 3.3-45 shows the spatial distribution of earthquakes in the project catalog with reported values of maximum intensity,  $I_0$ , which is assumed to be epicentral intensity. The red symbols denote those earthquakes that also have a reported value of **M**. The blue symbols denote offshore earthquakes where the assessment of  $I_0$  is problematic. The offshore earthquakes were not used in the development of the  $I_0$  to E[**M**] scaling.

Figure 3.3-46 shows the  $I_0$ - $M$  data from the project catalog. The red curves show a locally weighted least-squares (Loess) fit to the CEUS data, treating the  $I_0$  values as numeric quantities. The blue dashed curve shows the relationship derived by Johnston (1996b) from a worldwide data set of SCR earthquakes consisting primarily of values for  $I_0$  of V and larger. The Johnston (1996b) relationship overpredicts the value of  $M$  derived from the CEUS data set for intensities values between IV and VII.

The Loess fit to the CEUS data shows a pronounced change in slope at about  $I_0$  equal to V. Similar changes in scaling have been observed previously in developing relationships between  $I_0$  and  $m_b$ . Figure 3.3-47 shows the  $I_0$  and  $m_b$  data pairs from the NCEER-91 catalog (Seeber and Armbruster, 1991), together with the relationships between  $I_0$  and  $m_b$  developed by the EPRI-SOG project (EPRI, 1988) and Sibol et al. (1987). EPRI-SOG (EPRI, 1988) proposed that a linear fit was adequate for the intensity range of interest, although the observed data for  $I_0$  III fall generally above the fitted relationship. Sibol et al. (1987) proposed a variety of fits, including the nonparametric fits to the data for individual intensity classes shown on Figure 3.3-47. The Sibol et al. (1987) nonparametric fits were used by Seeber and Armbruster (1991) to develop the intensity-based magnitude estimates in the NCEER-91 catalog.

The departure from a linear  $I_0$ -magnitude relationship is much less pronounced for the  $m_b$  magnitude data shown on Figure 3.3-47 than for the  $M$  data shown on Figure 3.3-46, particularly at  $m_b$  values of 3 and larger that have been used to develop earthquake occurrence relationships by EPRI-SOG (EPRI, 1988) and by the USGS (e.g., Petersen et al., 2008). Therefore, the nonlinearity likely has had minimal effect on the estimation of seismicity parameters. However, the stronger departure from linear scaling observed for the  $I_0$ - $M$  pairs, coupled with the incorporation of uncertainty in magnitude estimates through the use of  $M^*$  or  $N^*$  adjustments, produced significant departures from exponential behavior in initial estimates of earthquake recurrence rates as a function of magnitude as well as possible overestimation of magnitudes from small intensities. The change in scaling slope may be due to inherent nonlinearity in the  $I_0$ - $M$  relationship, or it may be affected by truncation in the observed data at the lower magnitude and intensity levels. Truncation of the data is likely on the magnitude axis because of the limited number of small values of  $M$  reported in the literature and in various catalogs. Truncation of the data is likely on the intensity axis because of the lack of intensity reporting for recent earthquakes in earthquake catalogs and the limited felt areas of small earthquakes.

In order to investigate the possible effects of magnitude truncation on the scaling, the  $I_0$ - $M$  data were analyzed in reverse order (i.e.,  $I_0$  is estimated a function of  $M$ ). Figure 3.3-48 shows the data from Figure 3.3-46 plotted with  $M$  as the independent variable. The value of  $I_0$  as a function of  $M$  can be considered as a categorical response, one that falls into discrete categories. For the intensity data, the categories are ordered. One method of modeling ordered categorical responses is the proportional odds model (e.g., Fox, 2002), which provides the probability of a response being in the individual classes as a function of the predictor variables. This is a generalization of the logistic model for dichotomous (0-1) response variables. The result of fitting the model is a relationship between  $M$  and the probability of observing a specific category of  $I_0$ . Figure 3.3-49 shows examples of these relationships from fits to the data shown on Figure 3.3-48. The magnitude at which the maximum probability is obtained for each intensity class is shown by the red circles on Figure 3.3-48. These results indicate an approximately linear relationship between the value of  $M$  that maximizes the probability of observing a particular intensity class and the nominal intensity class value for  $M$  3 and greater and  $I_0$  IV and greater.

The proportional odds model imposes the requirement that the logistic models for each intensity class differ only by their intercepts; that is, they have the same coefficient applied to magnitude. A less restrictive model is the multinomial logit model, in which the order of the categories is not important. Applying this model produces the values of  $\mathbf{M}$  that maximize the probability of observing a particular intensity class shown by the blue diamonds on Figure 3.3-48. These results are more scattered at the edges of the data as the model parameters are less restricted by the functional form. However, the multinomial results also suggest an approximately linear trend over the same range as the proportional odds model. Based on these results it is concluded that a linear relationship between  $I_0$  and  $\mathbf{M}$  is appropriate for the CEUS SSC catalog data, at least for  $I_0$  above IV.

Initial analysis of the  $I_0$ - $\mathbf{M}$  data produced scaling relationships that appeared inconsistent with published relationships between  $I_0$  and  $m_b$  and the relationships between  $m_b$  and  $\mathbf{M}$  developed here, suggesting a possible bias in the data sample. Figure 3.3-50 shows the data from the project catalog for earthquakes with reported values of  $I_0$  and  $m_b$  ( $m_b$ ,  $m_{bLg}$ ,  $M_N$ ,  $m_{Lg(f)}$ ). The solid circles indicate those earthquakes that also have a value of  $\mathbf{M}$ . The blue and red curves show locally weighed least-squares (Loess) fits to the entire data set and only those earthquakes with reported values of  $\mathbf{M}$ , respectively. As can be seen, there is an offset in the fit for the subset of earthquakes with reported values of  $\mathbf{M}$  compared to the fit of the larger data set. Also shown on Figure 3.3-50 are the relationships between  $I_0$  and  $m_b$  developed by EPRI (1988) and Sibol et al. (1987).

As discussed above, linear relationship between  $I_0$  and magnitude is appropriate in the magnitude range of interest for this study. Figure 3.3-51 shows a linear least-squares fit to the data for values of  $I_0 \geq V$ . Again, the subset with  $\mathbf{M}$  shows an offset in the scaling relationship compared to that obtained for the full  $I_0$ - $m_b$  data set. Figures 3.3-52 and 3.3-53 show the effect of repeating the analysis using values of  $m_b$  adjusted for differences in  $m_b$  to  $\mathbf{M}$  scaling found in Section 3.3.2.3. These results show the same effect as the analysis of the reported  $m_b$  values without adjustment.

To address the apparent bias in the sample of earthquakes with just  $I_0$  and  $\mathbf{M}$  data, the regression data set was augmented with the much larger data set of earthquakes, with  $I_0$  and  $m_b$  using  $\mathbf{M}$  estimated from  $m_b$  for those earthquakes without values of  $\mathbf{M}$ . However, the effect of the underlying exponential distribution in earthquake sizes needs to be accounted for in mixing the data from earthquakes with values of  $\mathbf{M}$  with data where  $\mathbf{M}$  is estimated from  $m_b$ . The reported values of moment magnitude are designated  $\hat{\mathbf{M}}$  to indicate that they are measured with uncertainty. As described in Section 3.3.1, regression of  $\mathbf{M}$  versus  $m_b$  produces the estimate  $E[\mathbf{M}]$ . Equation 3.3.1-5 shows that adjusting the values of  $E[\mathbf{M}|m_b]$  to be consistent with  $\hat{\mathbf{M}}$  requires addition of the factor  $\beta \sigma^2[\mathbf{M}|m_b]$ . Using the value of  $\sigma^2[\mathbf{M}|m_b]$  of 0.24 found in Section 3.3.2.3 and a  $b$ -value of 0.95 (the value typically obtained from analysis of the catalog), the estimated values of  $E[\mathbf{M}|m_b]$  were adjusted upward by 0.12 magnitude units before combining with the  $\hat{\mathbf{M}}$  data set.

Figure 3.3-54 shows the resulting composite data set used to estimate the  $I_0$  to  $\mathbf{M}$  conversion. Plotted on the figure is a locally weighted least-squares (Loess) fit to the data. Also plotted are the relationships of EPRI (1988) and Sibol et al. (1987) shifted by an average  $m_b$  to  $\mathbf{M}$  factor of

–0.32. The fit to the  $I_0$ - $\mathbf{M}$  data is now consistent with past models for the relationship between  $I_0$  and  $m_b$  and the relationship between  $m_b$  and  $\mathbf{M}$  found in this study.

The Loess model fit indicates a break in slope between  $I_0$  IV and V, consistent with the indication that a linear relationship between  $I_0$  and  $\mathbf{M}$  is appropriate for larger intensity values. Therefore, the data set was trimmed to remove  $I_0 \leq IV$ . Figure 3.3-55 shows a linear fit to the data for  $I_0 > IV$ . Although there is large scatter, tests of the residuals using the method of Grubbs (1950) did not indicate the presence of outliers in the data set. In addition, a robust regression produces a relatively small reduction in standard error from 0.56 to 0.49. The linear model has a slope of 2/3.

Cavallini and Rebez (1996) propose that a linear model is not appropriate for relating  $I_0$  to magnitude over the entire range because  $I_0$  is bounded; in particular, as magnitude increases,  $I_0$  is limited to a maximum of XII. They propose instead the use of an inverse sigmoid curve, which is represented by the inverse of the error function (Erf) and the function form:

$$M = C_1 + C_2 \sqrt{2} \text{Erf}^{-1} \left[ \frac{I_0}{6} - 1 \right] \quad (3.3.2-1)$$

The model represented by Equation 3.3.2-1 was also fit to the data, with the result of a very slight improvement in the fit. However, one issue with the form specified by Cavallini and Rebez (1996) is that it does not allow for  $I_0$  to reach its maximum of XII. There are insufficient data in the project catalog with which to define an appropriate shape at the upper end. In order to allow for  $I_0$  equal to XII, Equation 3.3.2-1 was modified to the following form:

$$M = C_1 + C_2 \sqrt{2} \text{Erf}^{-1} \left[ \frac{(I_0 - 6)}{6.5} \right] \quad (3.3.2-2)$$

The fit of Equation 3.3.2-2 to the project data is shown on Figure 3.3-55. The fit is essentially identical to the linear model over most of the range of the data, and is slightly better at the upper end. The inverse sigmoid model has a slightly lower AIC value.

The resulting linear model is

$$\begin{aligned} E[\mathbf{M}] &= 0.017 + 0.666I_0 \\ \sigma_{\mathbf{M}|I_0} &= 0.50 \end{aligned}$$

and the inverse sigmoid model is

$$\begin{aligned} E[\mathbf{M}] &= 4.008 + 3.411 \times \sqrt{2} \text{Erf}^{-1} \left[ \frac{(I_0 - 6)}{6.5} \right] \\ \sigma_{\mathbf{M}|I_0} &= 0.50 \end{aligned}$$

The value of  $\sigma_{\mathbf{M}|I_0} = 0.50$  reflects the value of 0.56 obtained from regression reduced by the average value of  $\sigma[\mathbf{M}|\hat{\mathbf{M}}] = 0.25$  for the earthquakes used in the regression (Equation 3.3.1-8), which includes the estimates of  $\mathbf{M}$  from  $m_b$ .

F-tests for unequal variances at  $I_0$  values above and below  $I_0$  VI and above and below  $I_0$  VII found no statistically significant differences.

Another issue with the form proposed by Cavallini and Rebez (1996) occurs at the lower end of the intensity scale. An assigned intensity value of  $I_0 = I$  means the event was too small to be felt, but this does not require an extremely small negative magnitude. For this project the differences between the linear and inverse sigmoid fit are insignificant over most of the  $I_0$  range of interest. Therefore, the linear fit was used for  $I_0 \leq VI$  and the inverse sigmoid fit was used for  $I_0 > VI$ .

### 3.3.2.9 Uniform Moment Magnitude Catalog of $E[\mathbf{M}]$ and $N^*$ Values

As described in Section 3.3.1, the uniform magnitude measure used in the CEUS SSC earthquake catalog is  $E[\mathbf{M}]$ , the expected value of moment magnitude given its uncertainty in estimation. The hierarchy of estimates used to develop this size measure is as follows:

1. If an estimate of moment magnitude from assessment of the long-period amplitude of the source spectrum is available (e.g., a Harvard Centroid Moment Tensor solution), then it is used as the only size measure. The estimate is designated  $\hat{\mathbf{M}}$  to indicate that it is measured with uncertainty. This is consistent with the approach used to develop the EPRI-SOG catalog and is based on the assumption that a direct estimate of moment magnitude is greatly preferred over one estimated from other size measures.
2. Special studies of larger pre-instrumental earthquakes have derived estimates of  $\mathbf{M}$  from the area of isoseismals (e.g., Johnston et al., 1994; Johnston, 1996b) or from the intensity field and its fall-off with distance (e.g., Bakun and Hopper, 2004b; Bakun et al., 2003). If these are available for an earthquake, then they are preferred over estimates developed from the regressions against intensity measures developed in this study. Moment magnitude estimates based on use of isoseismal areas given in Johnston et al. (1994) and Johnston (1996b) were used, as the Johnston et al. (1994) relationships between felt area and  $\mathbf{M}$  are consistent with the project catalog data, and the use of multiple isoseismal areas is considered preferable to the use of just felt area. However, moment magnitudes given in Johnston et al. (1994) based on conversion from  $I_0$  were not used because the conversion relationships developed for the CEUS SSC Project are considered more appropriate for moderate-sized earthquakes in the CEUS than the relationships developed by Johnston et al. (1994) and Johnston (1996b) from worldwide  $I_0$  data.
3. Approximate moment magnitudes from the studies of Atkinson (2004a, 2004b), Boatwright (1994), and Moulis (2002) provide estimates of  $\mathbf{M}$ . These are treated as estimates of  $\mathbf{M}$  from size measure  $X$  with its associated uncertainty and are combined with estimates from other size measures.
4. For the majority of earthquakes, the values of  $E[\mathbf{M}]$  are based on other size measures,  $\mathbf{X}$ . These include other magnitude scales and the macroseismic values of  $\ln(\text{FA})$  or  $I_0$ . The estimates from the available size measures  $\mathbf{X}$  are combined using the variance weighted approach of Equations 3.3.1-9 and 3.3.1-10.

The values of  $E[\mathbf{M}]$  and  $\sigma[\mathbf{M}]$  obtained for each earthquake are given in the project catalog listed in Appendix B, Table B-1. Using the values of  $\sigma[\mathbf{M}]$  and a  $b$ -value of 0.95 determined from initial analysis of the catalog, values of the equivalent counts  $N^*$  are computed using Equation 3.3.1-12. These values are also listed in the project catalog (Table B-1).

### 3.4 Identification of Independent Earthquakes

The PSHA formulation typically used to model the occurrence of distributed seismicity is based on the Poisson model for the occurrence of independent earthquakes. Therefore, dependent earthquakes (foreshocks and aftershocks) must be identified and not included in the earthquake statistics used to develop estimates of earthquake recurrence rates. This process is referred to as catalog declustering. There are several techniques in use for the identification of dependent earthquakes. One of the first methods to be developed was that proposed by Gardner and Knopoff (1974), in which all smaller earthquakes within a fixed time and distance window around a larger earthquake are classified as dependent earthquakes. Gardner and Knopoff (1974) developed estimates of the size of the time and distance windows as a function of earthquake magnitude from analyses of Southern California earthquakes. Their approach and time and distance windows are widely used and form the basis for the identification of dependent earthquakes in the earthquake catalog used by the USGS for seismic hazard mapping in the CEUS (Petersen et al., 2008). Other applications of this approach have developed alternative criteria for the magnitude-dependent time and distance windows of foreshock and aftershock sequences, such as those developed by Grünthal (1985) for central Europe earthquakes.

Another approach was developed by Reasenber (1985) based on fitting an Omori aftershock decay model to earthquakes in the space-time vicinity of a larger earthquake to define the length of an aftershock sequence. Again, all earthquakes that occur within a fitted aftershock sequence are identified as dependent earthquakes.

EPRI-SOG (EPRI, 1988, Vol. 1) developed a somewhat different approach for identification of dependent earthquakes involving the use of statistical testing to identify clusters of earthquakes. The basic concept is illustrated on Figure 3.4-1. The earthquake catalog is analyzed starting with the largest earthquake and proceeding to the smallest. In the vicinity of an earthquake selected from this ordered sequence, two space-time windows are constructed according to user specified criteria. The first is a local window,  $W_l$ , in the immediate vicinity of the selected earthquake with space-time volume  $V_l$ . The second is a much larger extended window,  $W_e$ , with volume  $V_e$ . The local and extended windows contain observed earthquake counts of  $n_l$  and  $n_e$ , respectively. Assuming that the occurrence of earthquakes in the space-time vicinity of the earthquake being tested is a stationary Poisson process with unknown intensity parameter  $\mu$ , then the random counts of earthquakes in each window,  $N_l$ , and  $N_e$ , would have expected values proportional to the volume of each window,  $\mu V_l$  and  $\mu V_e$ , respectively. The null hypothesis that there is no elevated seismicity in the space-time vicinity of the earthquake being tested is given by

$$H_0 : \frac{E[N_l]}{V_l} = \frac{E[N_e]}{V_e} \quad (3.4-1)$$

The alternative hypothesis that the earthquake intensity  $\mu$  is higher in the local window (i.e., there is local clustering in space and time) is given by

$$H_1 : \frac{E[N_l]}{V_l} > \frac{E[N_e]}{V_e} \quad (3.4-2)$$

Citing Lehmann (1959), EPRI (1988, Vol. 1) indicates that under the null hypothesis  $H_0$  and assuming that the expected value of  $N_e$  equals the observed value  $n_e$ , the hypothesis can be tested assuming that the number of earthquakes in the local window  $N_l$  had a binomial distribution with  $n_e$  trials and probability of success  $p = V_l/V_e$ . The distribution for  $N_l$  is given by

$$P(N_l = n_l | N_e = n_e) = \binom{n_e}{n_l} p^{n_l} (1-p)^{n_e - n_l} \quad (3.4-3)$$

The hypothesis  $H_0$  is rejected when  $n_l$  exceeds the rejection limit  $n_l^R$  given by

$$n_l^R = \min \{ n \text{ for which } P(N_l > n | N_e = n_e) \leq \alpha \} \quad (3.4-4)$$

where  $\alpha$  is a suitable low significance level. A value of 0.02 is recommended for  $\alpha$  in EPRI (1988, Vol. 3).

Parts (b) and (c) of Figure 3.4.1 illustrate two additional tests performed if the null hypothesis is not rejected. Part (b) applies to the case where a local cluster extends outside the initial local window  $W_l$  such that the counts affect the estimated background rate in the extended window. A buffer around the local window is defined,  $W_b$ , and the volume and earthquake counts within the buffer are removed. The test of  $H_0$  is then performed comparing the number of earthquakes within the local volume to the rate estimated from the extended window without the buffer region. Part (c) applies to the case where the cluster is too small (in time and/or space) to be observed within the initial local space-time window. A contraction factor is applied to the local window parameters to construct a smaller local window and the test is repeated.

If the null hypothesis is rejected, then the procedure moves to identifying the extent of the local cluster. This is accomplished by testing adjacent space and time windows around the local window for clustering by comparing the counts in these adjacent portions with the counts in the extended window  $W_e$ , ignoring those earthquakes already identified as a cluster. The process is continued until no additional space-time segments are identified that reject the null hypothesis.

The final step is illustrated on Figure 3.4-2. The EPRI (1988) procedure does not classify all earthquakes within the identified space-time window of the cluster as secondary (dependent) earthquakes. Instead, it uses a process of thinning the earthquake counts in the cluster region to the point where the intensity matches the background rate in the extended window  $W_e$ . This is accomplished by simulating a Poisson process within the cluster region using the background intensity  $\mu$ . These simulated earthquakes are illustrated by the pluses in the top plot on Figure 3.4-2. The nearest neighbor among the recorded earthquakes to each simulated earthquake is identified as a primary earthquake (i.e., main shock). All the rest are then identified as secondary (dependent) earthquakes. The result is a space-time pattern of earthquakes that is consistent with the background rate, as shown in the bottom plot of Figure 3.4-2.

After the first pass through the earthquake catalog, the process is repeated for a second iteration with the secondary earthquakes identified in the first pass removed. It is suggested in EPRI (1988, Vol. 3) that two iterations are typically all that are needed.

The advantages of the EPRI (1988) approach are that it is insensitive to incompleteness, as a homogeneous Poisson process is only assumed in the general vicinity of the earthquake sequence being tested (the extended window  $W_e$ ) and it does not assume a priori a shape for the clusters.

Testing during its development on synthetic catalogs generated by a Poisson process showed that it retained nearly all earthquakes as independent occurrences (Van Dyck, 1986).

Figure 3.4-3 shows the results of application of the EPRI (1988) declustering approach to the CEUS SSC catalog. The EPRI-SOG (EPRI, 1988) computer program EQCLUSTER was used for the calculations. The data points represent the length in days of individual clusters and the maximum distance between earthquakes assigned to a cluster and the identified mainshock. The red dashed lines indicate the average values as a function of  $E[M]$ . The blue dashed lines indicate the starting values for cluster size used in the declustering algorithm. These were taken from EPRI (1988), adjusting for the conversion from  $m_b$  to  $E[M]$ . Shown for comparison are the time and distance windows developed by Gardner and Knopoff (1974) for Southern California earthquakes and by Grünthal (1985) for central Europe earthquakes. The Gardner and Knopoff (1974) time windows shown are their published aftershock time windows multiplied by 1.5 to add a foreshock window based on the difference between the Grünthal (1985) aftershock and foreshock time windows. It should be noted that the time and distance windows developed by Gardner and Knopoff (1974) and Grünthal (1985) represent optimized envelopes to their observations. The average spatial dimension of the clusters identified in the project catalog is less than the published distance window envelopes, and the average time length of a cluster is comparable to the published envelope values. The EPRI (1988) procedure does identify some clusters that have a much longer duration than the published time windows.

In order to provide a comparison of the effect of alternative declustering approaches, the Gardner and Knopoff (1974) method was applied to the CEUS SSC catalog using the computer program CAT3E developed by Dr. Charles Mueller at the USGS for use in earthquake catalog processing for seismic hazard estimation. Table 3.4-1 compares the results of the two methods in terms of the number of independent earthquakes in various magnitude intervals. The two methods produce very similar results, with the overall difference in the number of independent earthquakes being about 1.5 percent. The largest difference is the numbers in the  $E[M]$  2.9 to 3.6 magnitude bin, but this difference is only 4.4 percent. Thus, it is concluded that the use of the alternative Gardner and Knopoff (1974) declustering approach would not have a significant effect on earthquake recurrence rates computed from the declustered catalog.

The dependent earthquakes identified with the EPRI (1988) procedure are indicated in the earthquake catalog listed in Appendix B, Table B-1.

### 3.5 Catalog Completeness

The assessment of earthquake catalog completeness is necessary in order to prevent underestimation of earthquake recurrence rates. One approach is to evaluate the detection capability of seismic networks as a function of time on the basis of density of stations and type of instrumentation. An example is McLaughlin et al.'s (1997) analysis of the capability of the U.S. National Seismic Network (USNSN). However, the more common approach is the use of the general technique first proposed by Stepp (1972). This approach evaluates the catalog completeness for specific magnitude ranges by starting at the present and moving back in time and counting the total number of earthquakes in the catalog in each magnitude interval. At each point in time when an earthquake in the specified magnitude interval occurred, the rate of earthquakes in the magnitude interval is computed by dividing the sum of the number of earthquakes from that point in time to the end of the catalog by the length in time from that point

to the end of the catalog. Assuming that the rate of earthquakes is constant in time, plotting these values versus date for the complete portion of the catalog will show an approximately horizontal line. As one moves further back in time, eventually the plotted line will start to trend downward, indicating that not all earthquakes are being reported (again assuming stationarity in time of the true rate). The point at which this downward trend begins indicates the beginning of the complete period of catalog reporting for the specific magnitude interval. These plots are sometimes referred to as “Stepp” plots, after their originator.

A common practice is to use this technique to identify the period of complete catalog reporting for each magnitude interval and then use only the data from that portion of the catalog to assess earthquake recurrence parameters. The length of catalog completeness is typically a function of magnitude, with larger magnitudes having longer completeness periods. The data identified in this way would be used to assess recurrence parameters using a procedure such as Weichert’s (1980) maximum likelihood formulation for binned magnitude data.

Using only the complete portion of the catalog may be quite satisfactory where the change in slope on a Stepp plot can be clearly defined and often may correspond to known seismic network changes. However, in regions with a long history of earthquake reporting through felt effects, there may be a long gradual decline in the level of completeness. Ignoring the data from the partially complete period may mean discarding information that is important to the assessment of seismic hazards.

The EPRI-SOG Project (EPRI, 1988, Vol. 1) developed an approach for incorporating the catalog data in the partially complete period into the assessment of earthquake recurrence parameters. Assuming that earthquakes in magnitude interval  $i$  occur as a constant Poisson process in time with rate  $\lambda_i$ , then the expected number of earthquakes to have occurred during the period of complete reporting  $T_i^C$  for magnitude interval  $i$  is equal to  $\lambda_i T_i^C$ . The maximum likelihood estimator for  $\lambda_i$  is given by

$$\lambda_i = \frac{N_i^C}{T_i^C} \quad (3.5-1)$$

where  $N_i^C$  is the number of earthquakes in magnitude interval  $i$  observed during the period of complete recording  $T_i^C$ . EPRI (1988) extended this concept into the period of incomplete recording. A parameter called the probability of detection,  $P^D$ , was defined that represented the probability that an earthquake in any point in time would be recorded and would appear in the seismic record. Again under the assumption of a stationary Poisson process, the expected number of earthquakes that would be observed in any time interval  $T_j$  is given by the expression

$$E[N_{ij}] = \lambda_i \times T_j \times P^D(m_i, T_j, X) \quad (3.5-2)$$

where  $E[N_{ij}]$  is the expected number of earthquakes and  $P^D(m_i, T_j, X)$  is the average probability of detection of earthquakes in magnitude interval  $m_i$  during time period  $T_j$  and over spatial locations  $X$ . Assessment of the rate parameter  $\lambda_i$  requires knowledge of  $P^D$ . If one assumes that the larger magnitudes are complete at present, and imposes the constraints that  $P^D$  should decrease more or less monotonically with increasing time into the past and should increase monotonically with magnitude at each point in time, then—again invoking stationarity—the parameters  $\lambda_i$  and  $P^D$  can be estimated jointly from the earthquake catalog data. Considering only

a single magnitude interval and ignoring the spatial aspect for the moment, the likelihood function for the observed number of earthquakes over the total duration of the catalog is given by

$$L = \prod_j \frac{(\lambda_i P_{ij}^D T_j)^{N_{ij}} \exp(-\lambda_i P_{ij}^D T_j)}{N_{ij}!} \quad (3.5-3)$$

where  $P_{ij}^D$  is a shortened notation for  $P^D(m_i, T_j)$ . The maximum likelihood solution for  $\lambda_i$  becomes

$$\lambda_i = \frac{\sum_j N_{ij}}{\sum_j P_{ij}^D T_j} \quad (3.5-4)$$

If the values of  $P_{ij}^D$  are known (or have been estimated previously), then the term in the denominator of Equation 3.5-4 can be replaced by what is called the effective period of completeness,  $T_{ij}^E$ , given by the expression

$$T_{ij}^E = \sum_j P_{ij}^D T_j \quad (3.5-5)$$

The maximum likelihood estimator of  $\lambda_i$  becomes equal to the total number of earthquakes in the catalog in magnitude interval  $i$  divided by the effective period of completeness for that magnitude interval.

EPRI (1988) developed an approach to jointly estimate the recurrence parameters that define  $\lambda_i$  and its spatial variability along with  $P^D(m_i, T_j, X)$ . The approach is termed penalized likelihood and is described in detail in Section 5.3.2, along with refinements developed for the CEUS SSC Project. The original formulation assessed earthquake recurrence parameters and  $P^D(m_i, T_j, X)$  using a one-degree-longitude-by-one-degree-latitude discretization of the CEUS. While the enhancements of the methodology presented in Section 5.3.2 extend the methodology to smaller cell sizes, the original discretization is sufficient for the estimation of the probability of detection, as it is not expected to vary rapidly spatially across the CEUS. The original formulation as implemented in the EPRI-SOG program EQPARAM (EPRI, 1988, Vol. 3) was used to perform the assessment of  $P^D(m_i, T_j, X)$ . The program was modified to use the concept of  $N^*$  by changing the counting of earthquakes to the summing of the  $N^*$  values.

Through analysis of the history of population growth and earthquake recording, EPRI (1988) defined 13 completeness regions covering most of the CEUS. These regions represent portions of the CEUS where catalog completeness as a function of time and magnitude is assessed to be sufficiently similar such that it can be treated as the same. These completeness regions are shown on Figure 3.5-1 along with the independent earthquakes in the EPRI-SOG earthquake catalog. With the exceptions noted below, the information on the history of population growth and seismic network instrumentation has not changed significantly from what was available in the mid 1980's. Therefore, the EPRI (1988) completeness regions were used for the CEUS SSC Project with some modifications. The revised completeness regions together with the CEUS SSC Project catalog are shown on Figure 3.5-2. The modifications address additional sources of historical earthquakes used in the CEUS SSC Project that modify the history of catalog reporting

used in the EPRI-SOG study, and the extension of the completeness regions to cover the entire SSC model.

Two interior boundary modifications were made. First, the analysis of historical records, principally by Metzger et al. (2000), has extended the catalog coverage in the area around New Madrid. Consequently, the western boundary of Completeness Region 4 was extended to the southwest to incorporate the longer period of reporting in that area into the relatively long period of catalog reporting centered on New Madrid. The second significant change was to Completeness Regions 3 and 12. As shown on Figure 3.5-1, Completeness Region 3 covers both the Midwestern states west of New Madrid and the southern states all the way to eastern Tennessee and northern Georgia. The review of historical documents by various investigations, principally Munsey (2006), has greatly extended the completeness in the eastern portion of Completeness Region 3. Based on discussions with Jeffrey Munsey (pers. comm., 2011), Completeness Region 12 was expanded to cover this area, as the history of newspaper publishing in eastern Tennessee and northern Georgia is more similar to that of the western Carolinas than to the Midwestern states west of New Madrid. Other modifications include combining and extending Completeness Region 11 to cover the area north of the U.S.-Canada border, extending Completeness Region 11 into the northeastern Great Plains, and extending Completeness Region 1 to cover Texas. An additional Completeness Region 14 was added to cover the Gulf of Mexico, as offshore earthquakes in that area are important to the assessment of seismic hazards along the Gulf Coast.

EPRI (1988) defined time periods over which catalog completeness was assessed to be relatively constant. These time periods were 1625–1779, 1780–1859, 1860–1909, 1910–1949, 1950–1974, and post-1974. Figure 3.5-3 shows space-time plots of the independent earthquakes in the CEUS SSC catalog. The red lines denote the boundaries of the time periods defined by EPRI (1988). For the most part, these time periods coincide with changes in the density of recorded earthquakes and were retained for use in estimating completeness for the CEUS SSC catalog. An additional time period of 1995–2008 was added to accommodate the potential for recent improvements in earthquake recording.

More detailed examinations of catalog completeness as a function of time can be made on Figure 3.5-4. Shown are “Stepp” plots for each completeness region. These plots show a long history of earthquake recording in many areas of the CEUS with the typical trend of a gradual decay in completeness with increasing time into the past. These results indicate the importance of using a methodology that allows for the incorporation of most of this history into the assessment of earthquake recurrence rates and their spatial variation across the CEUS.

The catalog completeness analysis and subsequent assessment of earthquake recurrence parameters uses earthquakes binned in magnitude intervals. These magnitude intervals were centered on  $E[M]$  values obtained from conversion of whole-degree values of  $I_0$  to mimic the grouping of the converted magnitudes. These magnitude intervals are 2.9 to 3.6, 3.6 to 4.3, 4.3 to 5.0, 5.0 to 5.7, 5.7 to 6.4, 6.4 to 7.1, and 7.1 and higher.

Following EPRI (1988), the probabilities of detection were calculated using no spatial smoothing on the rate parameter, and medium smoothing on  $b$ , and no prior on  $b$ . As discussed in Section 5.3.2, several analysis cases were performed that assign different weights to the lower magnitude intervals to address potential departures from exponential behavior. These are Case A, full weight on all magnitude intervals; Case B with a reduced weight of 0.1 on the lowest

magnitude interval; and Case E with elimination of the first magnitude interval and 0.3 weight on the second interval.

McLaughlin et al. (1997) analyzed the capability of the USNSN and associated regional networks to detect at least four P waves for each earthquake. The analysis shows that for most of the eastern United States, there is 80 percent probability of detecting earthquakes with  $m_{bLg} = 3.25$ . The detection capability decreases toward the Atlantic Ocean to the east and toward the Gulf of Mexico to the south. The probability of detection is less than 80 percent in parts of southern Indiana, Illinois, and western Kentucky due to the scarcity of stations in the upper Midwest. If the Canadian stations are added to the USNSN, the probabilities increase in the northern United States and southern Canada. During 2004–2006, the USNSN was upgraded and expanded to become the current ANSS backbone national network of nearly 100 stations, and many ANSS regional network stations have been added in the CEUS during the past decade. However, the USNSN analysis still serves as a useful baseline for assessing the level of catalog completeness at the end of the twentieth century.

Based on the results presented in McLaughlin et al. (1997), the earthquake catalog for the study region was assumed complete (probability of detection of 1.0) for all magnitude intervals in the time period 1995–2008 in most of the completeness regions. Locally, the probability of detection of the first two magnitude intervals was calculated, and the results are lower than 1.0.

The estimated probabilities of detection for the magnitude and time intervals are given in Tables 3.5-1, 3.5-2, and 3.5-3 for Cases A, B, and E, respectively.

The final step in the catalog analysis was the computation of regional  $b$ -values for the CEUS. These values were used as prior values to aid in the penalized-likelihood estimation of earthquake recurrence parameters as described in Section 5.3.2. The regional  $b$ -values were computed using the Weichert (1980) formulation, with  $N$  given by the sum of the  $N^*$  values and  $T$  defined as  $T^E$  for each magnitude and completeness region. The calculations were made assuming a homogeneous seismicity rate in each completeness region that was allowed to vary from completeness region to completeness region, but a constant  $b$ -value over the entire CEUS. The following table lists the computed regional  $b$ -values.

Regional  $b$ -Values Assessed for the CEUS SSC Project Catalog

Magnitude Weighting Case	Regional $b$ -value
A	1.02
B	0.99
E	1.00

**Table 3.2-1**  
**Summary of Earthquakes Added–USGS Earthquake Catalog by Time Period**

Time Period	Number of Earthquakes in E[M] Magnitude Range						Total
	2.9–3.6	3.6–4.3	4.3–5.0	5.0–5.7	5.7–6.4	≥6.4	
1558 through 1799	9	6	1	1	0	0	17
1800 through 1899	106	58	23	3	0	0	190
1900 through 1959	40	10	13	5	0	1	69
1960 through 2006	285	27	5	2	0	0	319
2007 and 2008	49	8	3	1	0	0	61

**Table 3.2-2**  
**Summary of Earthquakes Added–USGS Earthquake Catalog by Source**

Source	Number of Earthquakes in E[M] Magnitude Range						Total
	2.9–3.6	3.6–4.3	4.3–5.0	5.0–5.7	5.7–6.4	≥6.4	
Metzger et al. (2000)	20	21	9	2	0	0	52
Munsey (2006)	44	17	11	0	0	0	72
GSC/NEDB and Burke (2009)	44	6	1	2	0	0	53
SUSN only	54	2	2	1	0	0	59
Single source, such as Lamont-Doherty; Ohio Survey; Oklahoma Survey; Reinbold and Johnston (1987); Seeber and Armbruster (1987); Saint Louis University; Weston Observatory; Adams and Simmons (1991); Bent (2003); CERI; Ma and Atkinson (2006); SCSN; Stover and Coffman (1993); Sykes et al. (2008)	70	16	5	1	0	0	92
Contained in multiple other sources	208	39	14	5	0	1	267

**Table 3.3-1**  
**Conversion Relationships Used—Develop Uniform Moment Magnitudes E[M]**

Size Measure	Conversion Relationship	$\sigma[M X]$
Body-wave magnitude ( $m_b$ , $m_{bLg}$ , $m_{Lg(f)}$ , $M_N$ )	$E[M] = m_b - 0.316 - 0.118Z_{NE} - 0.192Z_{1997GSC} + 0.280Z_{1982NE}$ <p><math>Z_{NE} = 1</math> for earthquakes located in the Northeast (northeast of the dashed line on Figure 3.3-16, including GSC data), and 0 otherwise</p> <p><math>Z_{1997GSC} = 1</math> for earthquakes occurring after 1997 recorded by GSC, and 0 otherwise</p> <p><math>Z_{1982NE} = 1</math> for earthquakes occurring in the Northeast before 1982 recorded by other than GSC, and 0 otherwise</p>	0.24
$M_L$ reported by GSC	Compute $m_b = M_L - 0.21$ and use $m_b$ conversion	0.42
$M_S$	$E[M] = 2.654 + 0.334M_S + 0.040M_S^2$	0.20
$M_C$ , $M_D$ , $M_L$ in northeastern United States (other than GSC)	$E[M] = 0.633 + 0.806(M_C, M_D \text{ or } M_L)$	0.27
$M_C$ , $M_D$ , $M_L$ in midcontinent United States east of longitude 100°W	$E[M] = 0.869 + 0.762 (M_C, M_D, \text{ or } M_L)$	0.25
$M_C$ , $M_D$ , $M_L$ in midcontinent United States west of longitude 100°W	Use $m_b$ conversion	0.24
$\ln(FA)$ (in $\text{km}^2$ )	$E[M] = 1.41 + 0.218 \times \ln(FA) + 0.00087\sqrt{FA}$	0.22
$I_0$	<p>for <math>I_0 \leq VI</math></p> $E[M] = 0.017 + 0.666I_0$ <p>for <math>I_0 &gt; VI</math></p> $E[M] = 4.008 + 3.411 \times \sqrt{2} \text{Erf}^{-1} \left[ \frac{(I_0 - 6)}{6.5} \right]$	0.50

**Table 3.4-1**  
**Comparison of CEUS SSC Catalog Declustering Results Obtained Using the EPRI (1988) Approach with the Gardner Knopoff (1974) Approach**

E[M] Magnitude Range	Number of Earthquakes in E[M] Magnitude Range		
	Entire Catalog	Independent Earthquakes Using EPRI (1988) Approach	Independent Earthquakes Using Gardner Knopoff (1974) Approach
2.9–3.6	2333	1787	1865
3.6–4.3	696	554	530
4.3–5.0	204	168	155
5.0–5.7	44	36	33
5.7–6.4	13	13	13
6.4–7.1	4	4	3
7.1–7.8	3	2	0
7.8–8.3	1	1	1

**Table 3.5-1**  
**Probability of Detection and Equivalent Periods of Completeness for the CEUS for**  
**Magnitude Weighting Case A**

Magnitude Interval	Probability of Detection for Time Period							Equivalent period of Completeness, TE (years)	Beginning of Usable Period
	1625–1780	1780–1860	1860–1910	1910–1950	1950–1975	1975–1995	1995–2009		
<b>Region 1</b>									
2.9–3.6	0	0	0	0.141	0.265	0.595	0.673	33.6	1910
3.6–4.3	0	0	0	0.212	0.531	0.595	1	47.7	1910
4.3–5.0	0	0	0	0.212	0.713	0.751	1	55.3	1910
5.0–5.7	0	0	0	0.961	0.961	1	1	96.5	1860
5.7–6.4	0	0	1	1	1	1	1	149.0	1860
6.4–8.3	0	0	1	1	1	1	1	149.0	1860
<b>Region 2</b>									
2.9–3.6	0	0	0.111	0.239	0.391	1	1	58.9	1860
3.6–4.3	0	0	0.181	0.672	1	1	1	94.9	1860
4.3–5.0	0	0	0.261	0.672	1	1	1	98.9	1860
5.0–5.7	0	0	0.261	1	1	1	1	112.1	1860
5.7–6.4	0	0	0.261	1	1	1	1	112.1	1860
6.4–8.3	0	0	0.261	1	1	1	1	112.1	1860
<b>Region 3</b>									
2.9–3.6	0	0	0.08	0.199	0.243	0.859	1	49.2	1860
3.6–4.3	0	0.056	0.381	0.529	0.743	0.859	1	94.4	1780
4.3–5.0	0	0.056	0.977	0.977	0.977	0.977	1	150.4	1780
5.0–5.7	0	0.428	1	1	1	1	1	183.2	1780
5.7–6.4	0	0.428	1	1	1	1	1	183.2	1780
6.4–8.3	0	0.428	1	1	1	1	1	183.2	1780
<b>Region 4</b>									
2.9–3.6	0	0	0.242	0.431	0.449	1	1	74.6	1860
3.6–4.3	0	0.239	0.756	0.756	0.756	1	1	140.1	1780
4.3–5.0	0	0.288	1	1	1	1	1	172.0	1780
5.0–5.7	0	0.56	1	1	1	1	1	193.8	1780
5.7–6.4	0	0.621	1	1	1	1	1	198.7	1780
6.4–8.3	0	0.621	1	1	1	1	1	198.7	1780
<b>Region 5</b>									
2.9–3.6	0	0.072	0.444	0.636	0.839	1	1	108.4	1780
3.6–4.3	0	0.5	0.567	0.788	0.839	1	1	154.8	1780
4.3–5.0	0.345	0.5	1	1	1	1	1	242.5	1625
5.0–5.7	0.345	0.5	1	1	1	1	1	242.5	1625
5.7–6.4	1	1	1	1	1	1	1	384.0	1625
6.4–8.3	1	1	1	1	1	1	1	384.0	1625

Magnitude Interval	Probability of Detection for Time Period							Equivalent period of Completeness, TE (years)	Beginning of Usable Period
	1625–1780	1780–1860	1860–1910	1910–1950	1950–1975	1975–1995	1995–2009		
<b>Region 6</b>									
2.9–3.6	0	0.164	0.735	0.735	1	1	1	138.3	1780
3.6–4.3	0	0.981	0.981	0.981	1	1	1	225.8	1780
4.3–5.0	0.434	1	1	1	1	1	1	296.3	1625
5.0–5.7	0.434	1	1	1	1	1	1	296.3	1625
5.7–6.4	0.434	1	1	1	1	1	1	296.3	1625
6.4–8.3	0.434	1	1	1	1	1	1	296.3	1625
<b>Region 7</b>									
2.9–3.6	0	0	0.185	0.185	0.446	0.635	0.635	49.4	1860
3.6–4.3	0	0	1	1	1	1	1	149.0	1860
4.3–5.0	0	0	1	1	1	1	1	149.0	1860
5.0–5.7	0	0	1	1	1	1	1	149.0	1780
5.7–6.4	0	0.746	1	1	1	1	1	208.7	1780
6.4–8.3	0	0.948	1	1	1	1	1	224.8	1780
<b>Region 8</b>									
2.9–3.6	0	0	0	0	0.38	1	1	43.5	1950
3.6–4.3	0	0	0	0	0.499	1	1	46.5	1950
4.3–5.0	0	0	0	0	1	1	1	59.0	1950
5.0–5.7	0	0	0	0	1	1	1	59.0	1910
5.7–6.4	0	0	0	0	1	1	1	59.0	1910
6.4–8.3	0	0	0	1	1	1	1	99.0	1910
<b>Region 9</b>									
2.9–3.6	0	0	0	0.257	0.543	0.652	0.652	46.0	1910
3.6–4.3	0	0	0.146	0.332	0.932	0.932	1	76.5	1860
4.3–5.0	0	0	0.244	1	1	1	1	111.2	1860
5.0–5.7	0	0	0.244	1	1	1	1	111.2	1860
5.7–6.4	0	0	0.244	1	1	1	1	111.2	1860
6.4–8.3	0	0	0.424	1	1	1	1	120.2	1860
<b>Region 10</b>									
2.9–3.6	0	0	0.107	0.451	0.774	1	1	76.7	1860
3.6–4.3	0	0.045	0.295	1	1	1	1	117.3	1780
4.3–5.0	0	0.49	0.49	1	1	1	1	162.7	1625
5.0–5.7	0	1	1	1	1	1	1	229.0	1625
5.7–6.4	0	1	1	1	1	1	1	229.0	1625
6.4–8.3	0	1	1	1	1	1	1	229.0	1625

Magnitude Interval	Probability of Detection for Time Period							Equivalent period of Completeness, TE (years)	Beginning of Usable Period
	1625–1780	1780–1860	1860–1910	1910–1950	1950–1975	1975–1995	1995–2009		
<b>Region 11</b>									
2.9–3.6	0	0	0	0	0.192	0.371	0.371	17.4	1950
3.6–4.3	0	0	0	0	0.59	0.59	1	40.5	1950
4.3–5.0	0	0	0	0	1	1	1	59.0	1910
5.0–5.7	0	0	0	0	1	1	1	59.0	1910
5.7–6.4	0	0	0	0	1	1	1	59.0	1910
6.4–8.3	0	0	0	0.673	1	1	1	85.9	1910
<b>Region 12</b>									
2.9–3.6	0	0.033	0.224	0.243	0.419	1	1	68.0	1780
3.6–4.3	0	0.109	0.373	0.373	0.926	1	1	99.4	1780
4.3–5.0	0	0.597	1	1	1	1	1	196.8	1625
5.0–5.7	0	1	1	1	1	1	1	229.0	1625
5.7–6.4	0	1	1	1	1	1	1	229.0	1625
6.4–8.3	0	1	1	1	1	1	1	229.0	1625
<b>Region 13</b>									
2.9–3.6	0	0	0.419	0.834	0.834	0.834	1	105.8	1860
3.6–4.3	0	0	0.995	1	1	1	1	148.7	1860
4.3–5.0	0	0	0.995	1	1	1	1	148.7	1860
5.0–5.7	0	0	0.995	1	1	1	1	148.7	1860
5.7–6.4	0	0	0.995	1	1	1	1	148.7	1860
6.4–8.3	0	0	0.995	1	1	1	1	148.7	1860
<b>Region 14</b>									
2.9–3.6	0	0	0	0	0	0	0.505	7.1	1995
3.6–4.3	0	0	0	0	0	0.364	0.505	14.3	1975
4.3–5.0	0	0	0	0	0.901	0.901	1	54.5	1950
5.0–5.7	0	0	0	0	0.901	0.901	1	54.5	1950
5.7–6.4	0	0	0	0	0.901	0.901	1	54.5	1950
6.4–8.3	0	0	0	0	1	1	1	59.0	1950

**Table 3.5-2**  
**Probability of Detection and Equivalent Periods of Completeness for the CEUS for**  
**Magnitude Weighting Case B**

Magnitude Interval	Probability of Detection for Time Period							Equivalent Period of Completeness, TE (years)	Beginning of Usable Period
	1625–1780	1780–1860	1860–1910	1910–1950	1950–1975	1975–1995	1995–2009		
<b>Region 1</b>									
2.9–3.6	0	0	0	0.156	0.292	0.587	0.746	35.7	1910
3.6–4.3	0	0	0	0.218	0.553	0.587	1	48.3	1910
4.3–5.0	0	0	0	0.218	0.697	0.735	1	54.8	1910
5.0–5.7	0	0	0	0.885	0.885	1	1	91.5	1860
5.7–6.4	0	0	1	1	1	1	1	149.0	1860
6.4–8.3	0	0	1	1	1	1	1	149.0	1860
<b>Region 2</b>									
2.9–3.6	0	0	0.109	0.235	0.386	1	1	58.5	1860
3.6–4.3	0	0	0.175	0.651	1	1	1	93.8	1860
4.3–5.0	0	0	0.252	0.651	1	1	1	97.6	1860
5.0–5.7	0	0	0.252	1	1	1	1	111.6	1860
5.7–6.4	0	0	0.252	1	1	1	1	111.6	1860
6.4–8.3	0	0	0.265	1	1	1	1	112.2	1860
<b>Region 3</b>									
2.9–3.6	0	0	0.072	0.178	0.217	0.697	1	44.1	1860
3.6–4.3	0	0.053	0.358	0.496	0.697	0.697	1	87.3	1780
4.3–5.0	0	0.053	0.964	0.964	0.964	0.964	1	148.4	1780
5.0–5.7	0	0.45	1	1	1	1	1	185.0	1780
5.7–6.4	0	0.45	1	1	1	1	1	185.0	1780
6.4–8.3	0	0.45	1	1	1	1	1	185.0	1780
<b>Region 4</b>									
2.9–3.6	0	0	0.201	0.356	0.372	0.735	1	62.3	1860
3.6–4.3	0	0.21	0.663	0.663	0.663	0.735	1	121.7	1780
4.3–5.0	0	0.267	1	1	1	1	1	170.4	1780
5.0–5.7	0	0.547	1	1	1	1	1	192.8	1780
5.7–6.4	0	0.644	1	1	1	1	1	200.5	1780
6.4–8.3	0	0.644	1	1	1	1	1	200.5	1780
<b>Region 5</b>									
2.9–3.6	0	0.078	0.482	0.69	0.958	0.958	1	115.1	1780
3.6–4.3	0	0.525	0.598	0.831	0.958	0.958	1	162.2	1780
4.3–5.0	0.352	0.525	1	1	1	1	1	245.6	1625
5.0–5.7	0.352	0.525	1	1	1	1	1	245.6	1625
5.7–6.4	1	1	1	1	1	1	1	384.0	1625
6.4–8.3	1	1	1	1	1	1	1	384.0	1625

Magnitude Interval	Probability of Detection for Time Period							Equivalent Period of Completeness, TE (years)	Beginning of Usable Period
	1625–1780	1780–1860	1860–1910	1910–1950	1950–1975	1975–1995	1995–2009		
<b>Region 6</b>									
2.9–3.6	0	0.175	0.782	0.782	1	1	1	143.4	1780
3.6–4.3	0	1	1	1	1	1	1	229.0	1780
4.3–5.0	0.438	1	1	1	1	1	1	296.9	1625
5.0–5.7	0.438	1	1	1	1	1	1	296.9	1625
5.7–6.4	0.438	1	1	1	1	1	1	296.9	1625
6.4–8.3	0.438	1	1	1	1	1	1	296.9	1625
<b>Region 7</b>									
2.9–3.6	0	0	0.187	0.187	0.466	0.646	0.646	50.4	1860
3.6–4.3	0	0	1	1	1	1	1	149.0	1860
4.3–5.0	0	0	1	1	1	1	1	149.0	1860
5.0–5.7	0	0	1	1	1	1	1	149.0	1780
5.7–6.4	0	0.72	1	1	1	1	1	206.6	1780
6.4–8.3	0	0.943	1	1	1	1	1	224.4	1780
<b>Region 8</b>									
2.9–3.6	0	0	0	0	0.537	1	1	47.4	1950
3.6–4.3	0	0	0	0	0.61	1	1	49.2	1950
4.3–5.0	0	0	0	0	1	1	1	59.0	1950
5.0–5.7	0	0	0	0	1	1	1	59.0	1910
5.7–6.4	0	0	0	0	1	1	1	59.0	1910
6.4–8.3	0	0	0	1	1	1	1	99.0	1910
<b>Region 9</b>									
2.9–3.6	0	0	0	0.329	0.696	0.834	0.834	58.9	1910
3.6–4.3	0	0	0.165	0.376	1	1	1	82.3	1860
4.3–5.0	0	0	0.24	1	1	1	1	111.0	1860
5.0–5.7	0	0	0.24	1	1	1	1	111.0	1860
5.7–6.4	0	0	0.24	1	1	1	1	111.0	1860
6.4–8.3	0	0	0.24	1	1	1	1	111.0	1860
<b>Region 10</b>									
2.9–3.6	0	0	0.131	0.554	0.949	1	1	86.4	1860
3.6–4.3	0	0.049	0.324	1	1	1	1	119.1	1780
4.3–5.0	0	0.479	0.479	1	1	1	1	161.3	1625
5.0–5.7	0	1	1	1	1	1	1	229.0	1625
5.7–6.4	0	1	1	1	1	1	1	229.0	1625
6.4–8.3	0	1	1	1	1	1	1	229.0	1625

Magnitude Interval	Probability of Detection for Time Period							Equivalent Period of Completeness, TE (years)	Beginning of Usable Period
	1625–1780	1780–1860	1860–1910	1910–1950	1950–1975	1975–1995	1995–2009		
<b>Region 11</b>									
2.9–3.6	0	0	0	0	0.229	0.442	0.442	20.8	1950
3.6–4.3	0	0	0	0	0.673	0.673	1	44.3	1950
4.3–5.0	0	0	0	0	1	1	1	59.0	1910
5.0–5.7	0	0	0	0	1	1	1	59.0	1910
5.7–6.4	0	0	0	0	1	1	1	59.0	1910
6.4–8.3	0	0	0	0.671	1	1	1	85.8	1910
<b>Region 12</b>									
2.9–3.6	0	0.04	0.27	0.293	0.506	1	1	75.1	1780
3.6–4.3	0	0.121	0.415	0.415	1	1	1	106.0	1780
4.3–5.0	0	0.619	1	1	1	1	1	198.5	1625
5.0–5.7	0	1	1	1	1	1	1	229.0	1625
5.7–6.4	0	1	1	1	1	1	1	229.0	1625
6.4–8.3	0	1	1	1	1	1	1	229.0	1625
<b>Region 13</b>									
2.9–3.6	0	0	0.277	0.469	0.552	0.552	1	71.4	1860
3.6–4.3	0	0	0.707	0.707	1	1	1	122.6	1860
4.3–5.0	0	0	0.707	0.707	1	1	1	122.6	1860
5.0–5.7	0	0	0.707	0.707	1	1	1	122.6	1860
5.7–6.4	0	0	0.707	0.86	1	1	1	128.7	1860
6.4–8.3	0	0	0.841	0.961	1	1	1	139.5	1860
<b>Region 14</b>									
2.9–3.6	0	0	0	0	0	0	0.209	2.9	1995
3.6–4.3	0	0	0	0	0	0.209	0.209	7.1	1975
4.3–5.0	0	0	0	0	0.633	0.633	1	42.5	1950
5.0–5.7	0	0	0	0	0.633	0.633	1	42.5	1950
5.7–6.4	0	0	0	0	0.633	0.633	1	42.5	1950
6.4–8.3	0	0	0	0	1	1	1	59.0	1950

**Table 3.5-3**  
**Probability of Detection and Equivalent Periods of Completeness for the CEUS for**  
**Magnitude Weighting Case E**

Magnitude Interval	Probability of Detection for Time Period							Equivalent Period of Completeness, TE (years)	Beginning of Usable Period
	1625–1780	1780–1860	1860–1910	1910–1950	1950–1975	1975–1995	1995–2009		
<b>Region 1</b>									
3.6–4.3	0	0	0	0.168	0.595	0.595	1	47.5	1910
4.3–5.0	0	0	0	0.168	0.743	0.784	1	55.0	1910
5.0–5.7	0	0	0	0.921	0.921	1	1	93.9	1860
5.7–6.4	0	0	1	1	1	1	1	149.0	1860
6.4–8.3	0	0	1	1	1	1	1	149.0	1860
<b>Region 2</b>									
3.6–4.3	0	0	0.177	0.584	1	1	1	91.2	1860
4.3–5.0	0	0	0.255	0.584	1	1	1	95.1	1860
5.0–5.7	0	0	0.255	1	1	1	1	111.7	1860
5.7–6.4	0	0	0.255	1	1	1	1	111.7	1860
6.4–8.3	0	0	0.255	1	1	1	1	111.7	1860
<b>Region 3</b>									
3.6–4.3	0	0.038	0.325	0.451	0.634	0.634	1	79.9	1780
4.3–5.0	0	0.038	0.939	0.939	0.939	0.939	1	143.8	1780
5.0–5.7	0	0.475	1	1	1	1	1	187.0	1780
5.7–6.4	0	0.475	1	1	1	1	1	187.0	1780
6.4–8.3	0	0.475	1	1	1	1	1	187.0	1780
<b>Region 4</b>									
3.6–4.3	0	0.15	0.473	0.473	0.473	0.473	1	89.9	1780
4.3–5.0	0	0.229	1	1	1	1	1	167.3	1780
5.0–5.7	0	0.568	1	1	1	1	1	194.4	1780
5.7–6.4	0	0.845	1	1	1	1	1	216.6	1780
6.4–8.3	0	0.845	1	1	1	1	1	216.6	1780
<b>Region 5</b>									
3.6–4.3	0	0.434	0.562	0.781	0.793	0.793	1	143.7	1780
4.3–5.0	0.324	0.434	1	1	1	1	1	233.9	1625
5.0–5.7	0.324	0.434	1	1	1	1	1	233.9	1625
5.7–6.4	1	1	1	1	1	1	1	384.0	1625
6.4–8.3	1	1	1	1	1	1	1	384.0	1625
<b>Region 6</b>									
3.6–4.3	0	1	1	1	1	1	1	229.0	1780
4.3–5.0	0.432	1	1	1	1	1	1	296.0	1625
5.0–5.7	0.432	1	1	1	1	1	1	296.0	1625
5.7–6.4	0.432	1	1	1	1	1	1	296.0	1625
6.4–8.3	0.432	1	1	1	1	1	1	296.0	1625

Magnitude Interval	Probability of Detection for Time Period							Equivalent Period of Completeness, TE (years)	Beginning of Usable Period
	1625–1780	1780–1860	1860–1910	1910–1950	1950–1975	1975–1995	1995–2009		
<b>Region 7</b>									
3.6–4.3	0	0	1	1	1	1	1	149.0	1860
4.3–5.0	0	0	1	1	1	1	1	149.0	1860
5.0–5.7	0	0	1	1	1	1	1	149.0	1780
5.7–6.4	0	0.681	1	1	1	1	1	203.5	1780
6.4–8.3	0	0.931	1	1	1	1	1	223.5	1780
<b>Region 8</b>									
3.6–4.3	0	0	0	0	0.53	0.628	0.628	34.6	1950
4.3–5.0	0	0	0	0	1	1	1	59.0	1950
5.0–5.7	0	0	0	0	1	1	1	59.0	1910
5.7–6.4	0	0	0	0	1	1	1	59.0	1910
6.4–8.3	0	0	0	1	1	1	1	99.0	1910
<b>Region 9</b>									
3.6–4.3	0	0	0.161	0.365	1	1	1	81.7	1860
4.3–5.0	0	0	0.218	1	1	1	1	109.9	1860
5.0–5.7	0	0	0.218	1	1	1	1	109.9	1860
5.7–6.4	0	0	0.218	1	1	1	1	109.9	1860
6.4–8.3	0	0	0.218	1	1	1	1	109.9	1860
<b>Region 10</b>									
3.6–4.3	0	0.055	0.362	1	1	1	1	121.5	1780
4.3–5.0	0	0.499	0.499	1	1	1	1	163.9	1625
5.0–5.7	0	0.991	1	1	1	1	1	228.3	1625
5.7–6.4	0	0.991	1	1	1	1	1	228.3	1625
6.4–8.3	0	0.991	1	1	1	1	1	228.3	1625
<b>Region 11</b>									
3.6–4.3	0	0	0	0	0.75	0.75	1	47.7	1950
4.3–5.0	0	0	0	0	1	1	1	59.0	1910
5.0–5.7	0	0	0	0	1	1	1	59.0	1910
5.7–6.4	0	0	0	0	1	1	1	59.0	1910
6.4–8.3	0	0	0	0.661	1	1	1	85.4	1910
<b>Region 12</b>									
3.6–4.3	0	0.123	0.422	0.422	1	1	1	106.8	1780
4.3–5.0	0	0.627	1	1	1	1	1	199.2	1625
5.0–5.7	0	1	1	1	1	1	1	229.0	1625
5.7–6.4	0	1	1	1	1	1	1	229.0	1625
6.4–8.3	0	1	1	1	1	1	1	229.0	1625

Magnitude Interval	Probability of Detection for Time Period							Equivalent Period of Completeness, TE (years)	Beginning of Usable Period
	1625–1780	1780–1860	1860–1910	1910–1950	1950–1975	1975–1995	1995–2009		
<b>Region 13</b>									
3.6–4.3	0	0	0.393	0.393	0.779	0.779	1	84.4	1860
4.3–5.0	0	0	0.393	0.393	0.779	0.779	1	84.4	1860
5.0–5.7	0	0	0.393	0.393	0.779	0.779	1	84.4	1860
5.7–6.4	0	0	0.535	0.798	1	1	1	117.7	1860
6.4–8.3	0	0	0.779	0.954	1	1	1	136.1	1860
<b>Region 14</b>									
3.6–4.3	0	0	0	0	0	0.155	0.155	5.3	1975
4.3–5.0	0	0	0	0	0.535	0.535	1	38.1	1950
5.0–5.7	0	0	0	0	0.535	0.535	1	38.1	1950
5.7–6.4	0	0	0	0	0.535	0.535	1	38.1	1950
6.4–8.3	0	0	0	0	1	1	1	59.0	1950

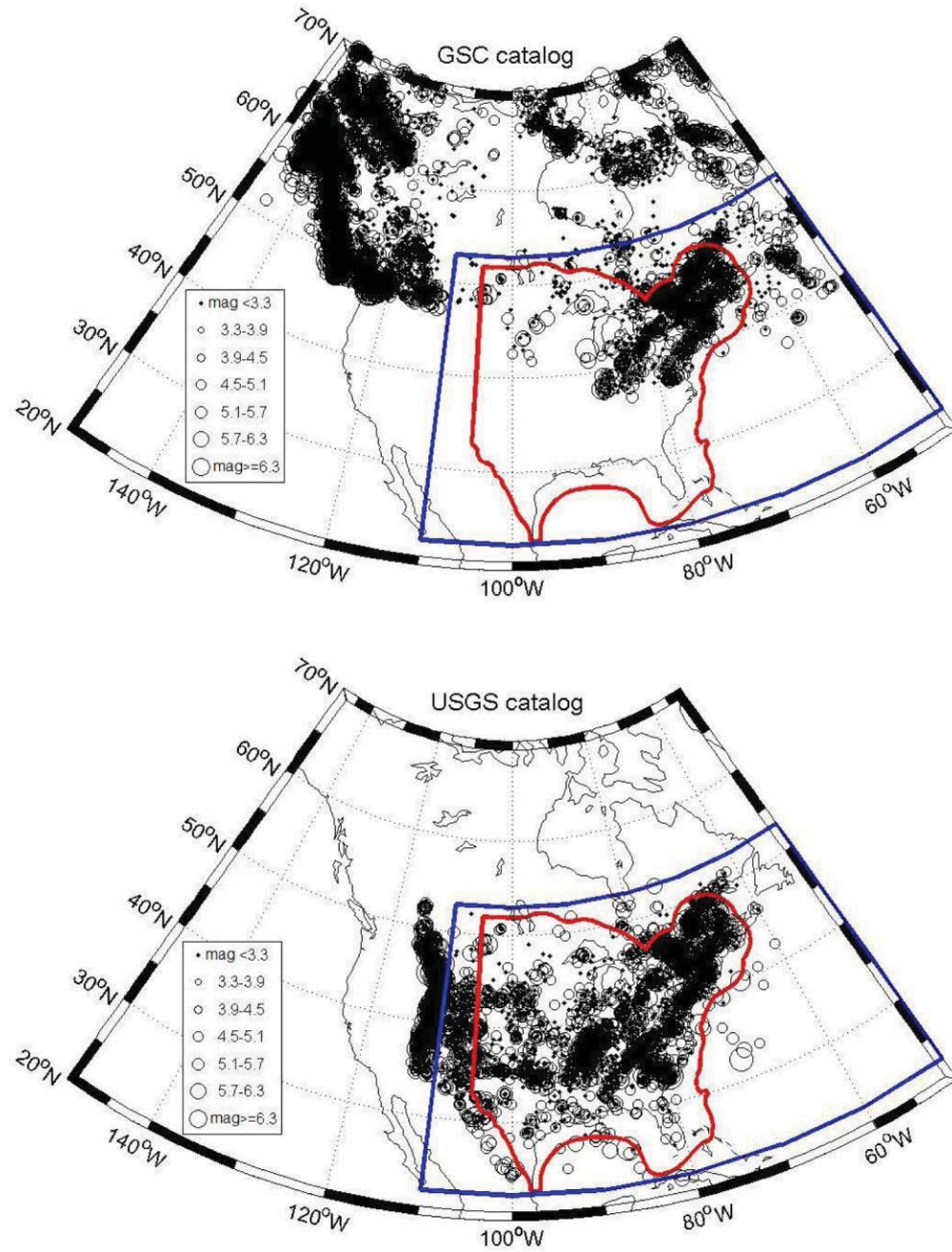


**Figure 3.2-1**  
Areal coverage of the primary earthquake catalog sources. Top: GSC catalog (Halchuk, 2009); bottom: USGS seismic hazard mapping catalog (Petersen et al., 2008). Red line denotes boundary of study region. Blue line denotes portion of each catalog used for development of project catalog.

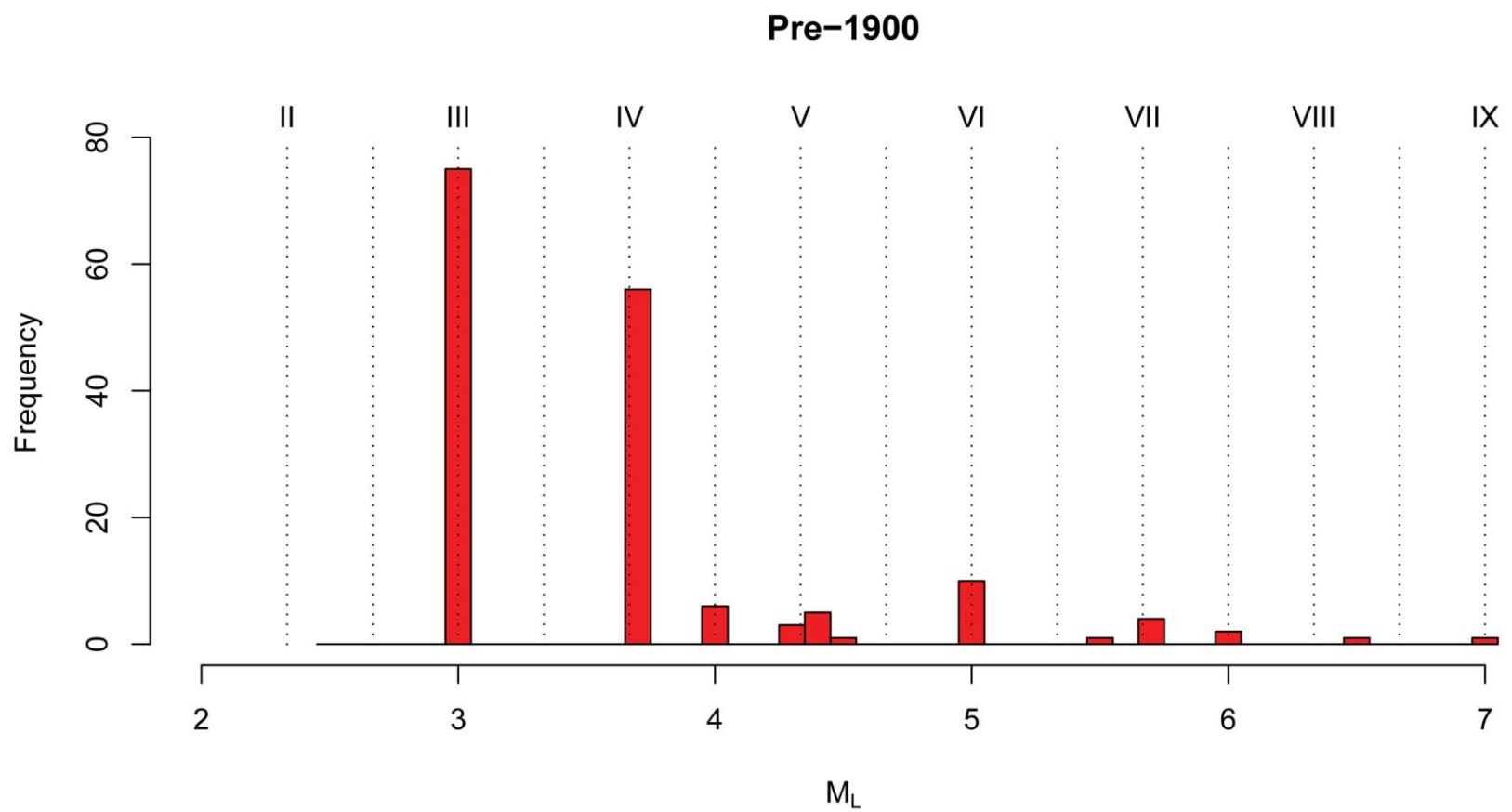


**Figure 3.2-2**  
Histogram of  $M_L$  magnitudes from the GSC SHEEF catalog for the time period 1600-1899 and the region east of longitude  $-105^\circ$  and south of latitude  $53^\circ$

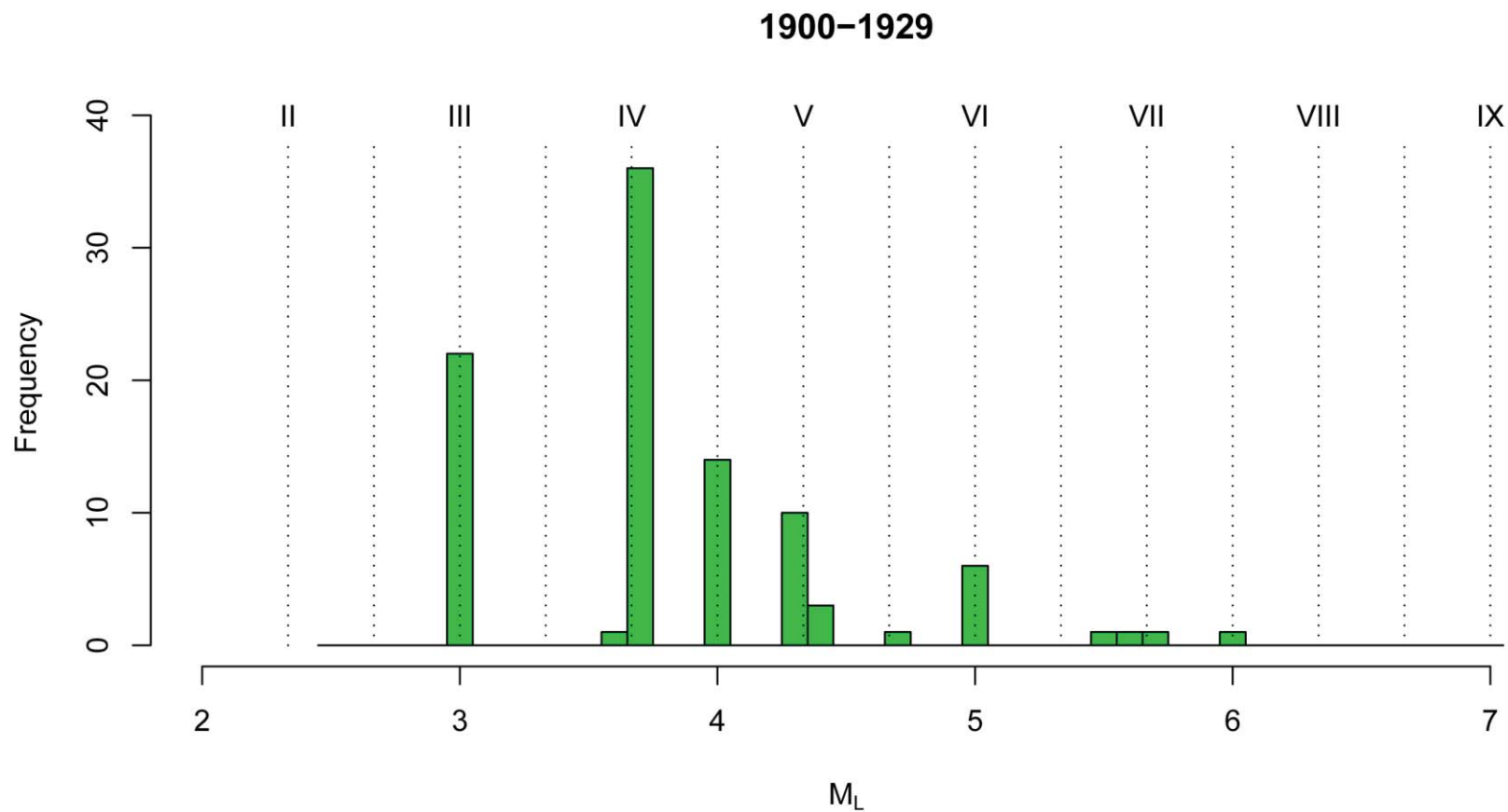


**Figure 3.2-3**  
Histogram of  $M_L$  magnitudes from the GSC SHEEF catalog for the time period 1900-1929 and the region east of longitude  $-105^\circ$  and south of latitude  $53^\circ$

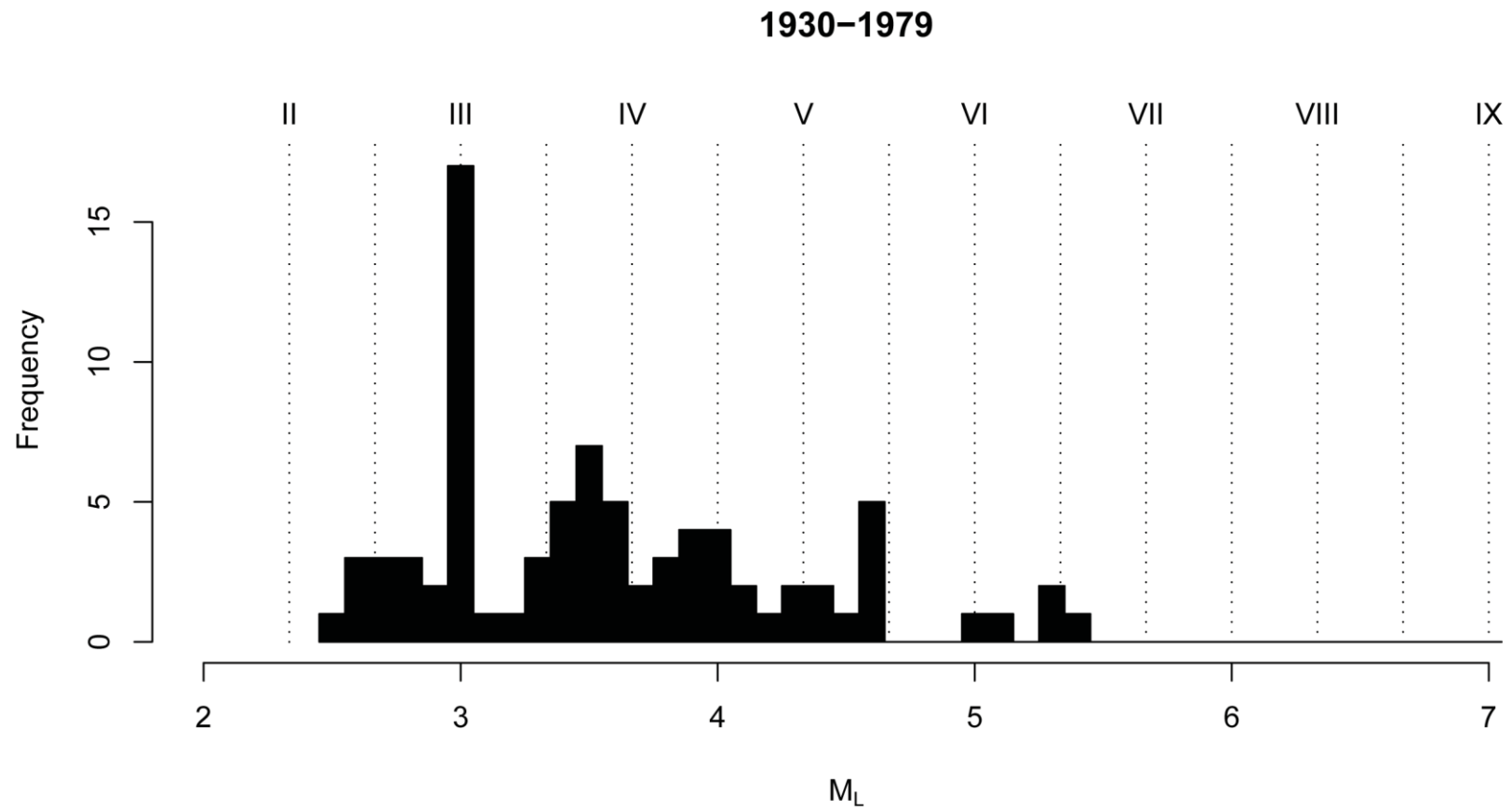


**Figure 3.2-4**  
Histogram of  $M_L$  magnitudes from the GSC SHEEF catalog for the time period 1930-1979 and the region east of longitude  $-105^\circ$  and south of latitude  $53^\circ$

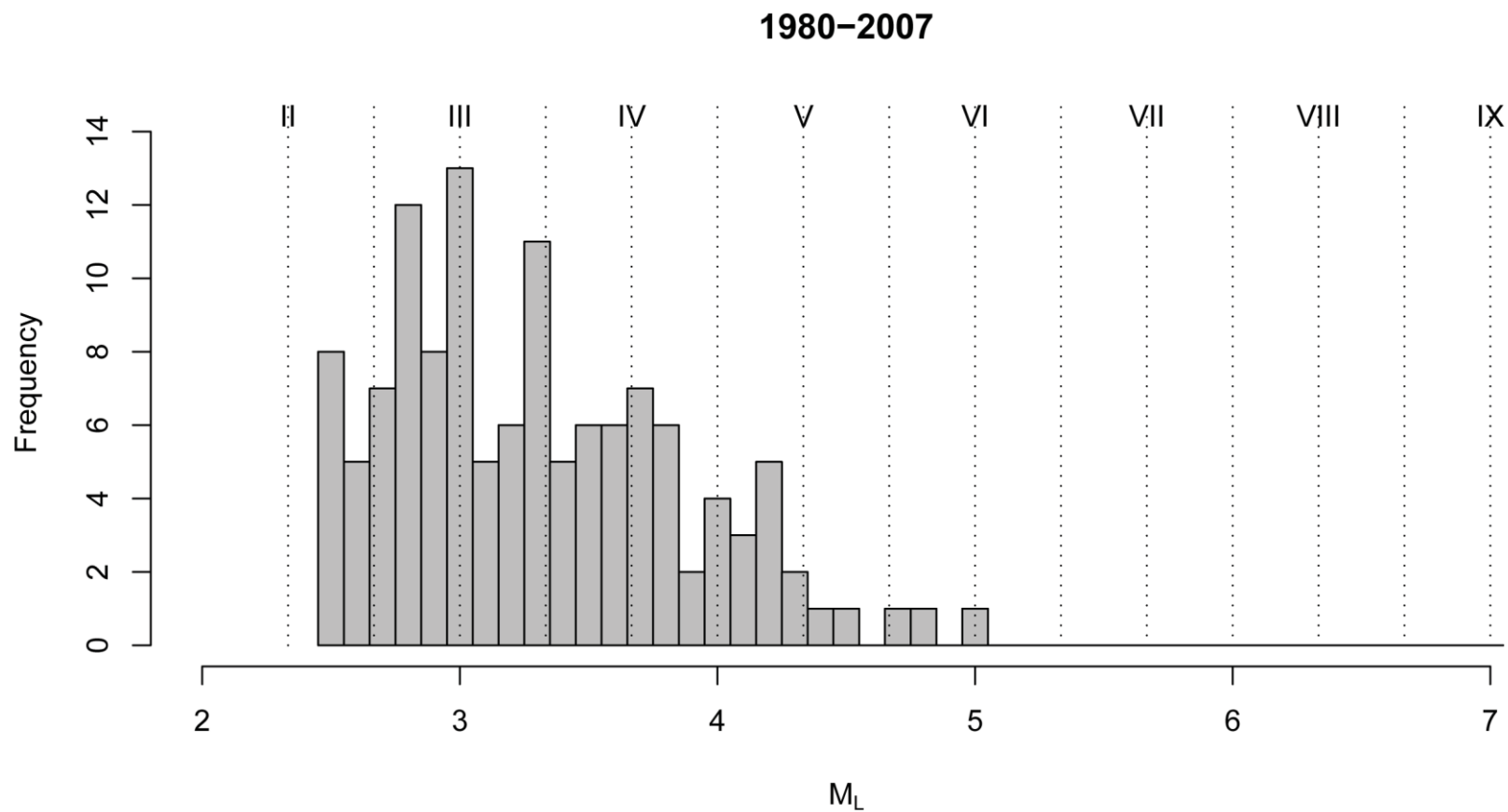


**Figure 3.2-5**  
Histogram of  $M_L$  magnitudes from the GSC SHEEF catalog for the time period 1980-2007 and the region east of longitude  $-105^\circ$  and south of latitude  $53^\circ$

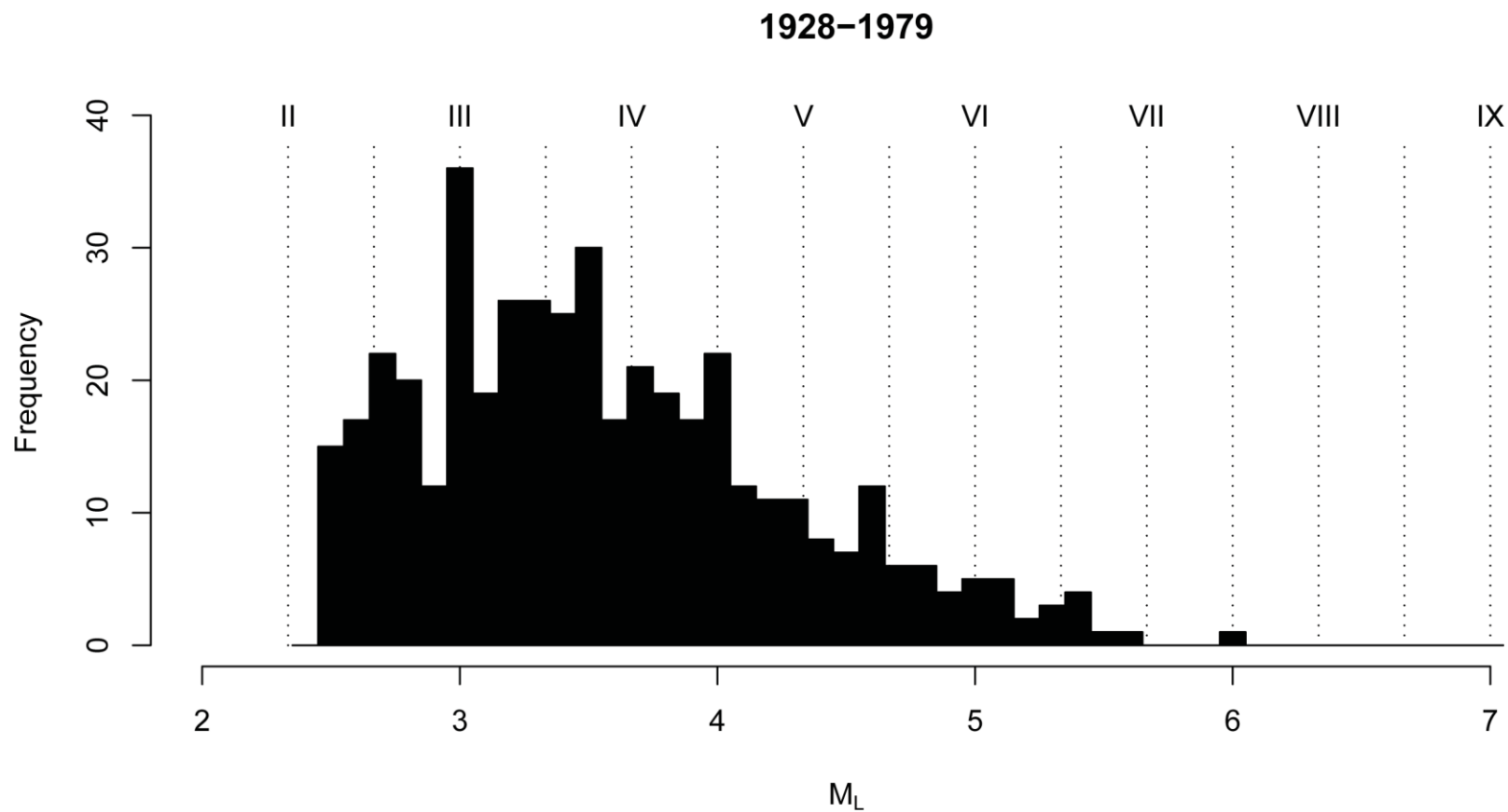


**Figure 3.2-6**  
Histogram of  $M_L$  magnitudes from the revised catalog with GSC as the source for the time period 1928-1979

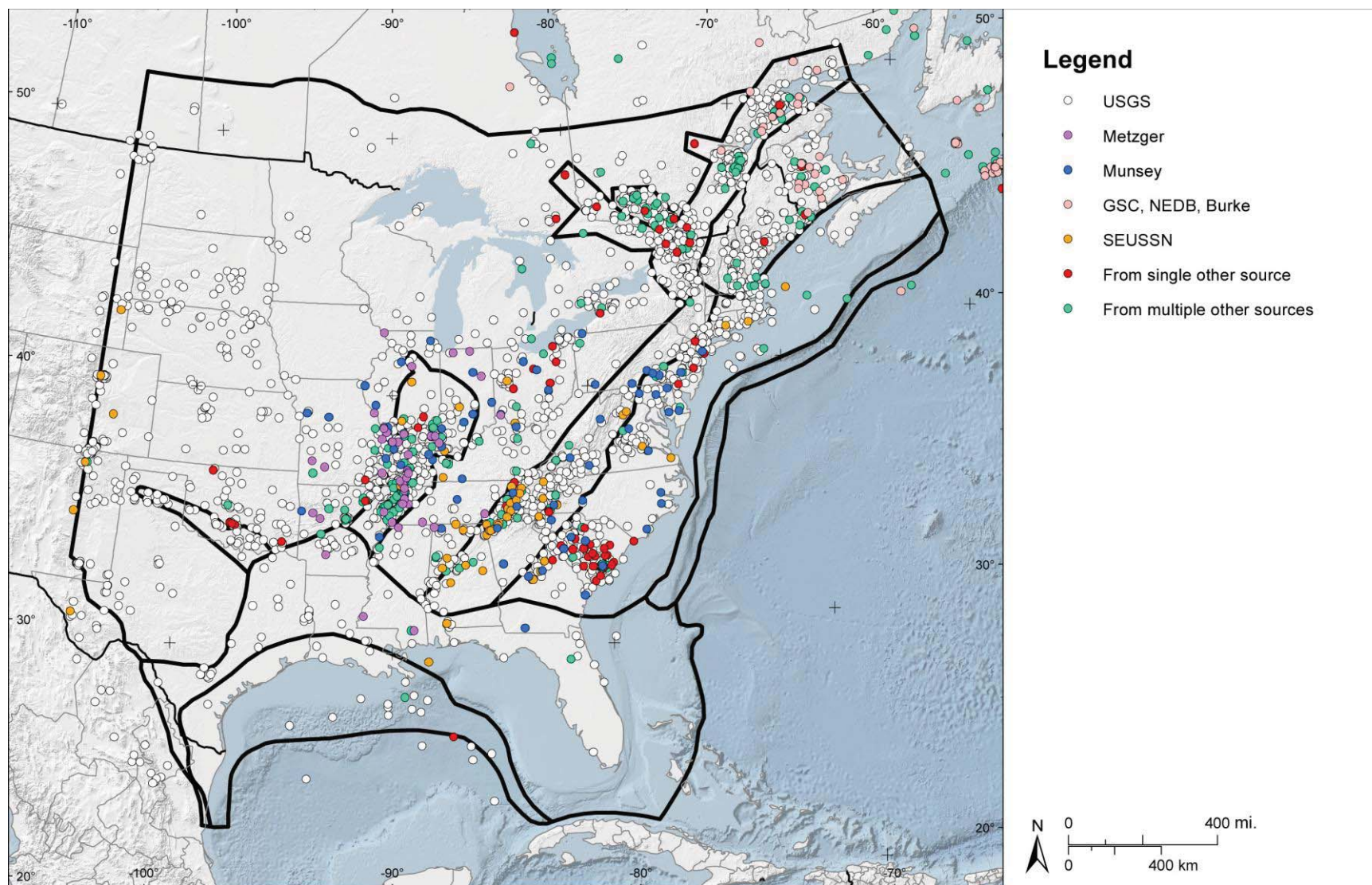


**Figure 3.2-7**  
Map of the CEUS SSC Project catalog showing earthquakes of uniform moment magnitude  $E[M]$  2.9 and larger. Colored symbols denote earthquakes not contained in the USGS seismic hazard mapping catalog.

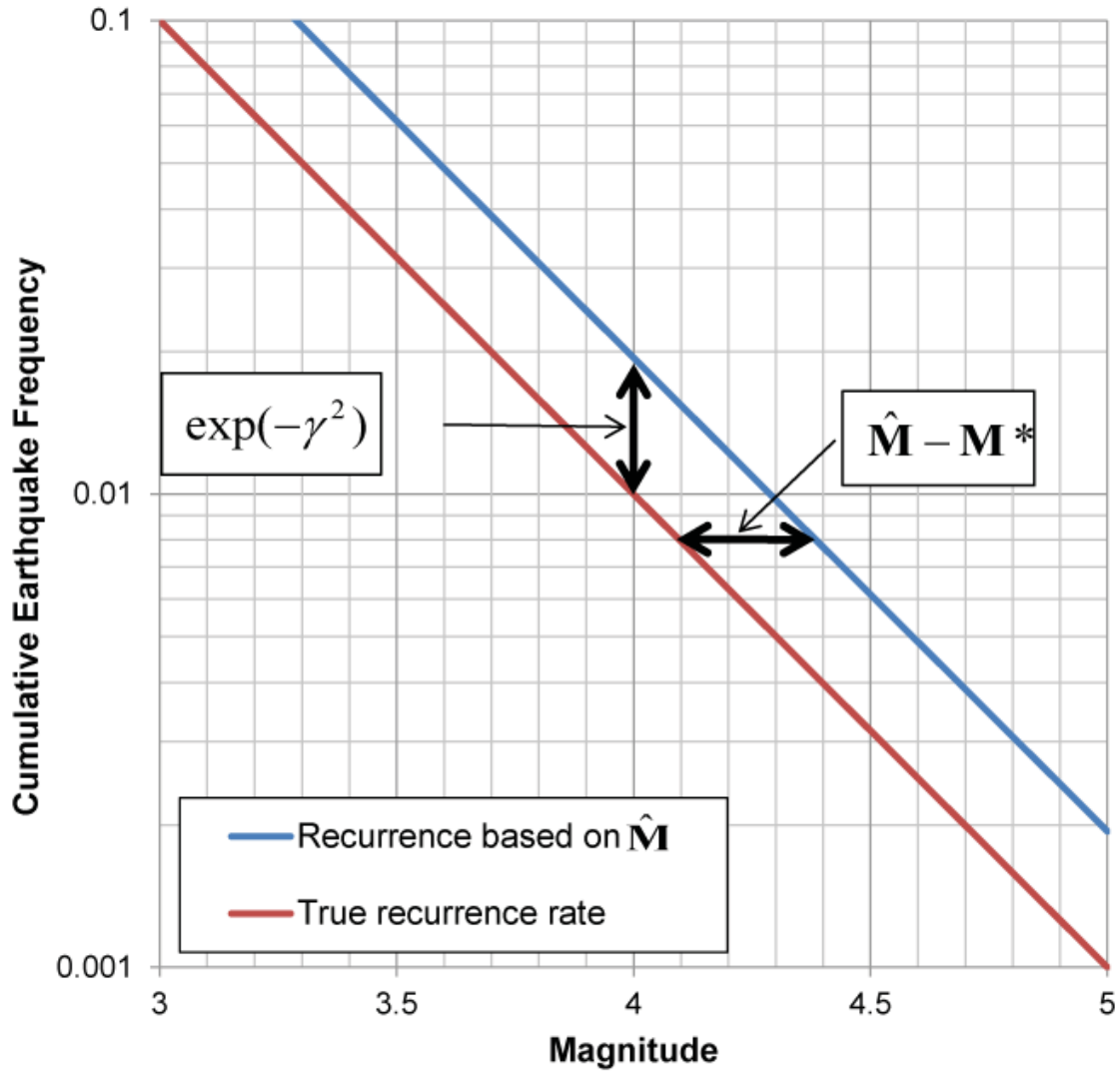
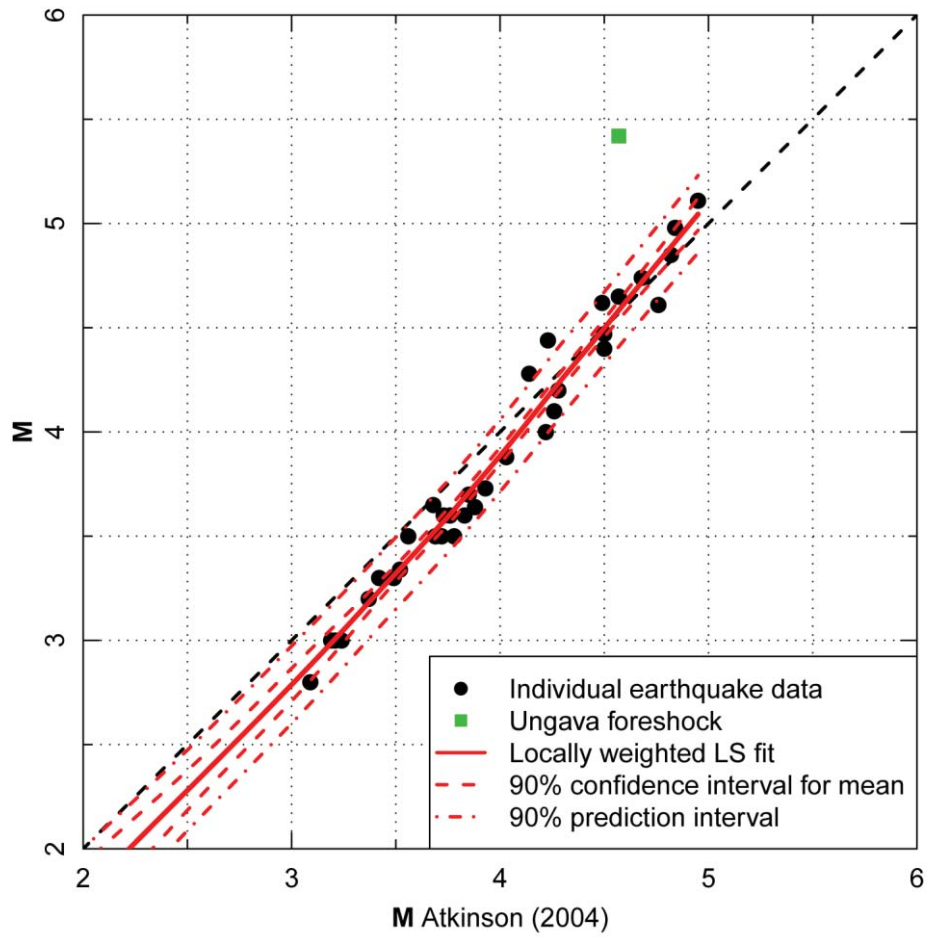
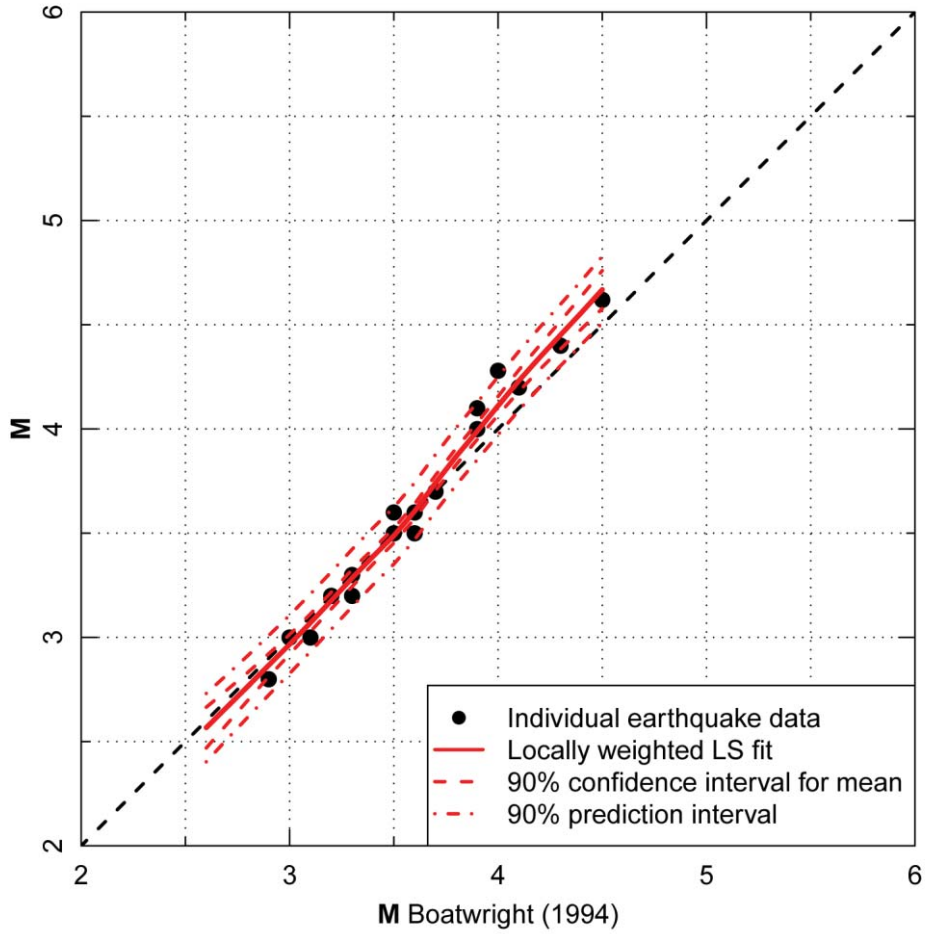


Figure 3.3-1  
Illustration of equivalence of the  $M^*$  and  $\gamma^2$  corrections to remove bias in earthquake recurrence relationships estimated from magnitudes with uncertainty,  $\hat{M}$



**Figure 3.3-2**  
Approximate moment magnitudes from Atkinson (2004b) compared to values of M given in Table B-2 in Appendix B for earthquakes in common



**Figure 3.3-3**  
Approximate moment magnitudes from Boatwright (1994) compared to values of M given in Table B-2 in Appendix B for earthquakes in common

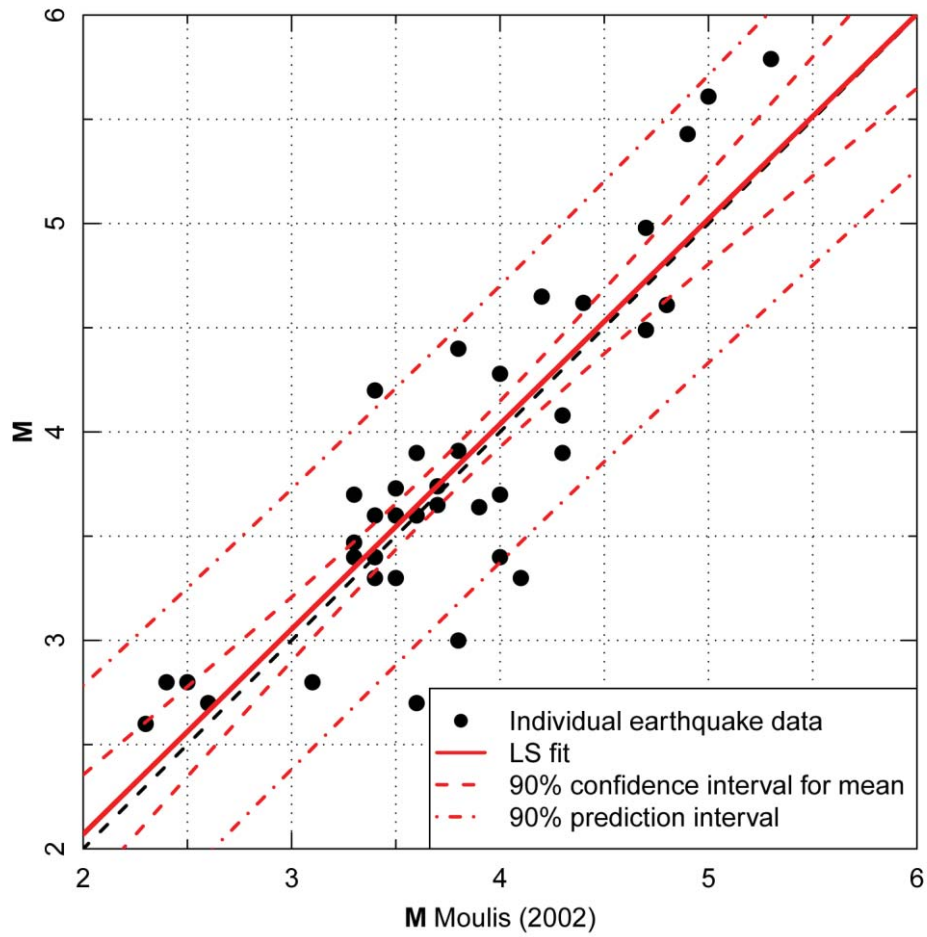


**Figure 3.3-4**  
Approximate moment magnitudes from Moulis (2002) compared to values of M given in Table B-2 in Appendix B for earthquakes in common

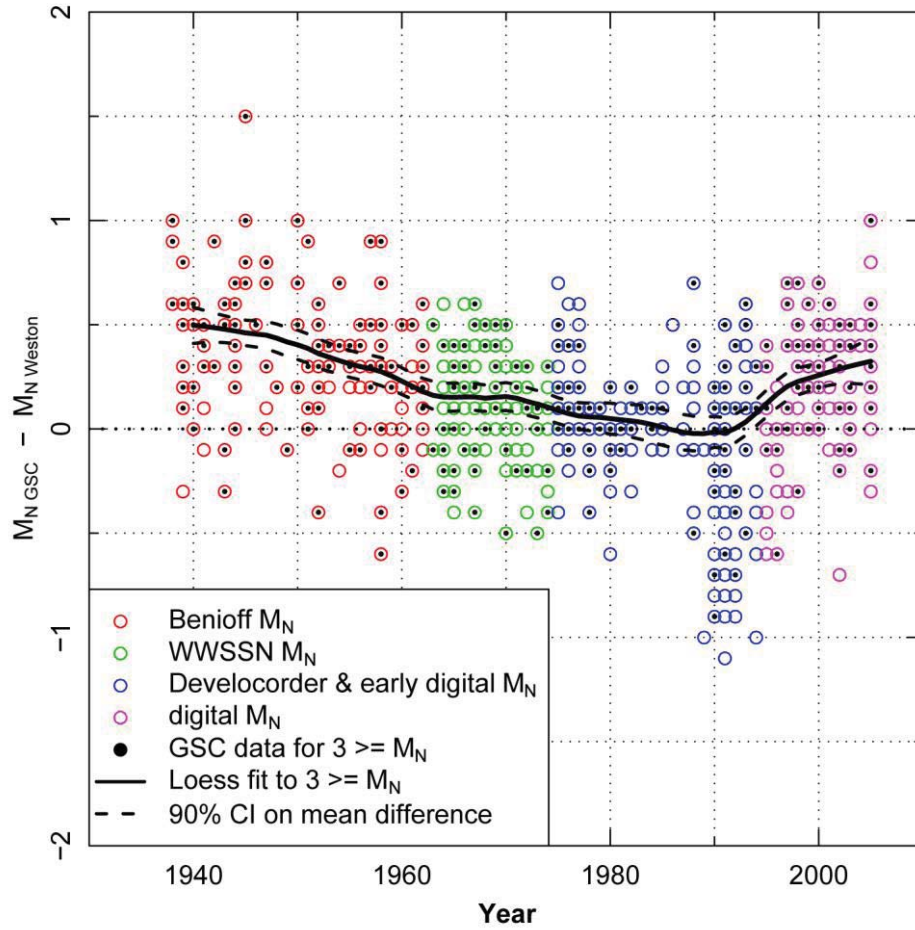


**Figure 3.3-5**  
Difference between  $M_N$  reported by the GSC and  $M_N$  or  $m_{Lg(f)}$  reported by the Weston Observatory catalog as a function of time

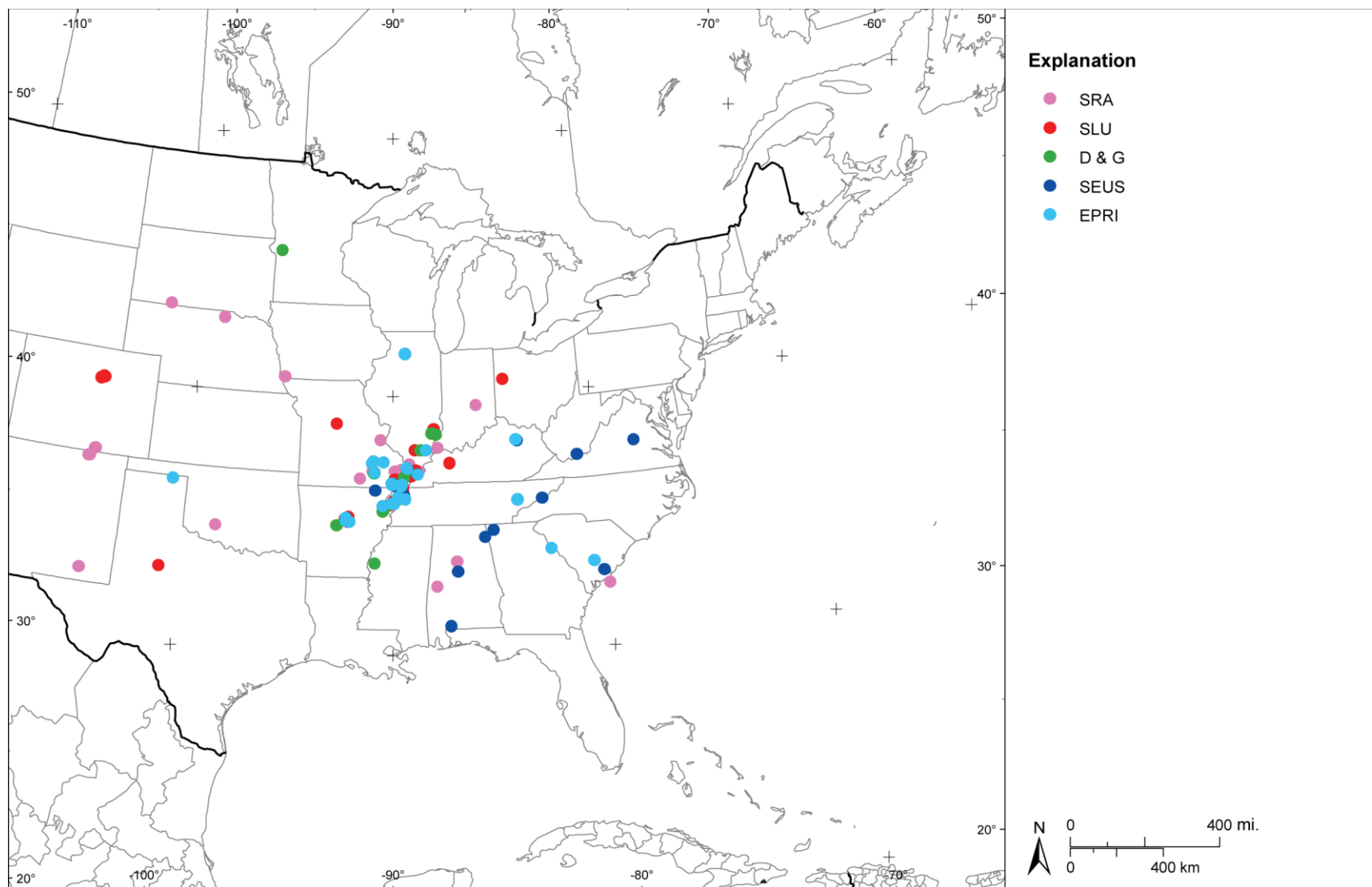


**Figure 3.3-6**  
Spatial distribution of earthquakes with body-wave ( $m_b$ ,  $m_{bLG}$ ,  $M_N$ ) and  $M$  magnitudes in the CEUS SSC Project catalog for the Midcontinent region. Color codes indicate the source of the body-wave magnitudes.

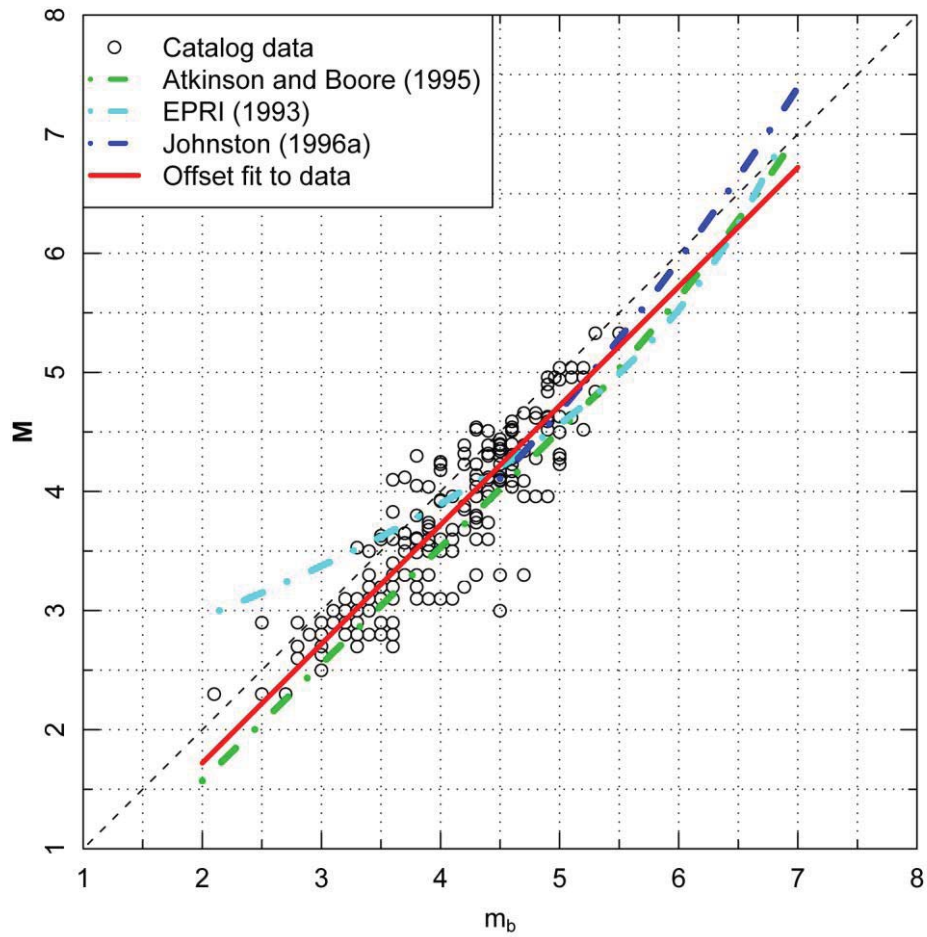


**Figure 3.3-7**  
 $m_b$ - $M$  data for the earthquakes shown on Figure 3.3-6. Red curve shows the preferred offset fit  $M = m_b - 0.28$ .

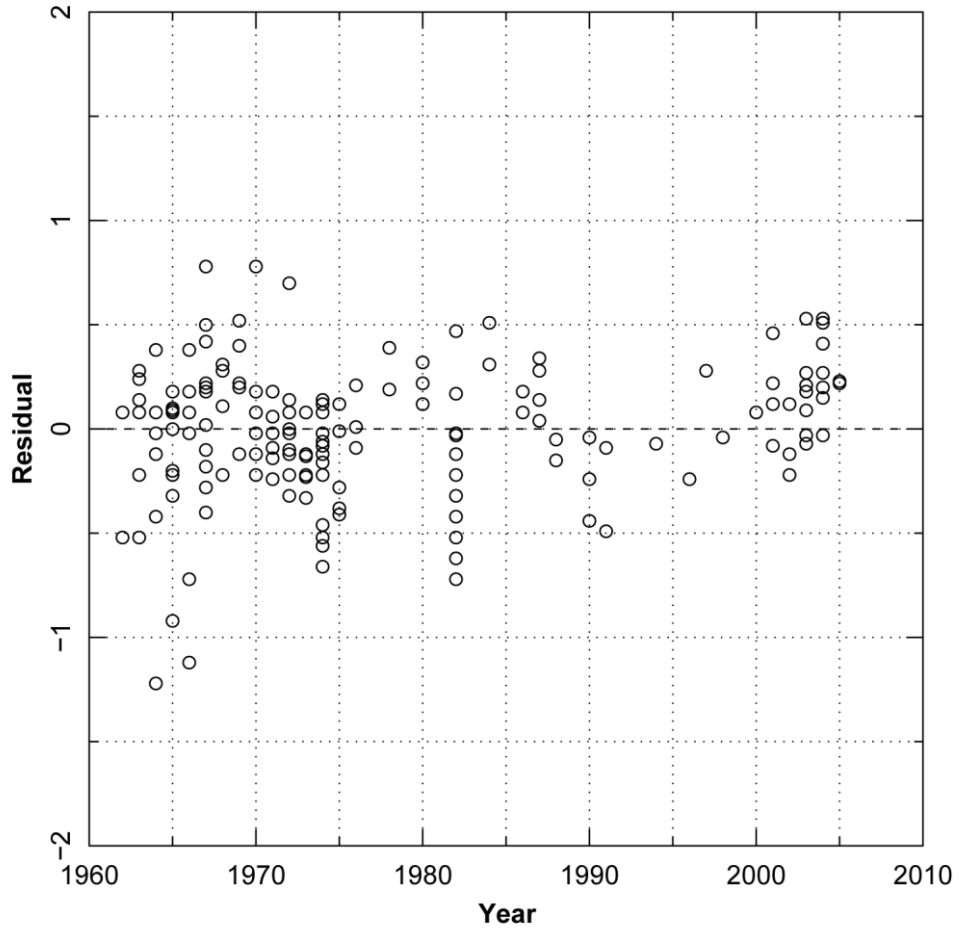


**Figure 3.3-8**  
Residuals from offset fit shown on Figure 3.3-7 plotted against earthquake year

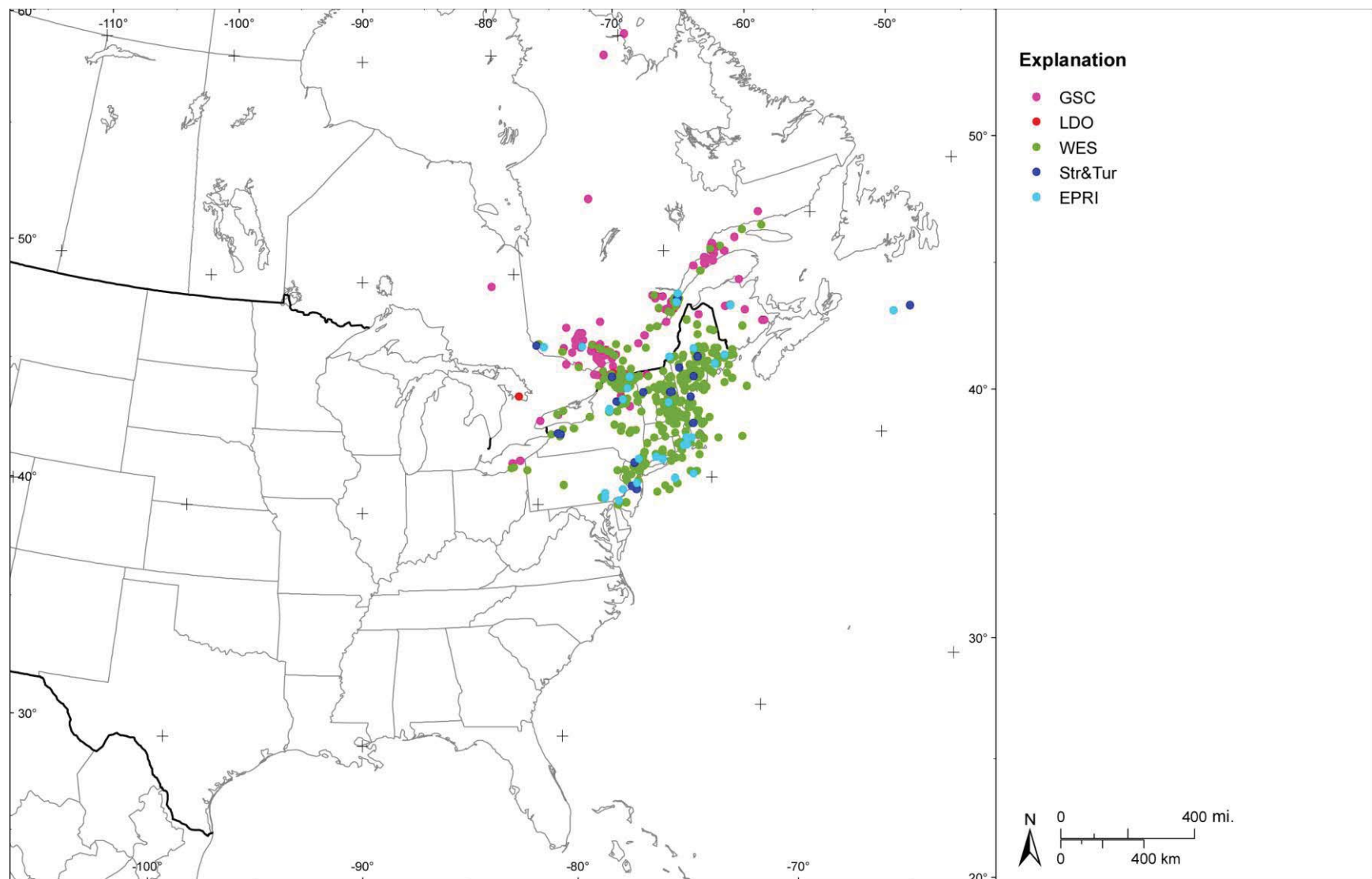


**Figure 3.3-9**  
Spatial distribution of earthquakes with body wave ( $m_b$ ,  $m_{bLG}$ ,  $M_N$ ) and  $M$  magnitudes in the CEUS SSC Project catalog for the northeastern portion of the study region. Color codes indicate the source of the body-wave magnitudes.

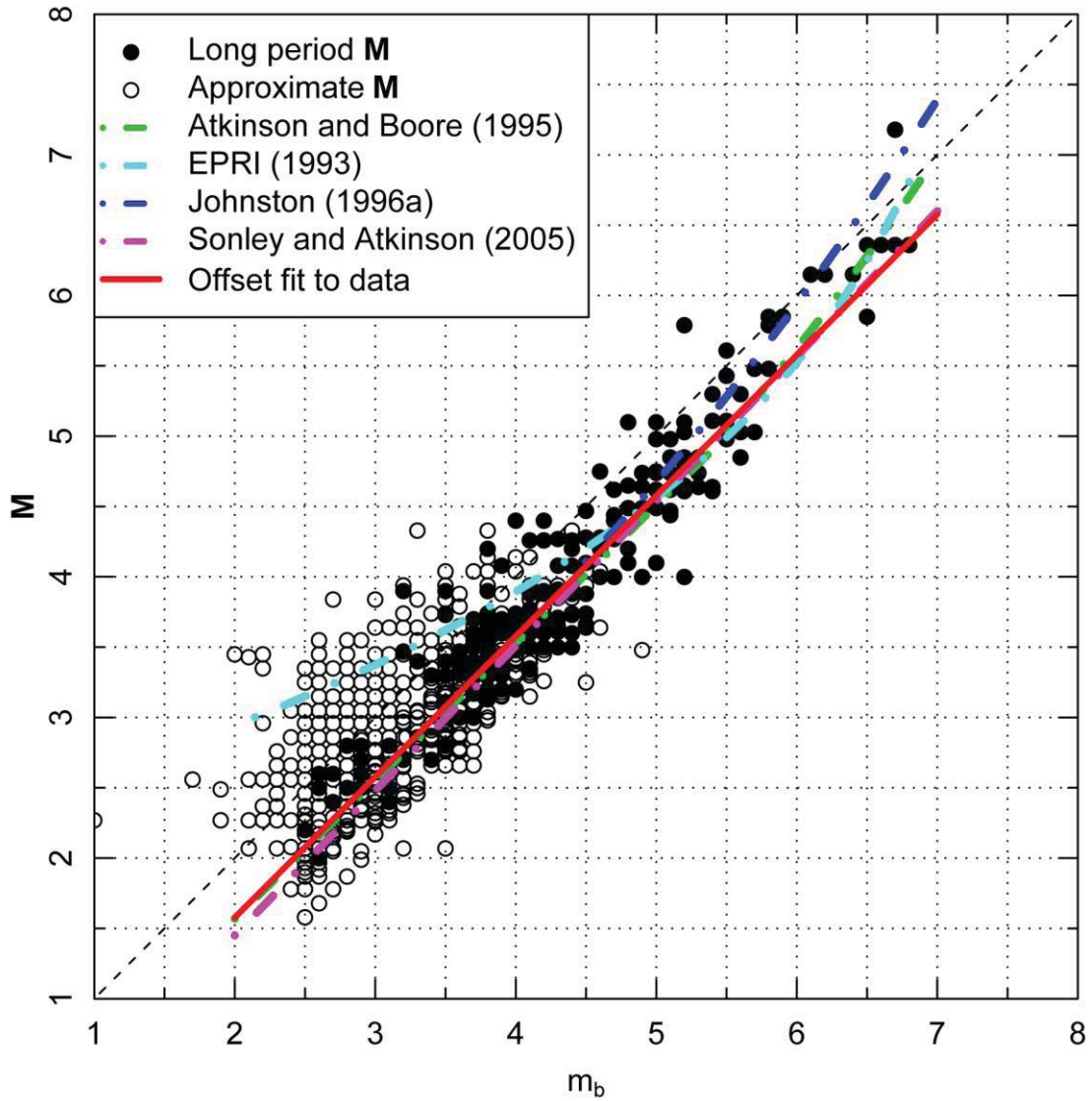
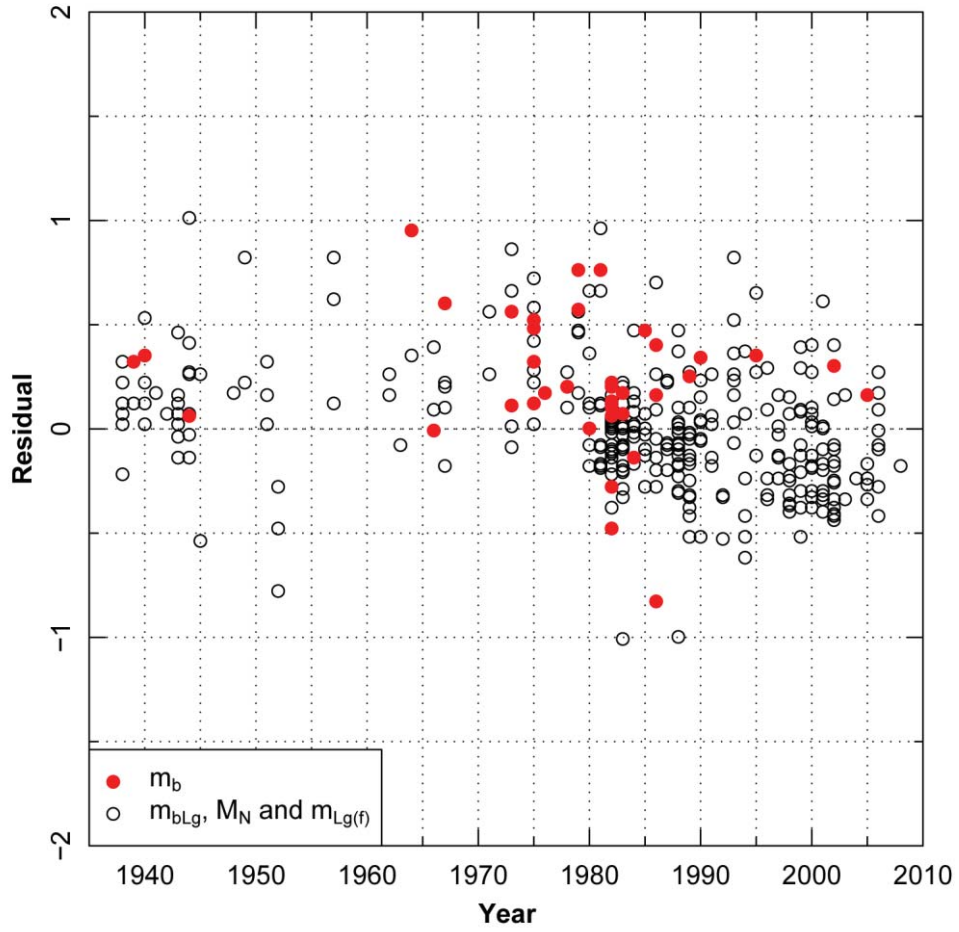


Figure 3.3-10  
 $m_b$ - $M$  data for the earthquakes shown on Figure 3.3-9. Red curve shows the preferred offset fit  $M = m_b - 0.42$ .



**Figure 3.3-11**  
Residuals from offset fit shown on Figure 3.3-10 plotted against earthquake year

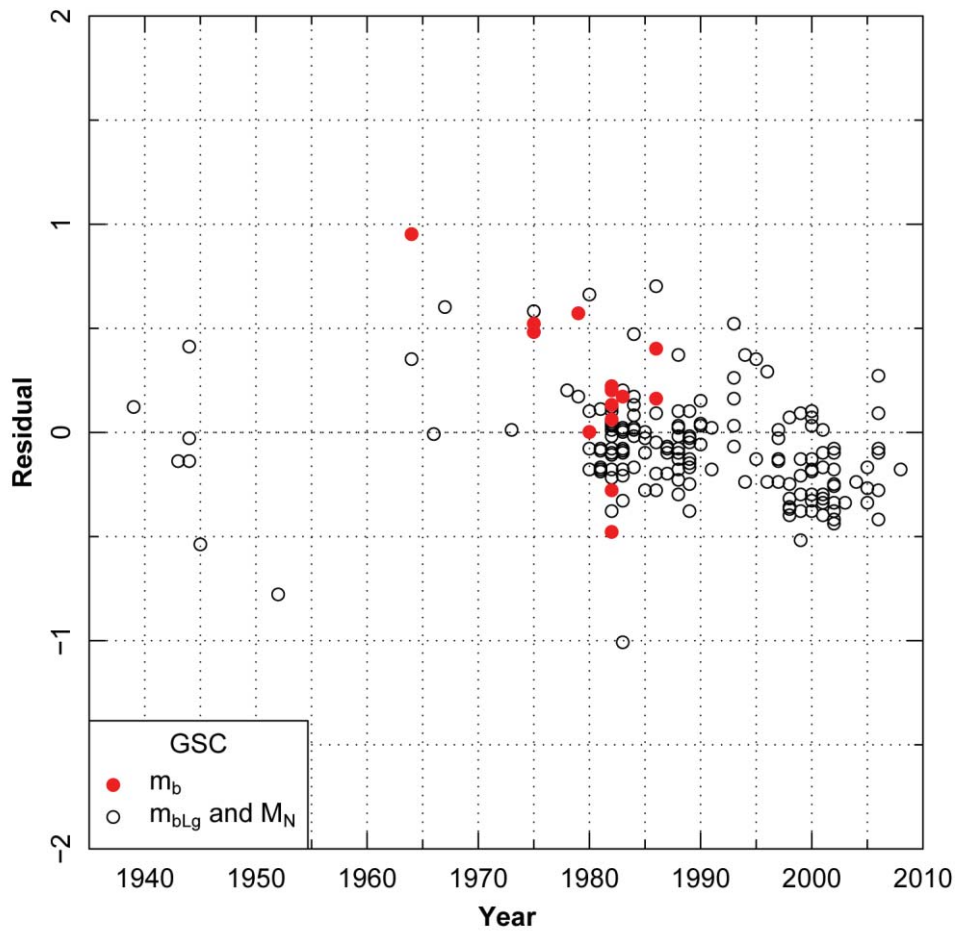
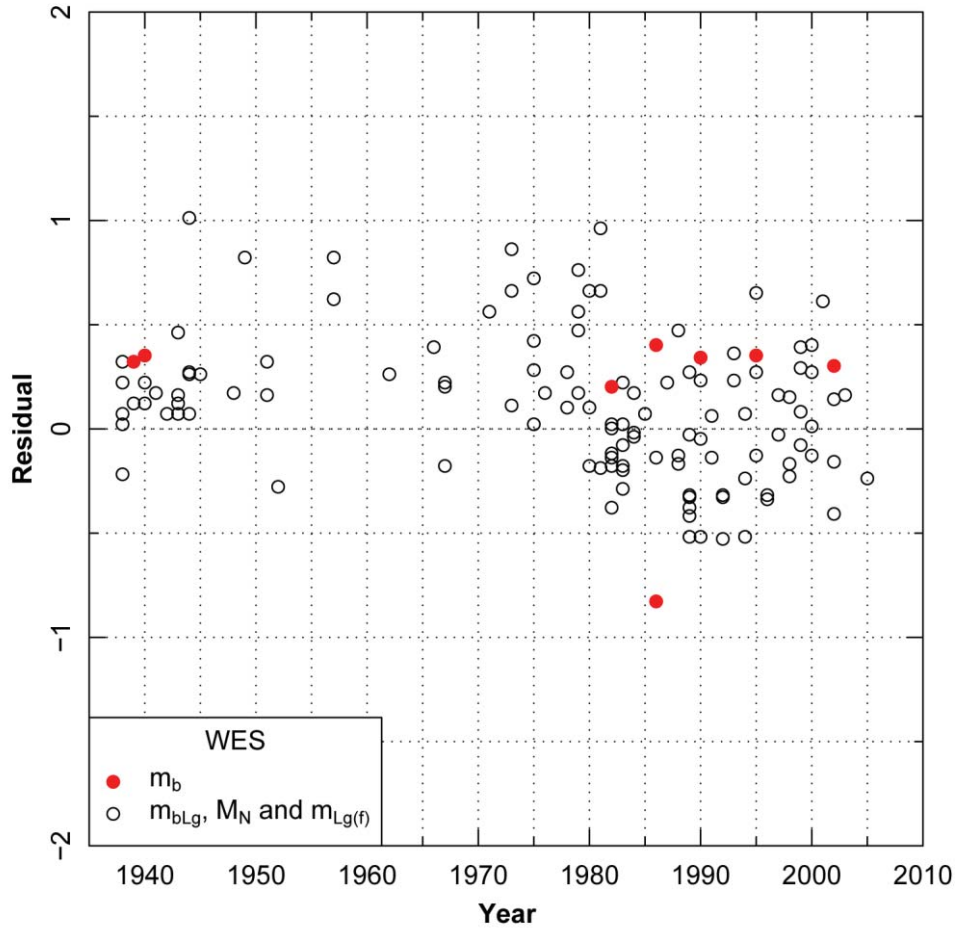
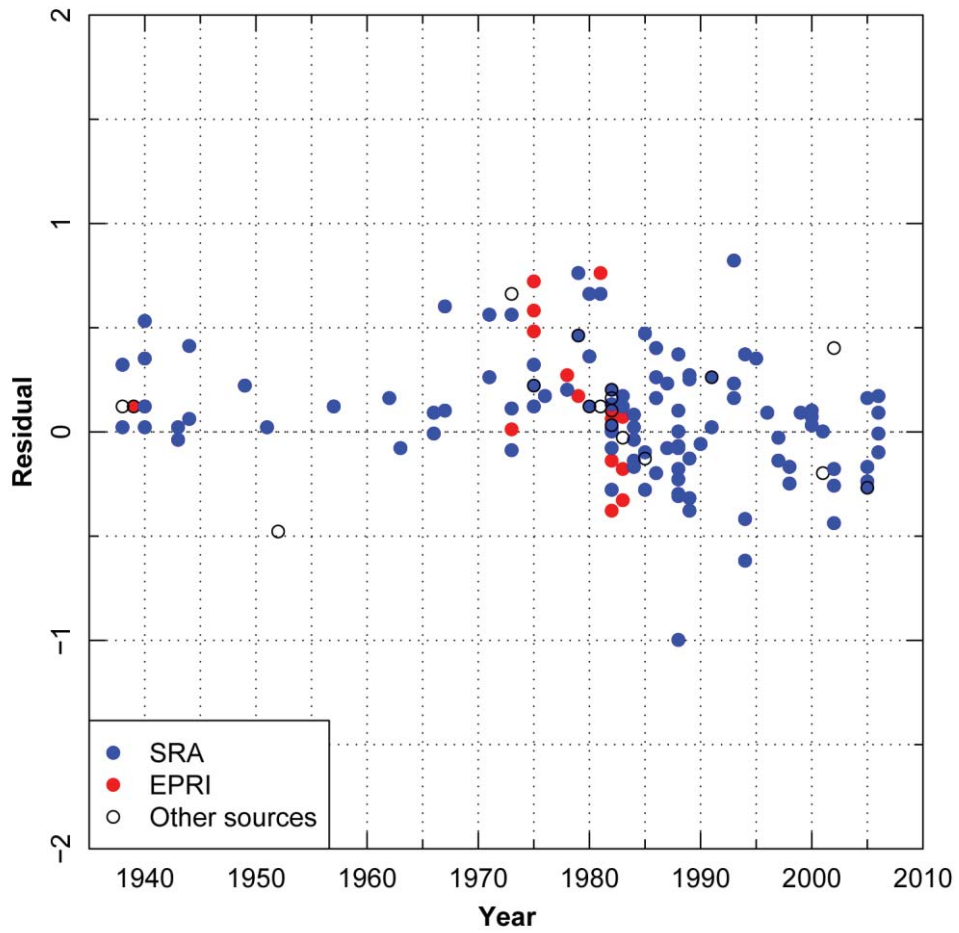


Figure 3.3-12  
Residuals for GSC data from offset fit shown on Figure 3.3-10 plotted against earthquake year



**Figure 3.3-13**  
Residuals for WES data from offset fit shown on Figure 3.3-10 plotted against earthquake year



**Figure 3.3-14**  
Residuals for data from sources other than GSC or WES from offset fit shown on Figure 3.3-10 plotted against earthquake year

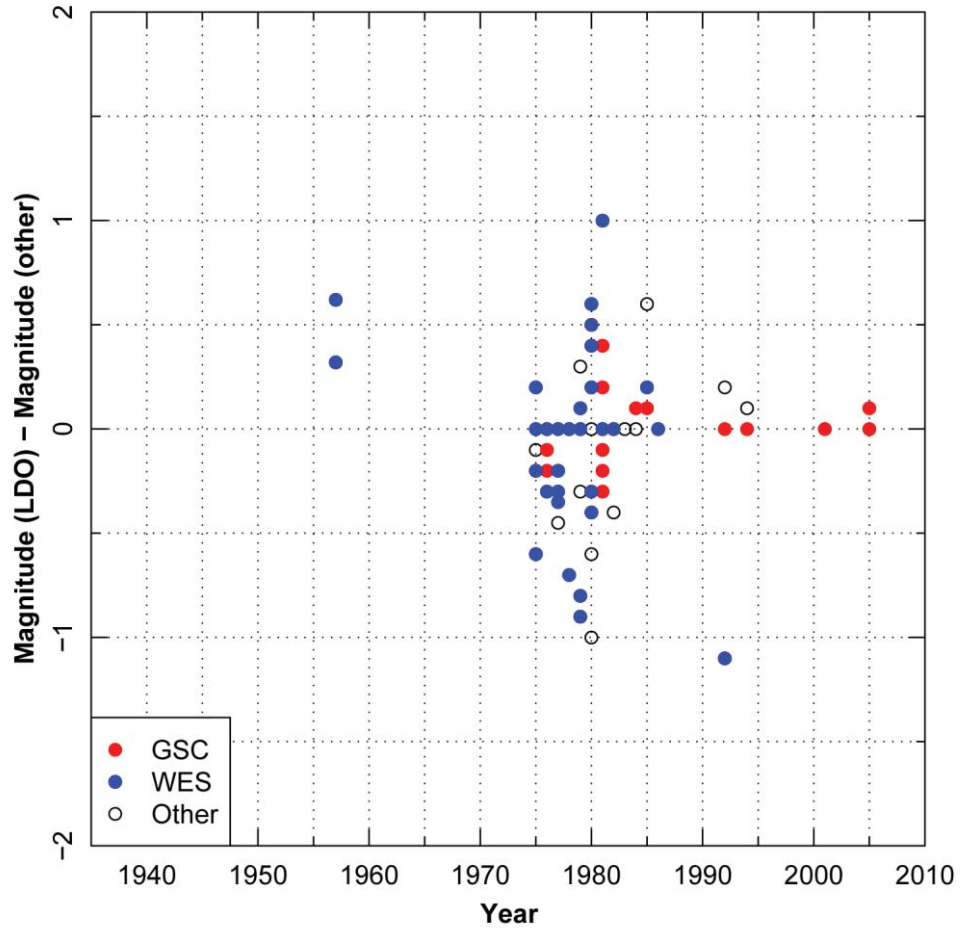


**Figure 3.3-15**  
Difference between body-wave magnitudes reported by LDO and those by other sources as a function of year

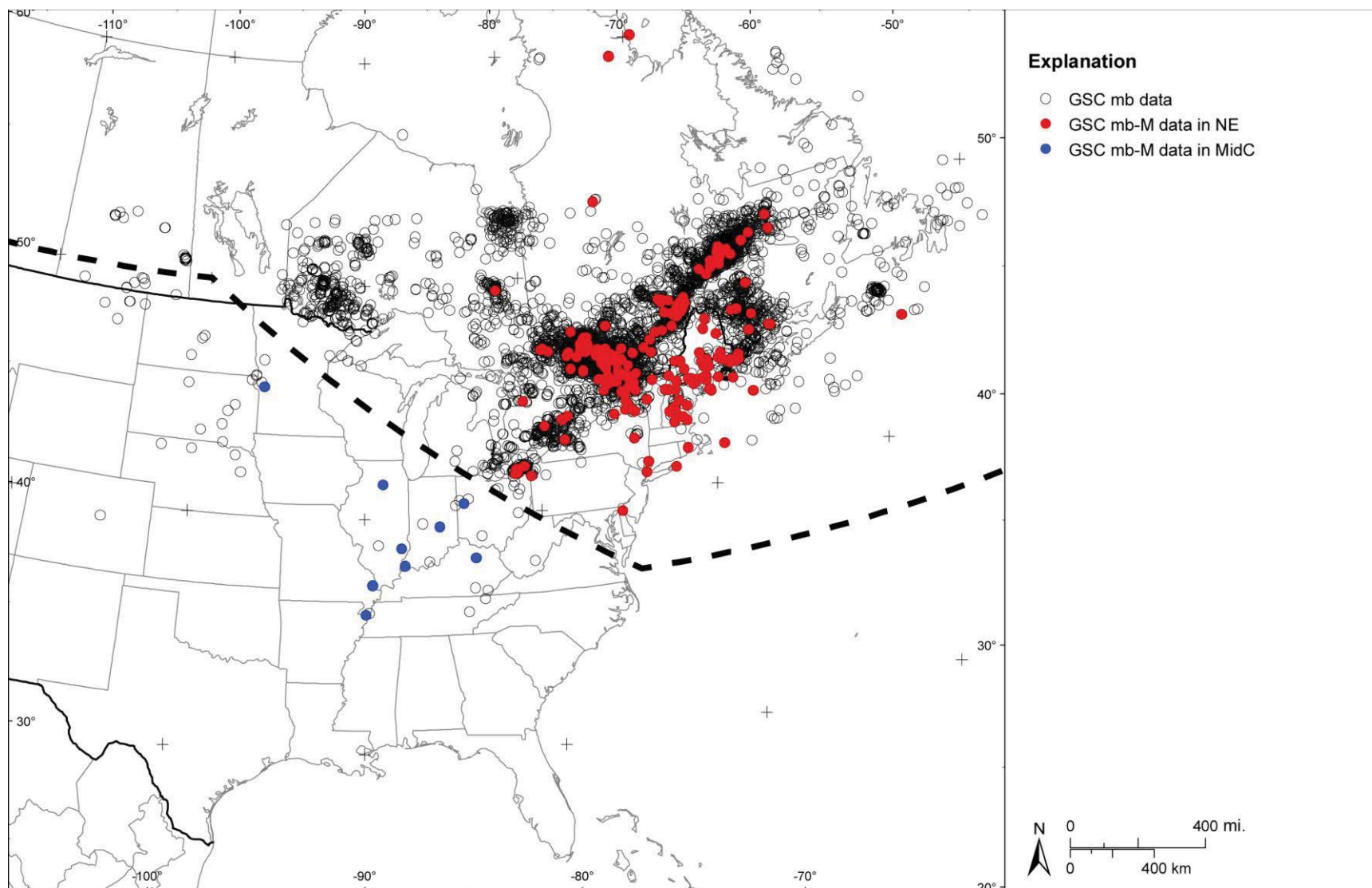


**Figure 3.3-16**  
Spatial distribution of earthquakes with reported GSC body-wave magnitudes. Red and blue symbols indicate earthquakes with both  $m_b$  and  $M$  magnitudes for  $m_b \geq 3.5$ . Dashed line indicates the portion of the study region considered the "Northeast" for purposes of magnitude scaling.

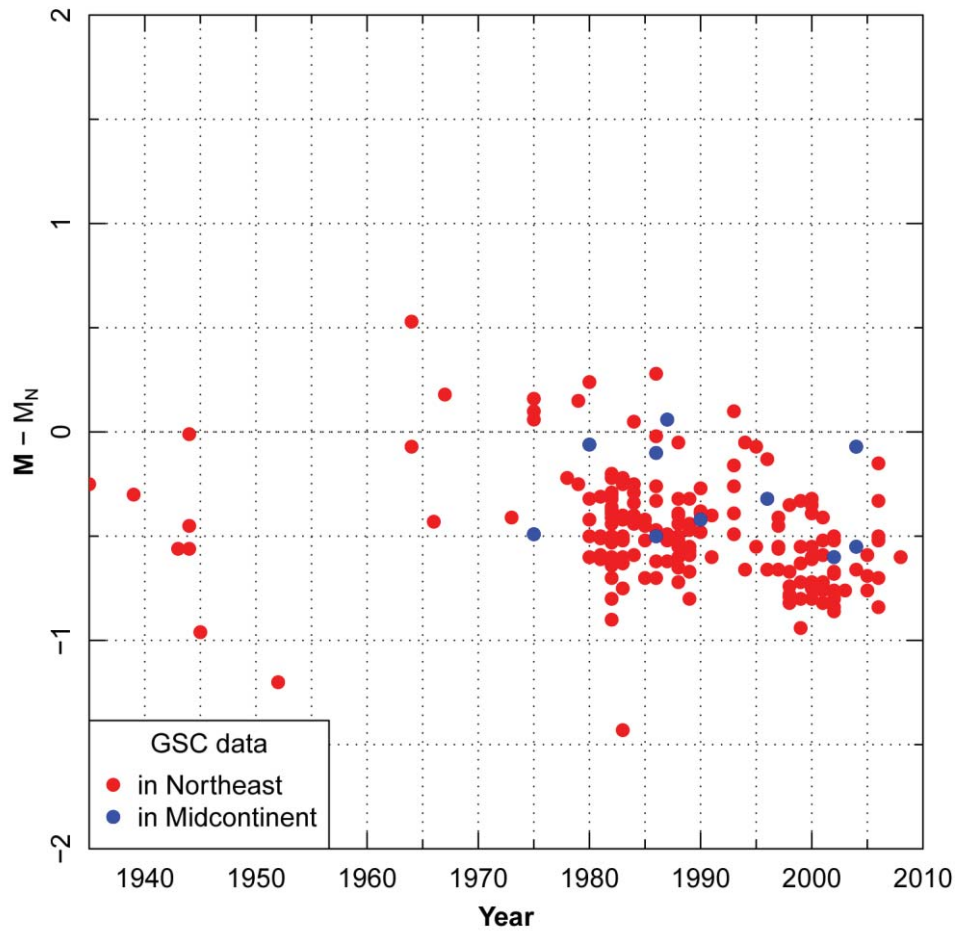


**Figure 3.3-17**  
 **$M - m_b$  as a function of time for  $m_b$  data from the GSC shown on Figure 3.3-16**

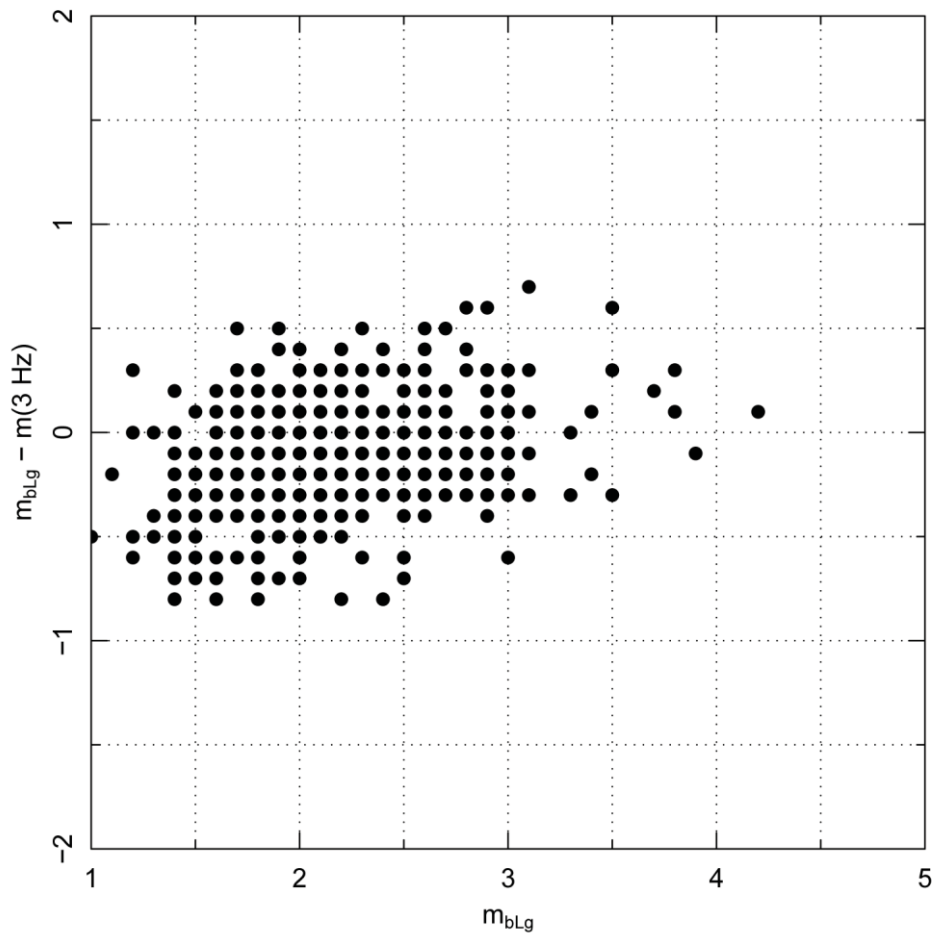


**Figure 3.3-18**  
Plot of magnitude differences  $m_{bLg} - m(3 \text{ Hz})$  for the OKO catalog

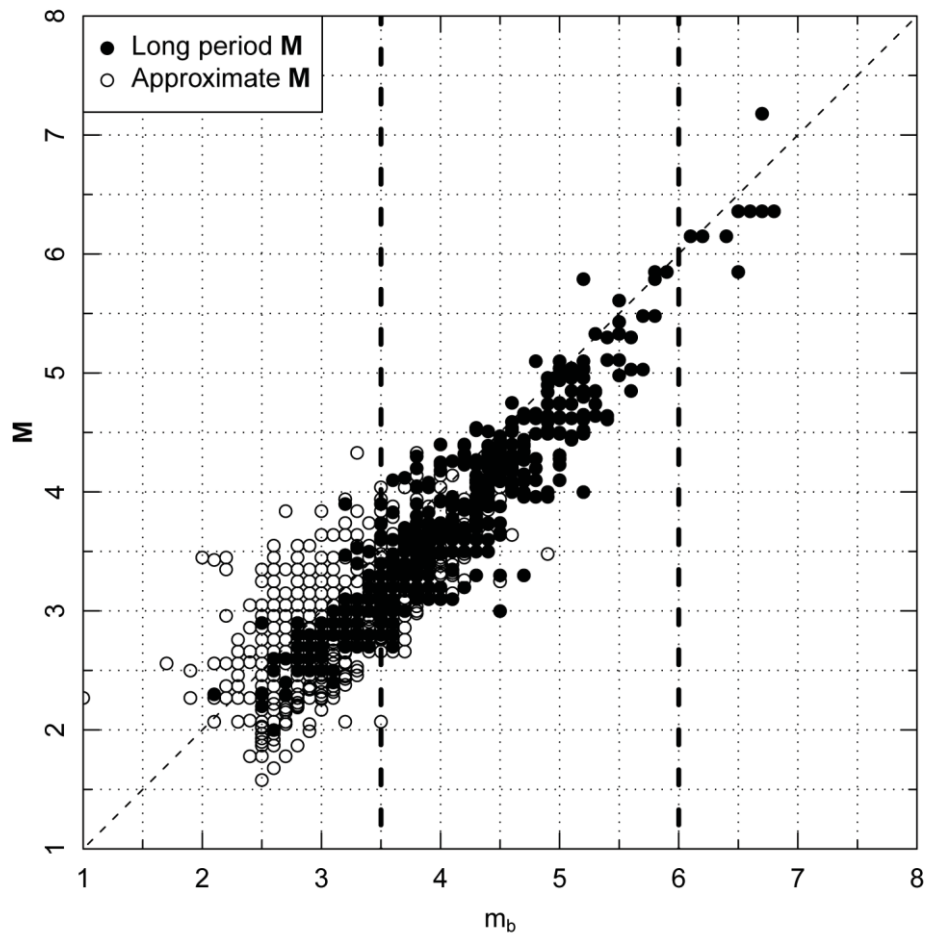


**Figure 3.3-19**  
Final  $m_b$ -M data set. Vertical dashed lines indicate the magnitude range used to develop the scaling relationship. Diagonal line indicates a one-to-one correlation.

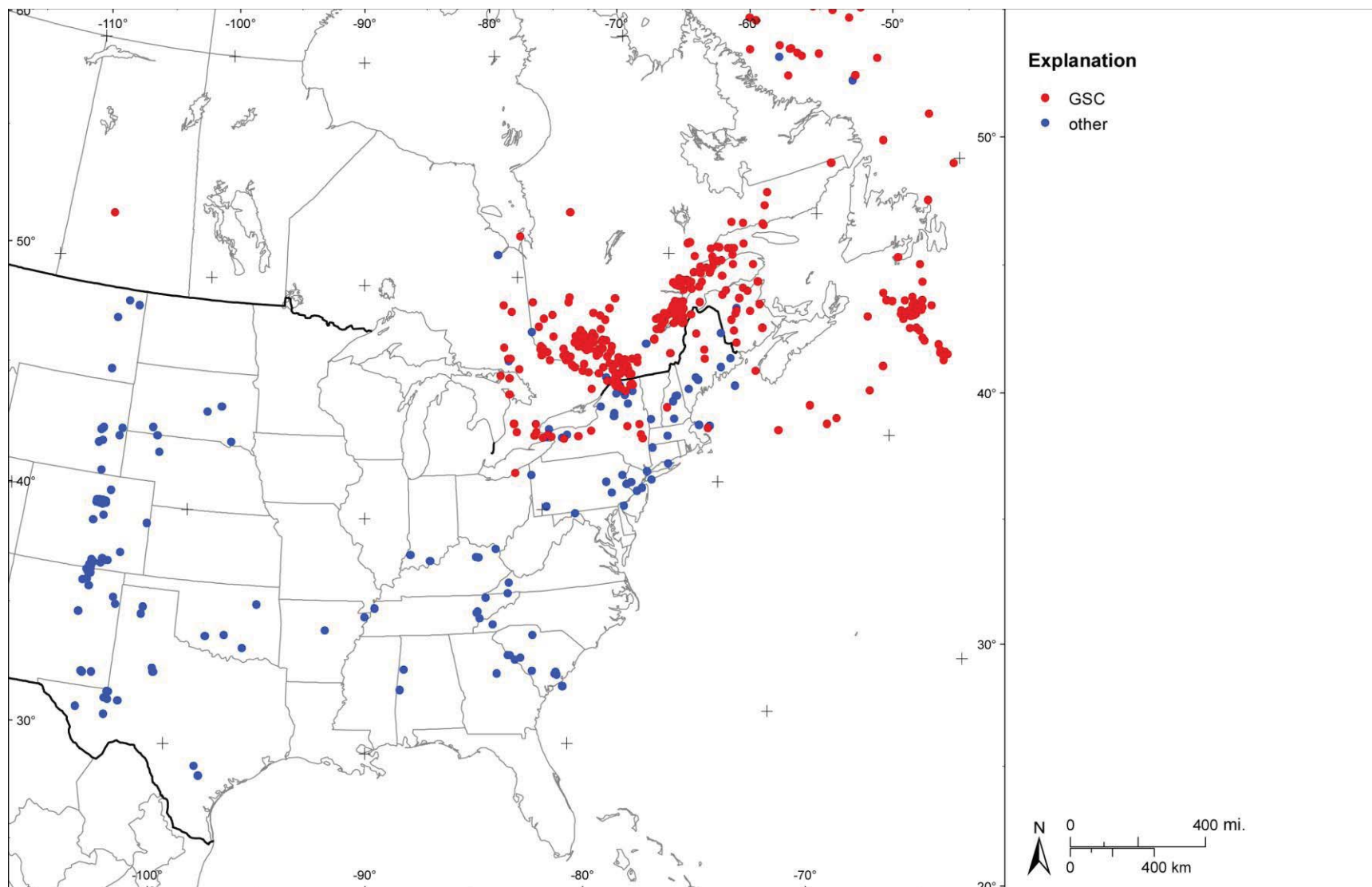


**Figure 3.3-20**  
Spatial distribution of earthquakes in the CEUS SSC Project catalog with instrumental  $M_L$  magnitudes

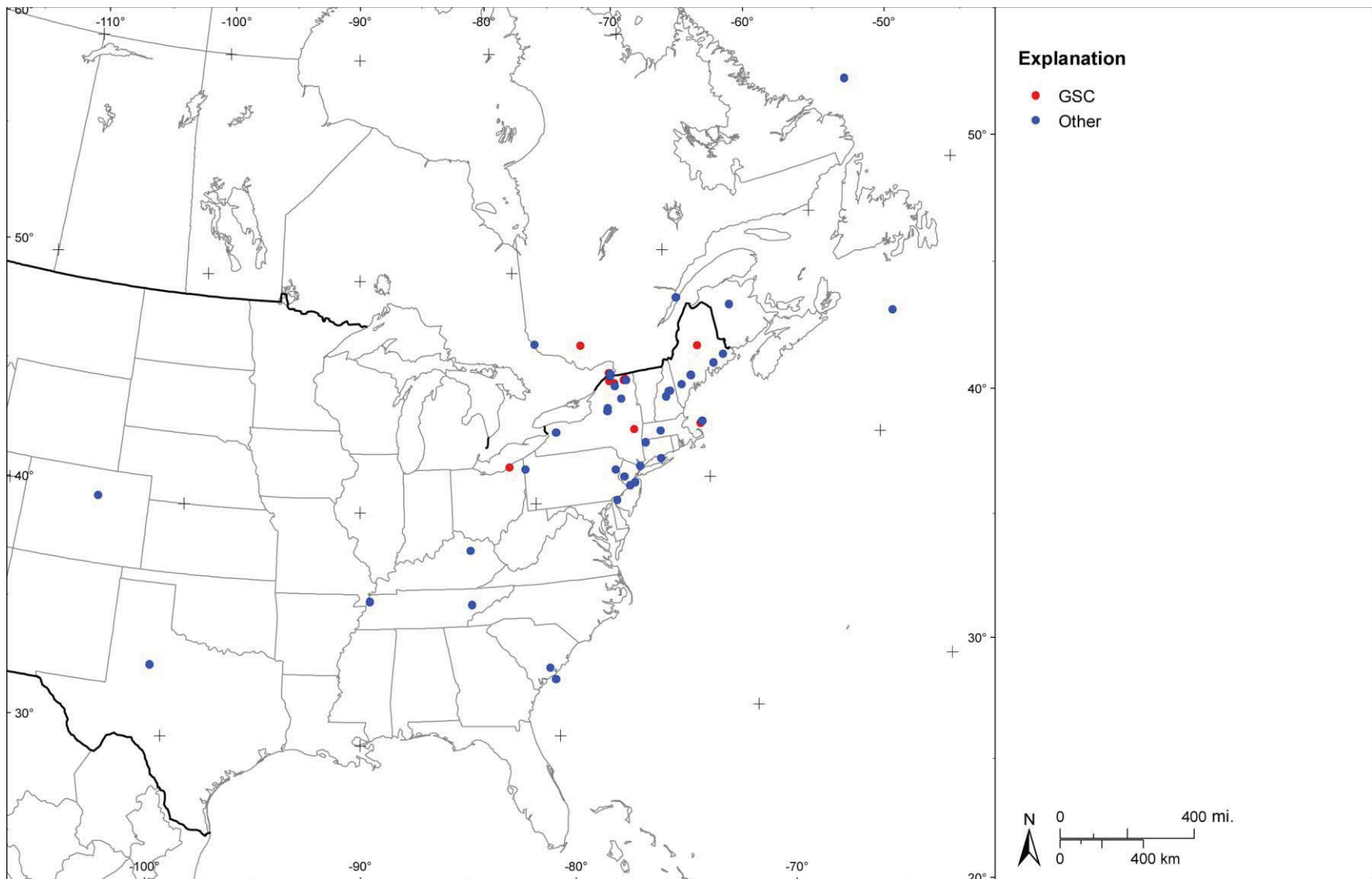


**Figure 3.3-21**  
Spatial distribution of earthquakes in the CEUS SSC Project catalog with instrumental  $M_L$  magnitudes and  $M$  magnitudes

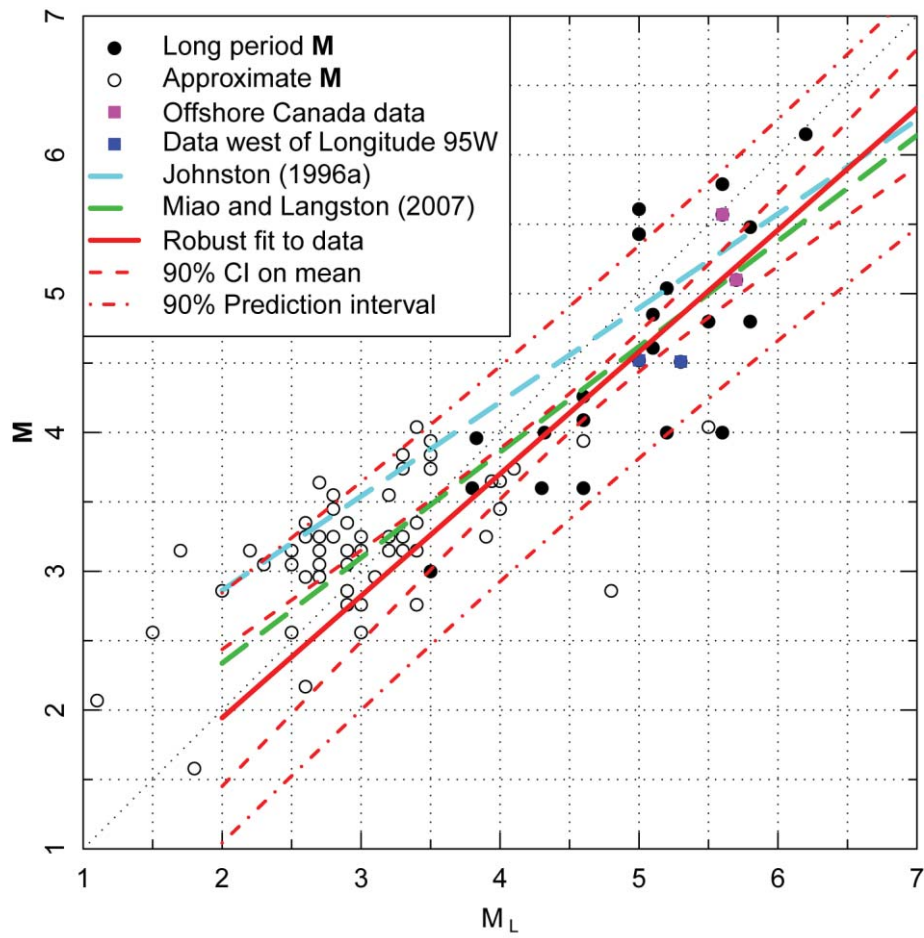


**Figure 3.3-22**  
 **$M_L$ - $M$  data from the CEUS SSC Project catalog and robust regression fit to the data**

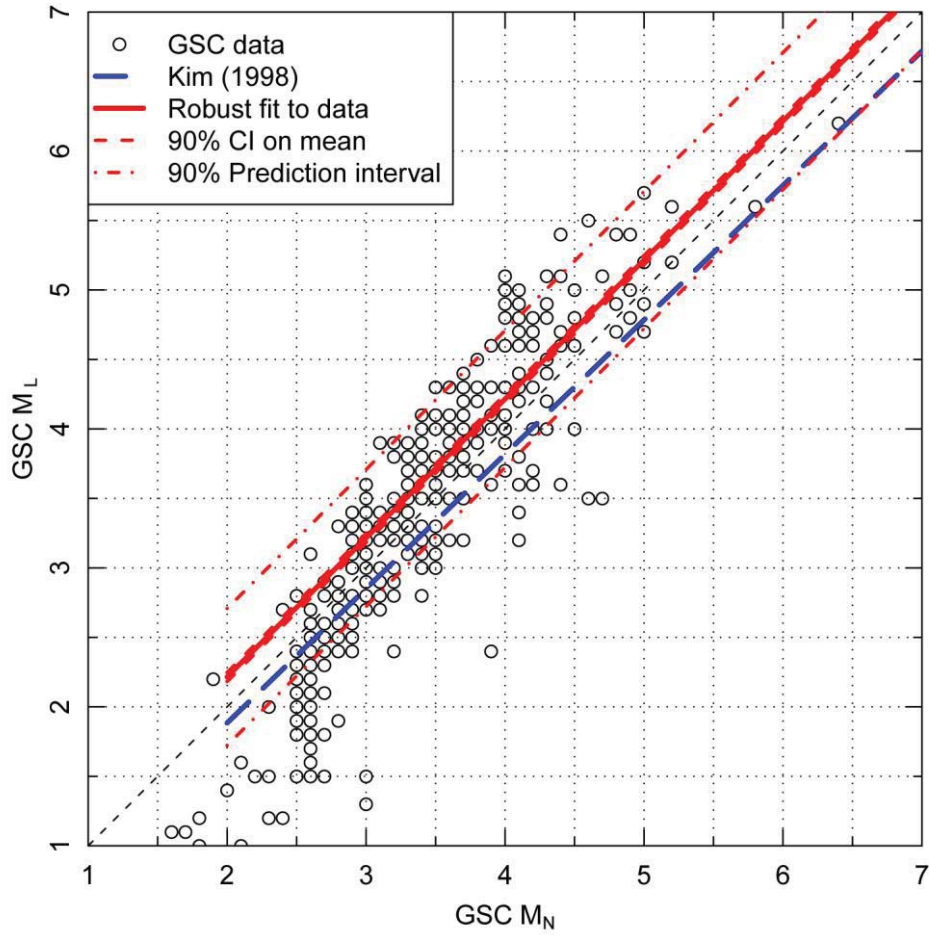


**Figure 3.3-23**  
Relationship between  $M_N$  and  $M_L$  for the GSC data

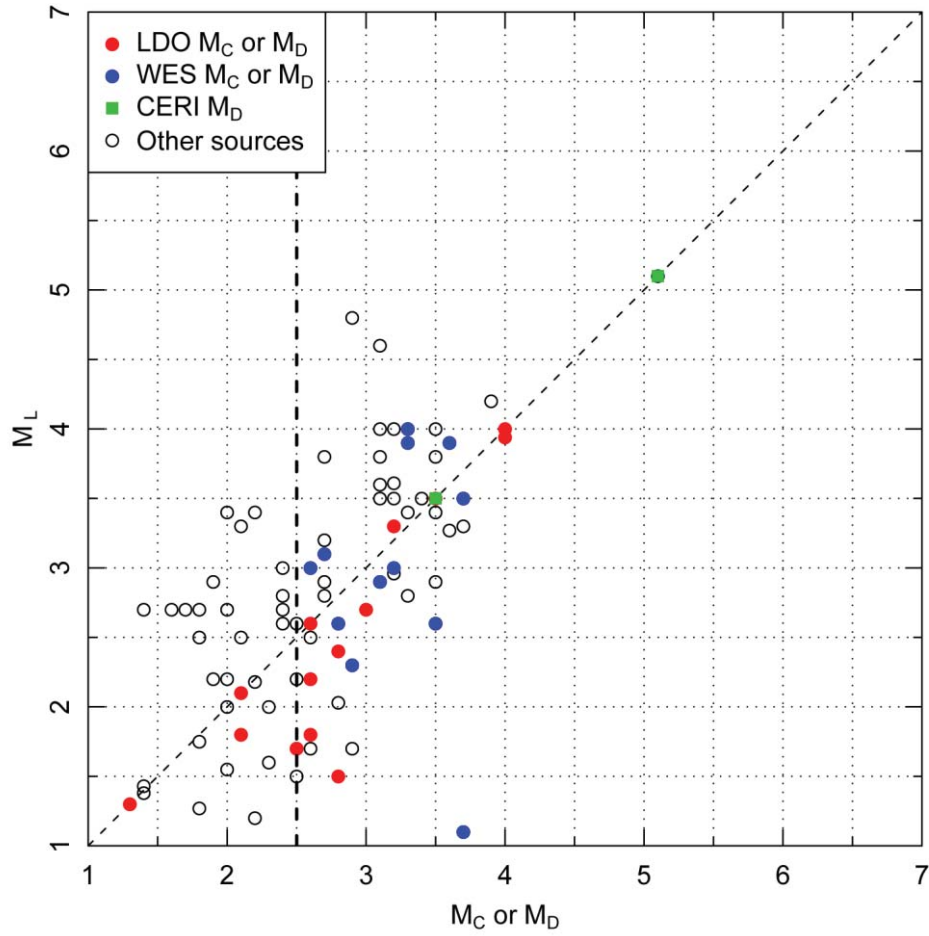


**Figure 3.3-24**  
Data from the northeastern portion of the study region with  $M_L$  and  $M_C$  or  $M_D$  magnitude from catalog sources other than the GSC

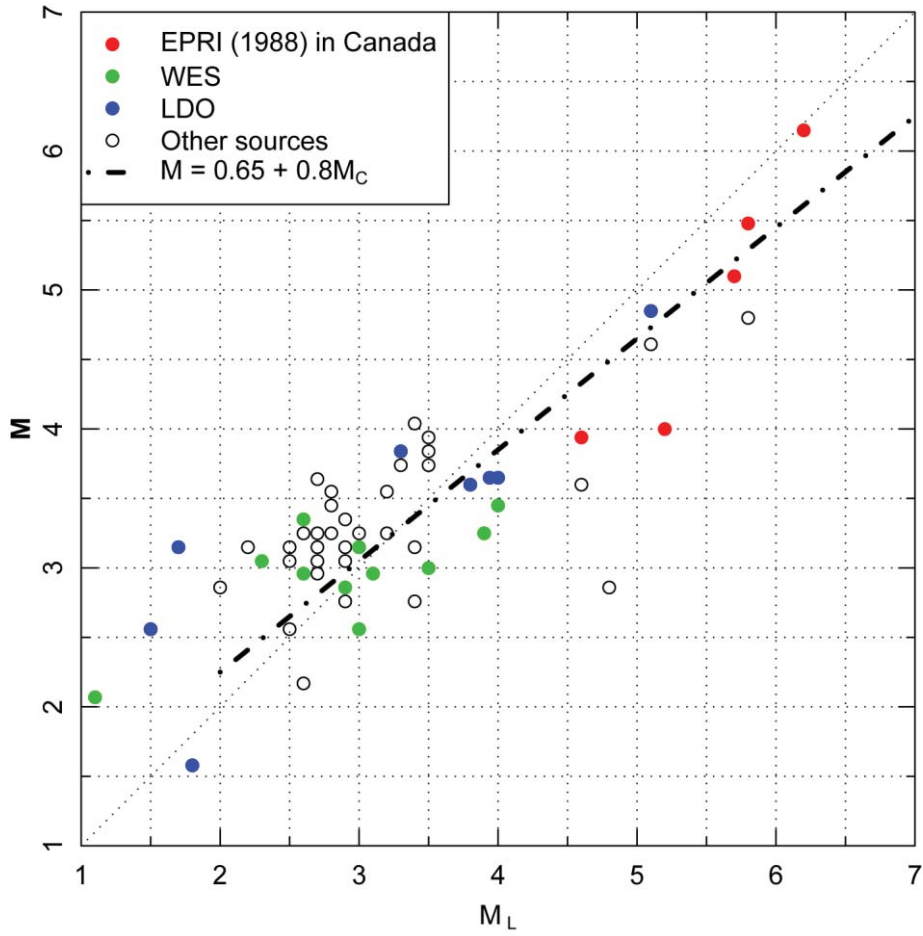


**Figure 3.3-25**  
Data from the northeastern portion of the study region with  $M_L$  and  $M$  magnitudes from sources other than the GSC

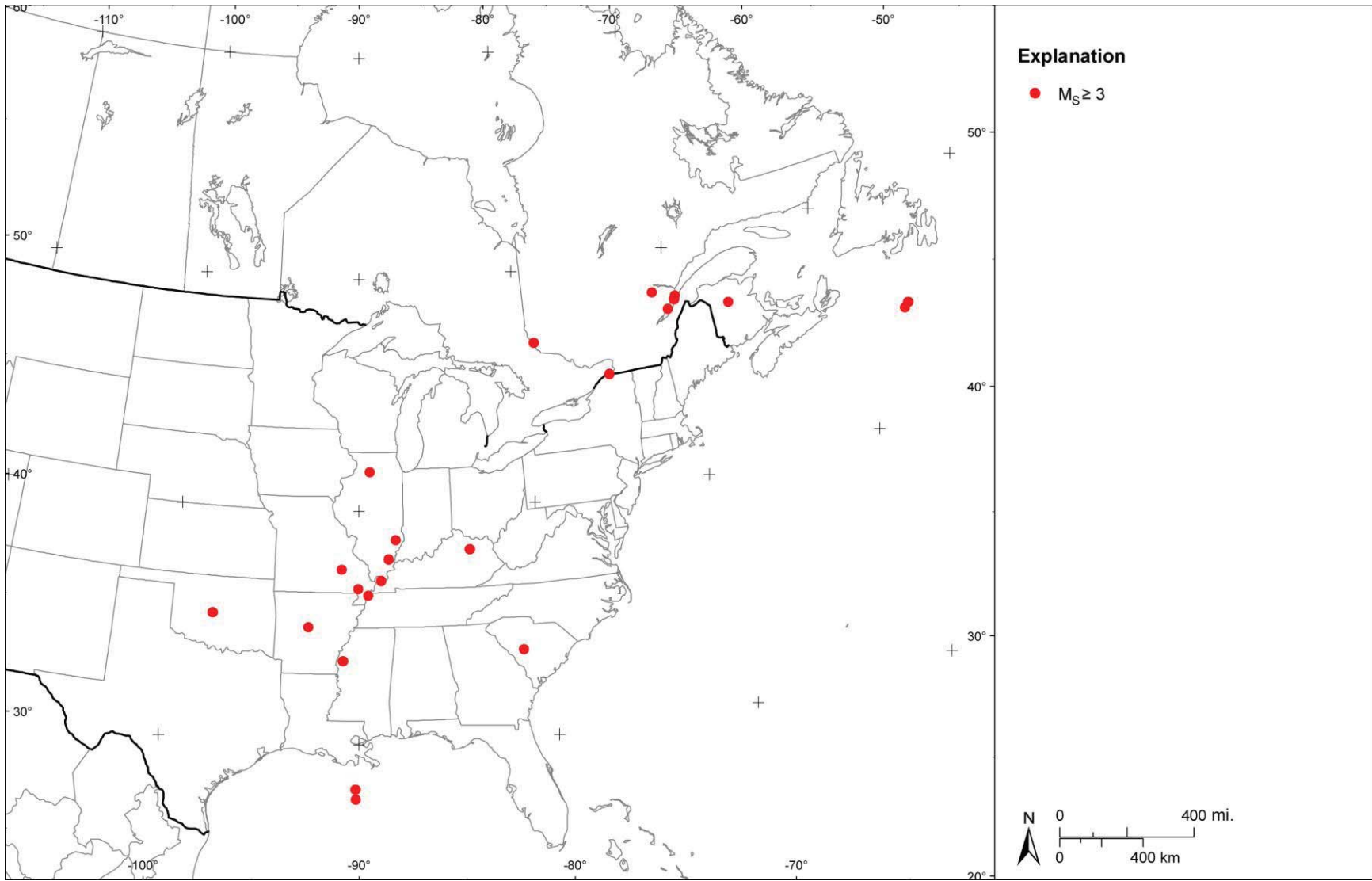


**Figure 3.3-26**  
Spatial distribution of earthquakes in the CEUS SSC Project catalog with  $M_S \geq 3$  magnitudes

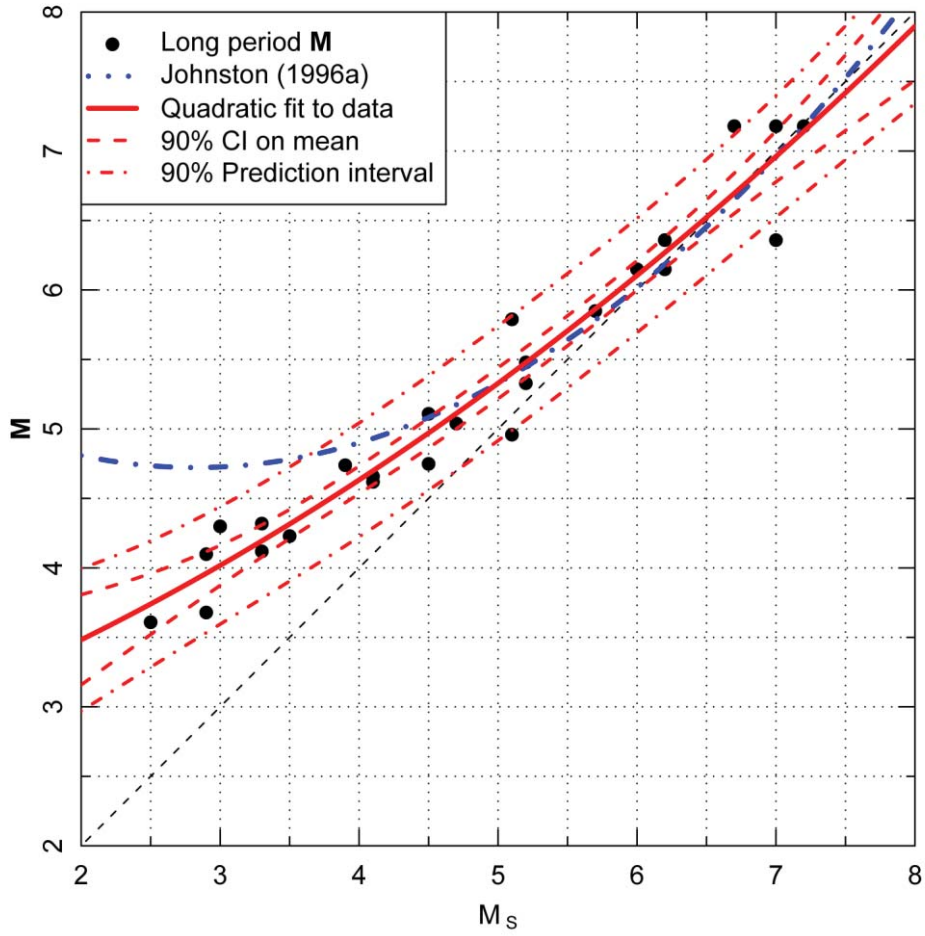


**Figure 3.3-27**  
 **$M_s$ - $M$  data from the CEUS SSC Project catalog and quadratic polynomial fit to the data**

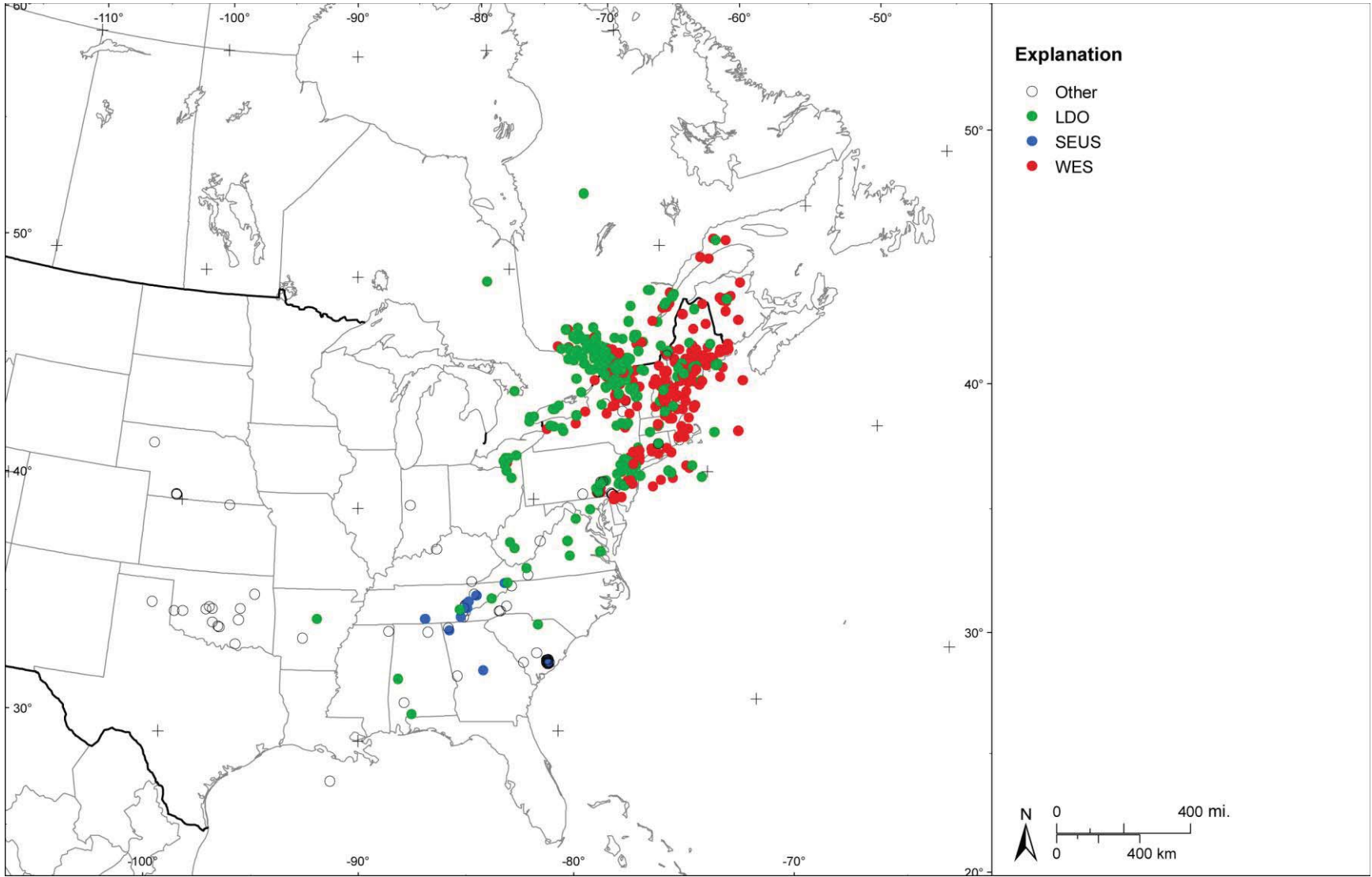


**Figure 3.3-28**  
Spatial distribution of earthquakes in the CEUS SSC Project catalog with  $M_C \geq 2.5$  magnitudes

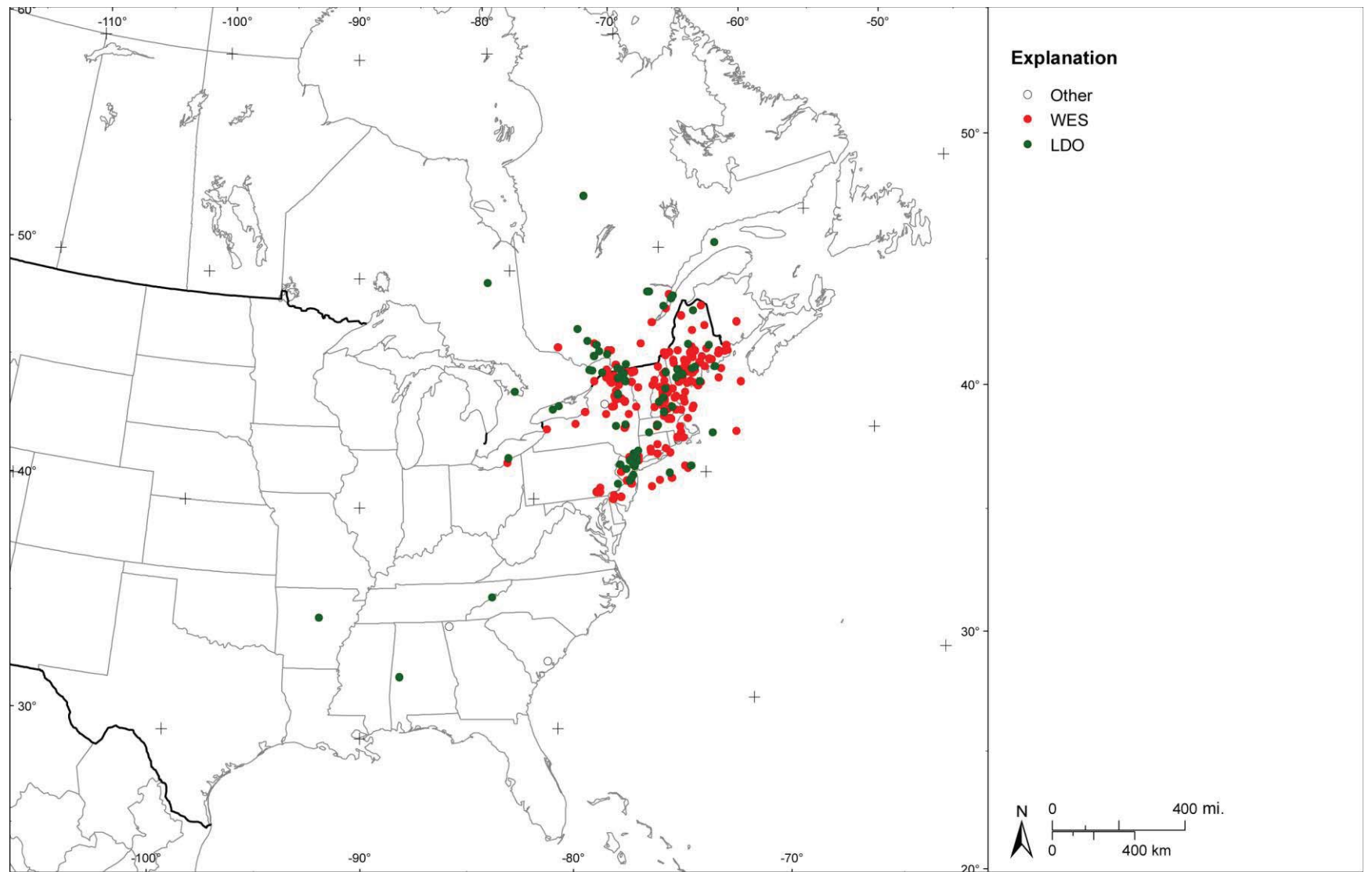


**Figure 3.3-29**  
Spatial distribution of earthquakes in the CEUS SSC Project catalog with  $M_C \geq 2.5$  and  $M$  magnitudes

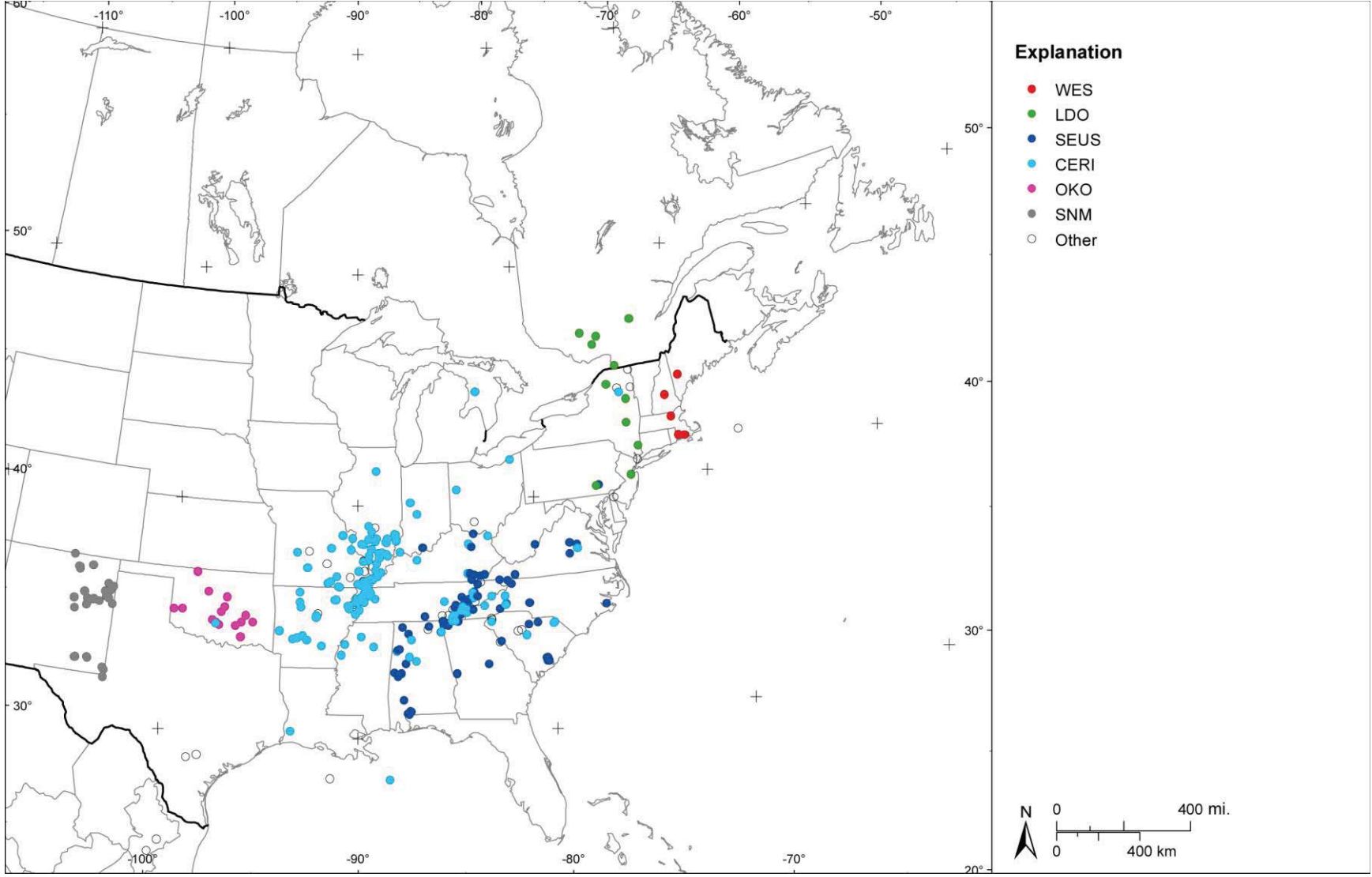


**Figure 3.3-30**  
Spatial distribution of earthquakes in the CEUS SSC Project catalog with  $M_D \geq 3$  magnitudes

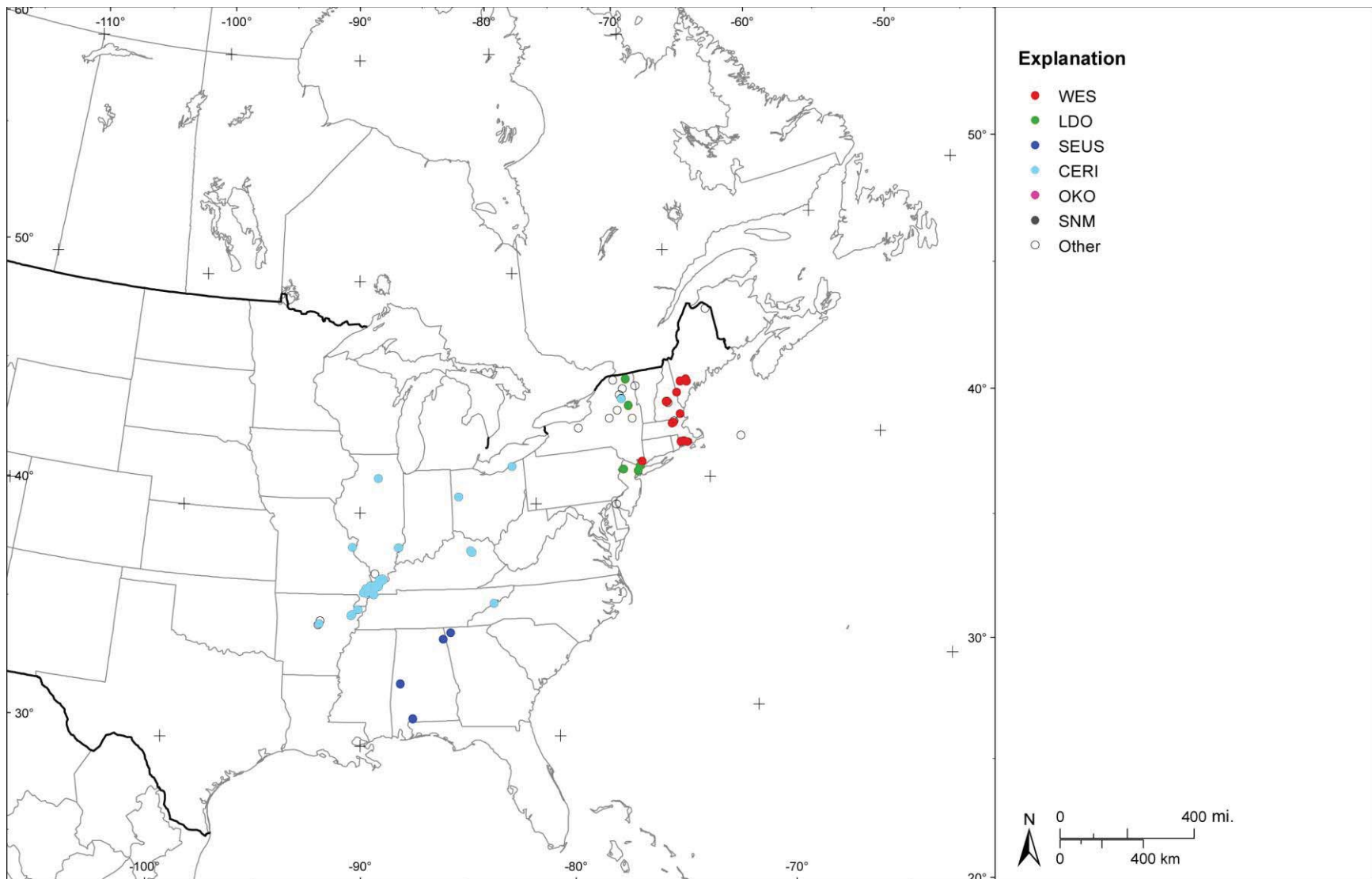


**Figure 3.3-31**  
Spatial distribution of earthquakes in the CEUS SSC Project catalog with both  $M_D$  and  $M$  magnitudes

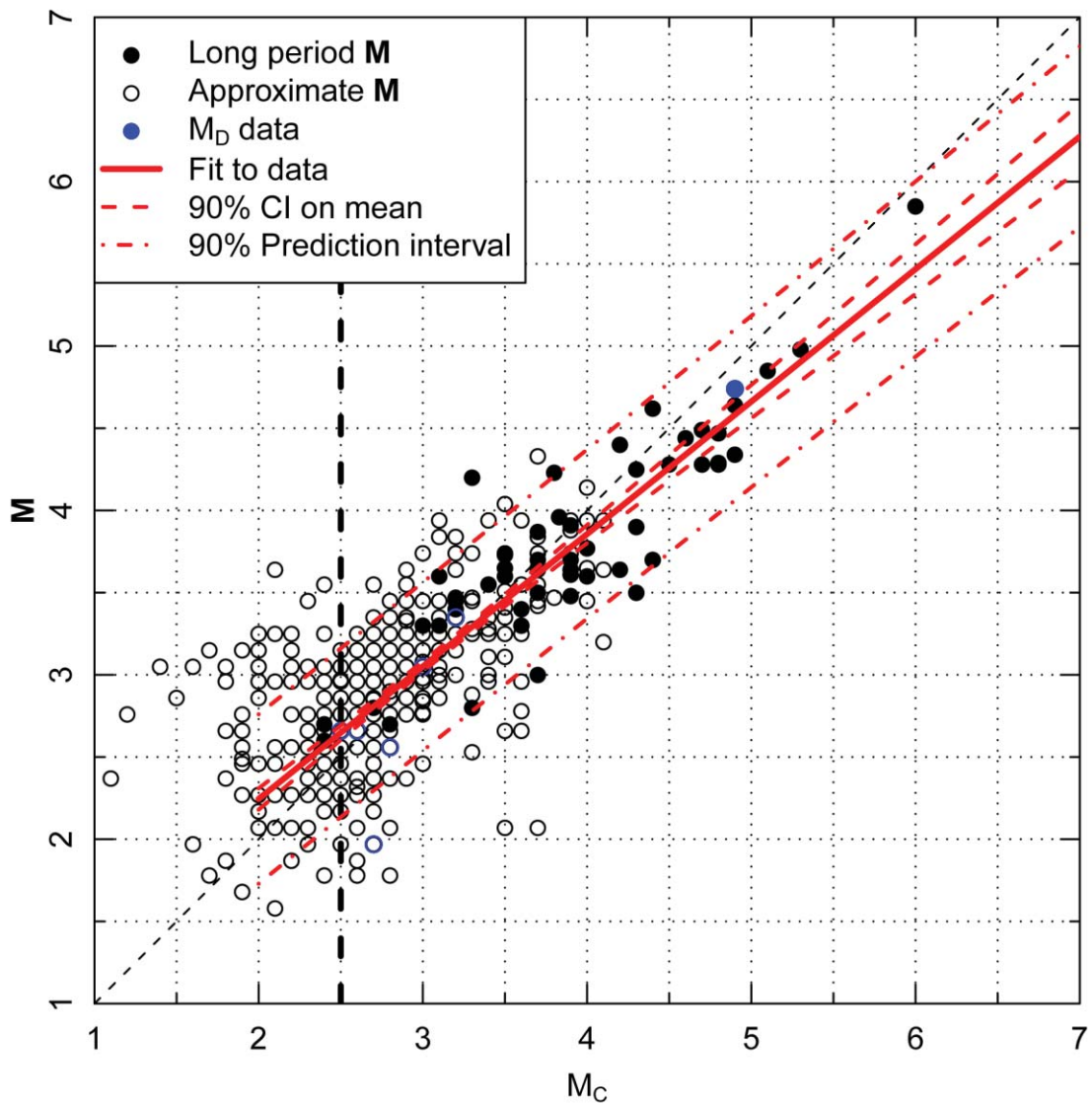
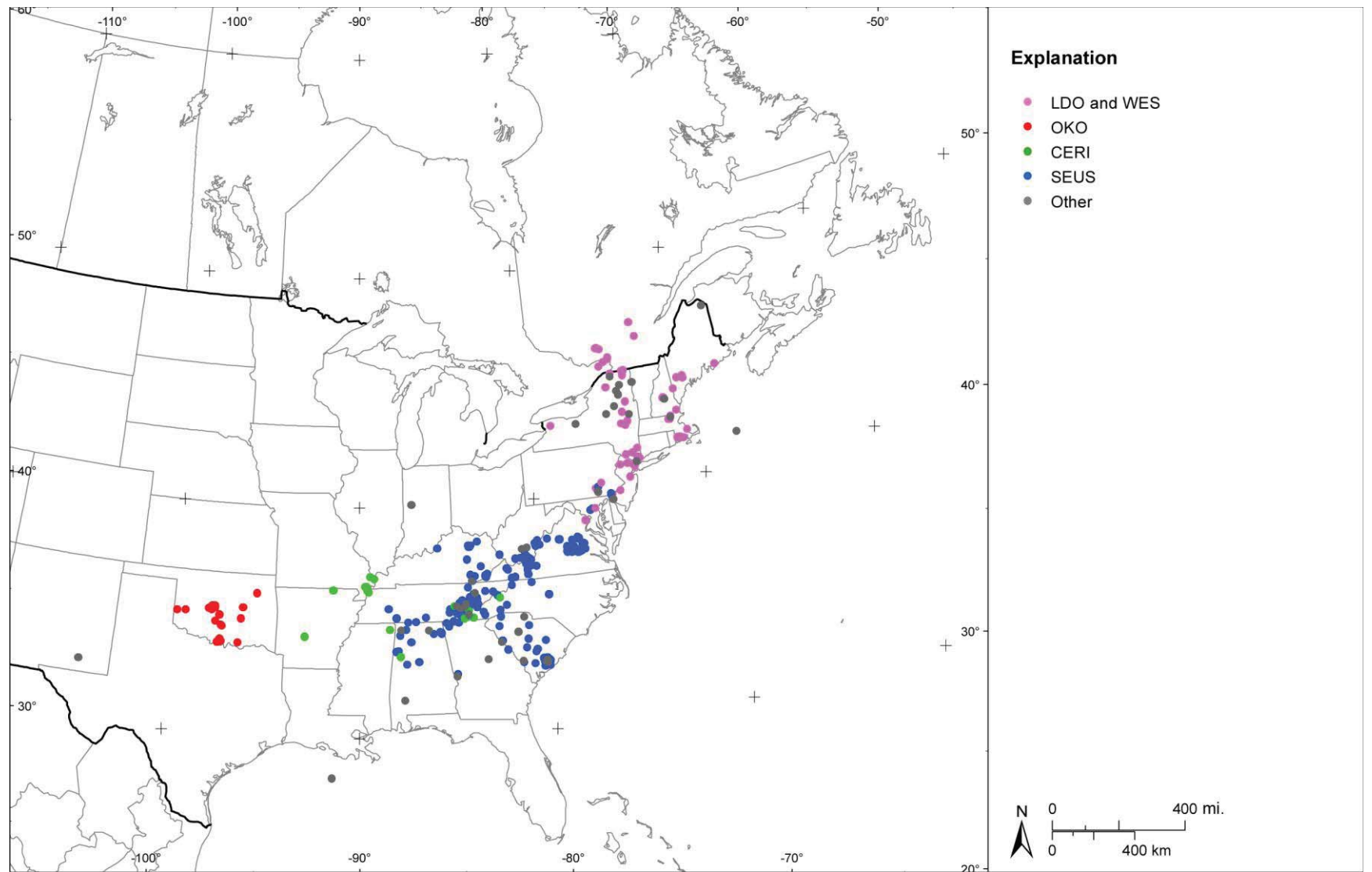


Figure 3.3-32  
 $M_C$ - $M$  data from the CEUS SSC Project catalog and linear regression fit to the data



**Figure 3.3-33**  
Spatial distribution of earthquakes with reported  $M_C$  and  $M_D$  magnitudes

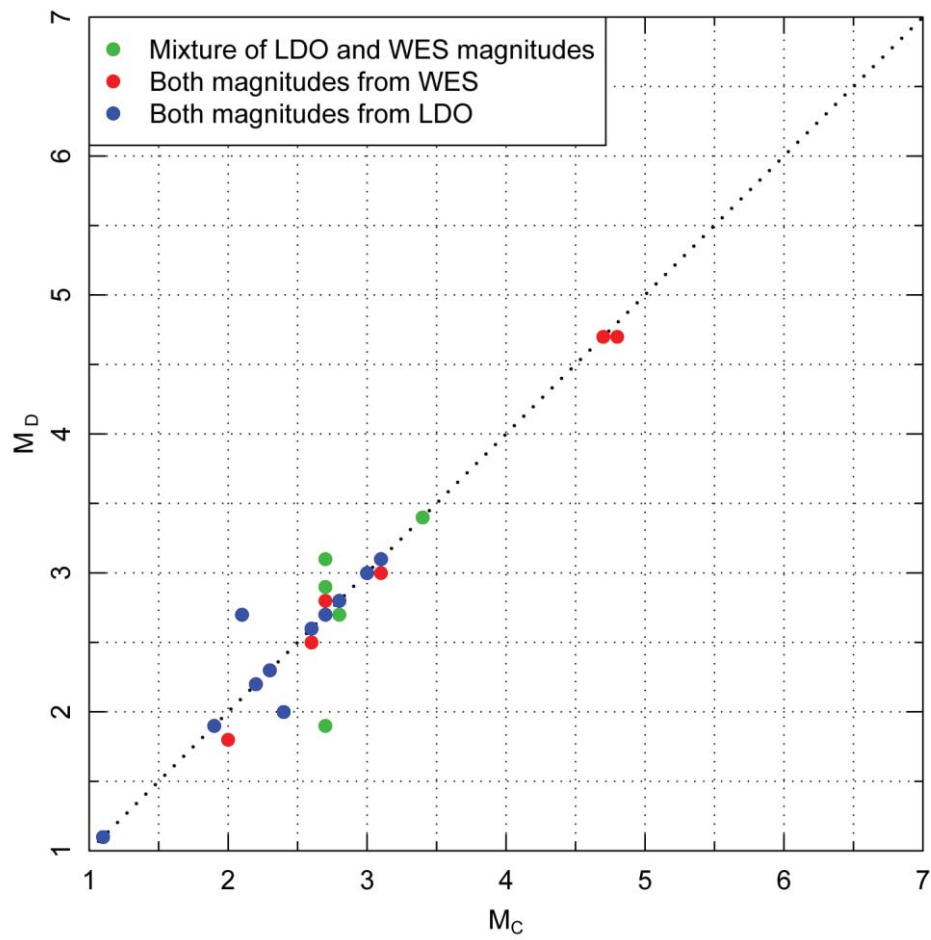
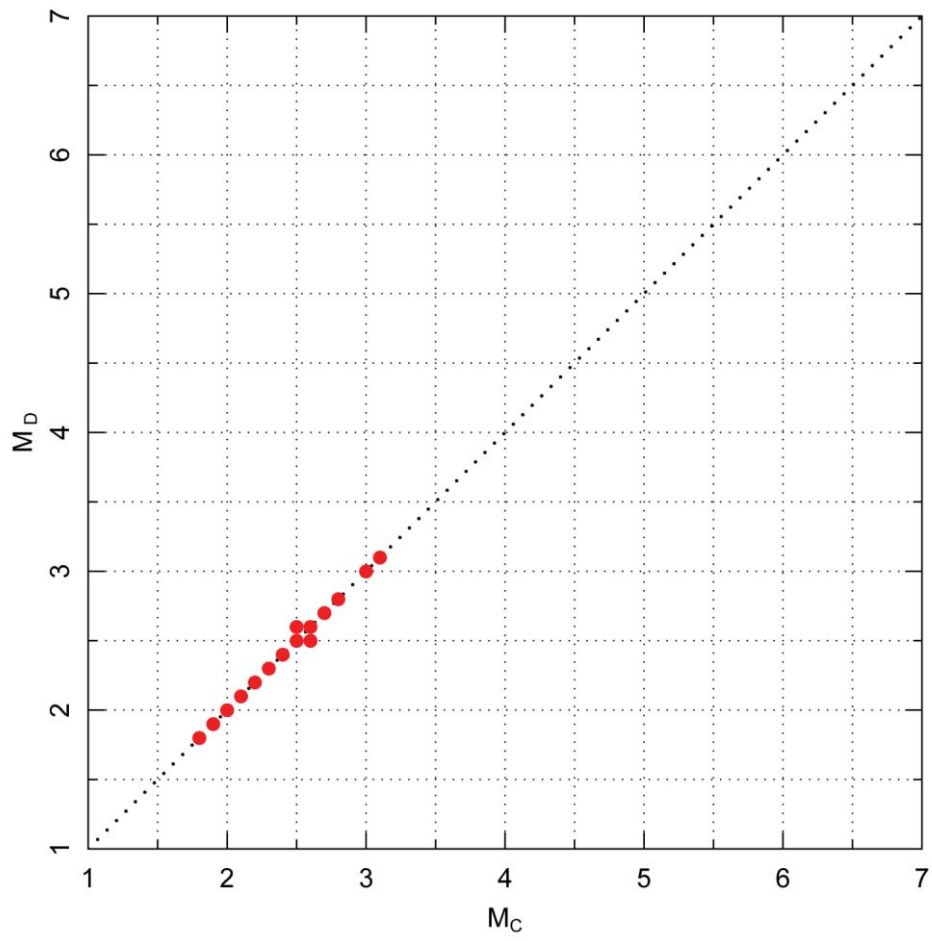
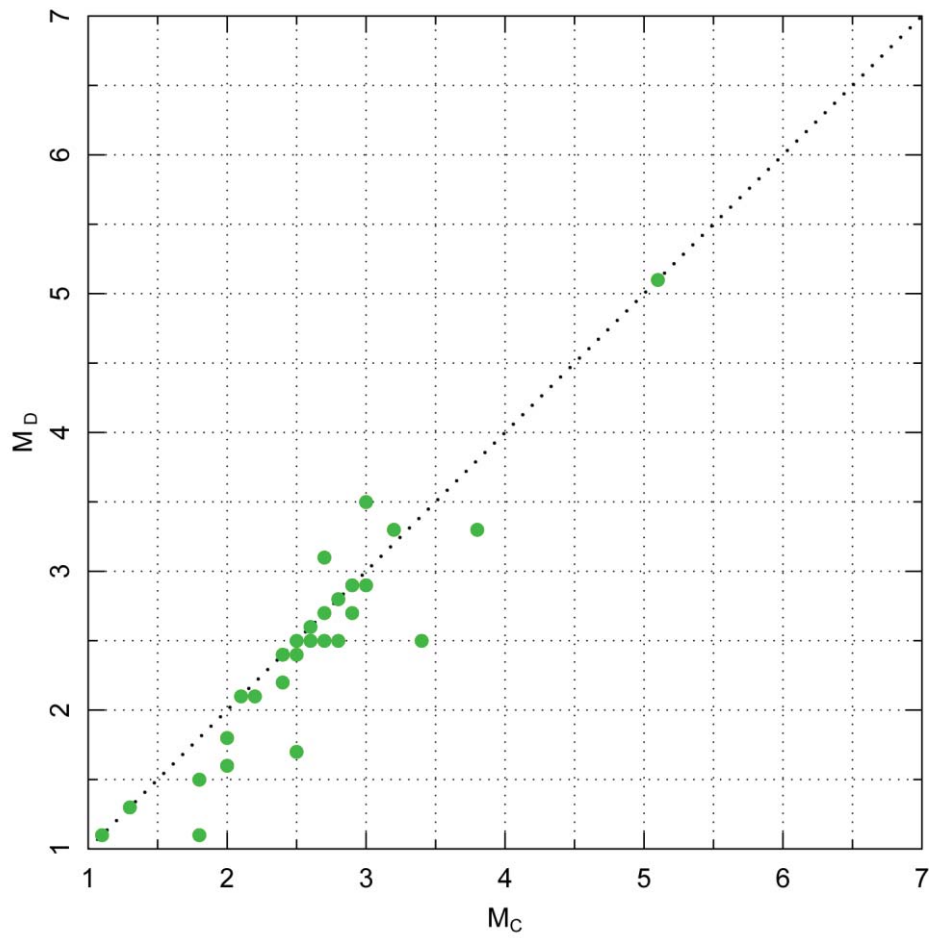


Figure 3.3-34  
Comparison of  $M_C$  and  $M_D$  magnitudes for the LDO and WES catalogs



**Figure 3.3-35**  
Comparison of  $M_C$  with  $M_D$  for at least one of the two magnitude types reported in the OKO catalog



**Figure 3.3-36**  
Comparison of  $M_C$  with  $M_D$  for at least one of the two magnitude types reported in the CERI catalog

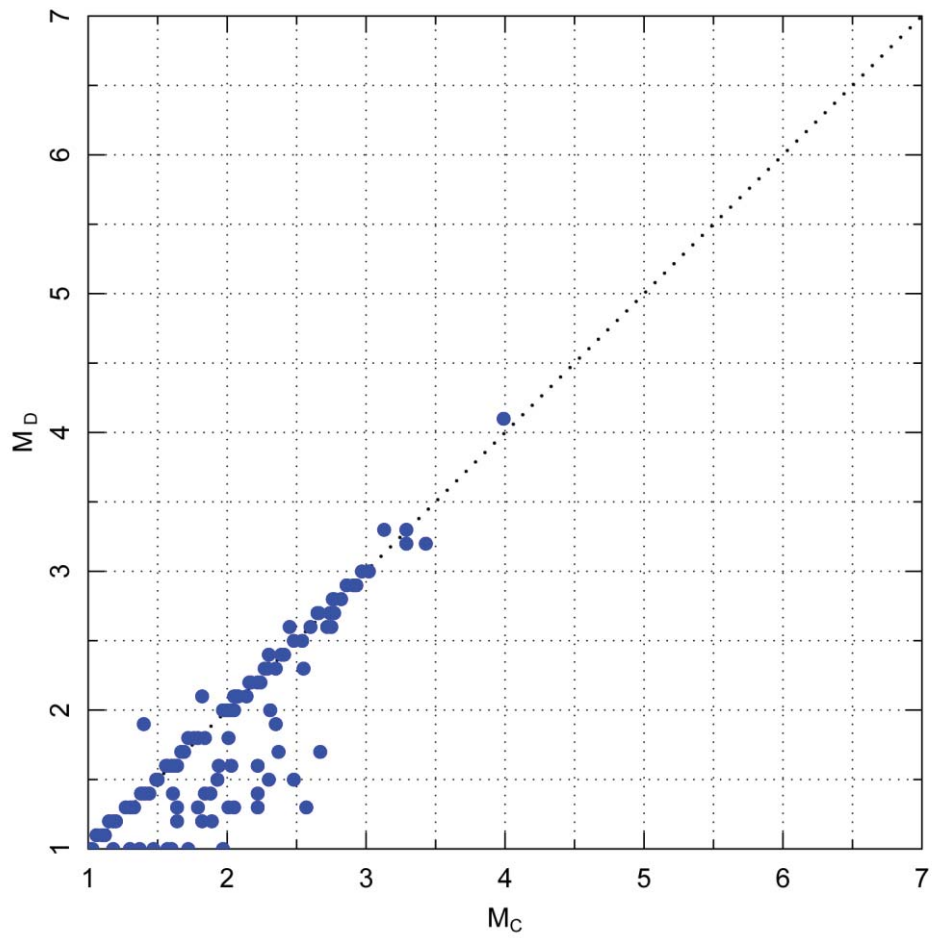


**Figure 3.3-37**  
Comparison of  $M_C$  with  $M_D$  for at least one of the two magnitude types reported in the SCSN catalog

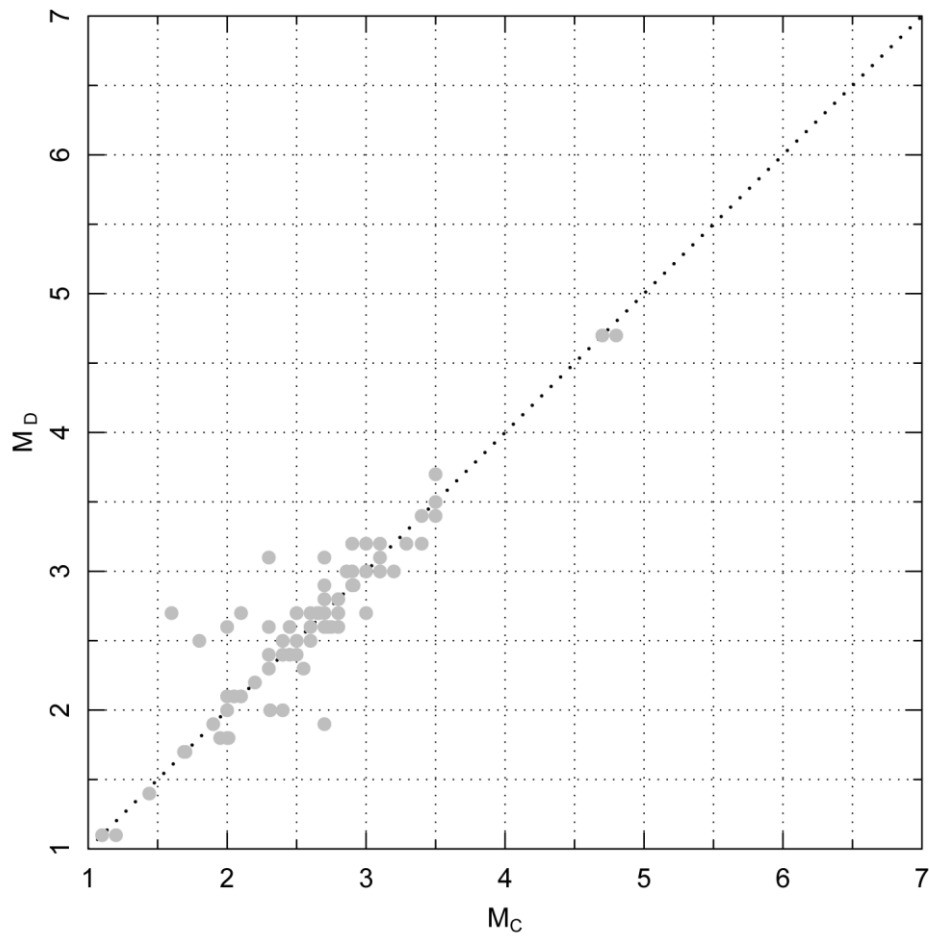


**Figure 3.3-38**  
Comparison of  $M_C$  with  $M_D$  for at least one of the two magnitude types reported in other catalogs for earthquakes in the Midcontinent portion of the study region

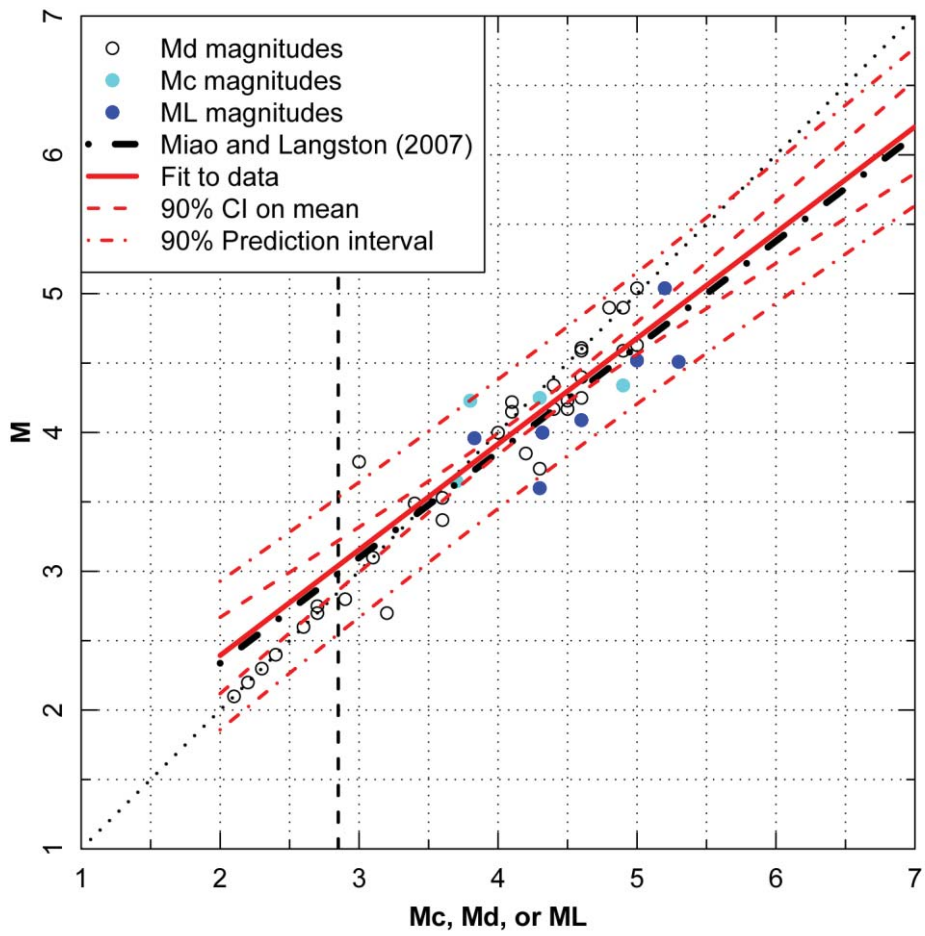


**Figure 3.3-39**  
Relationship between  $M$  and  $M_C$ ,  $M_D$ , or  $M_L$  for the Midcontinent portion of the study region

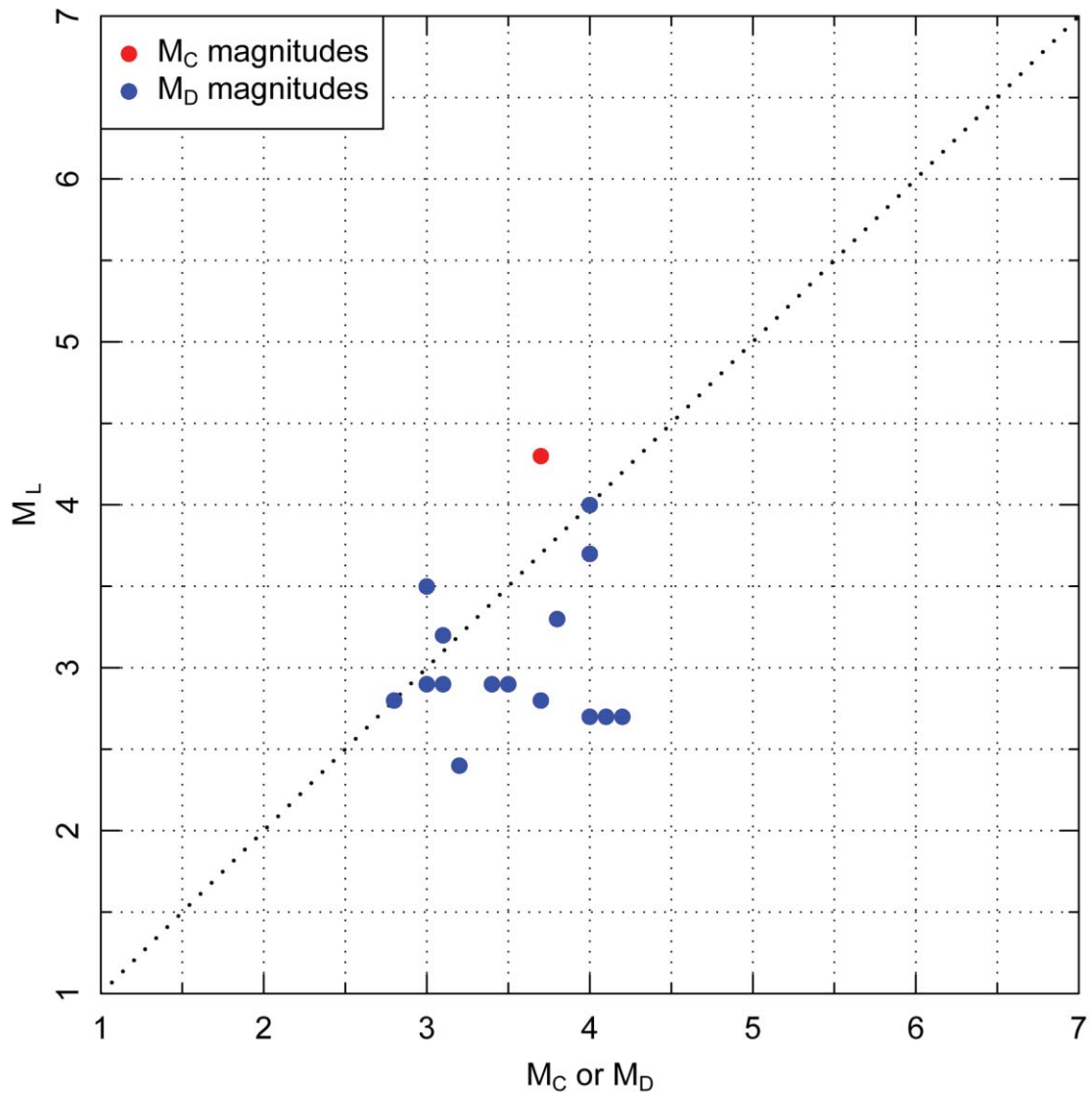
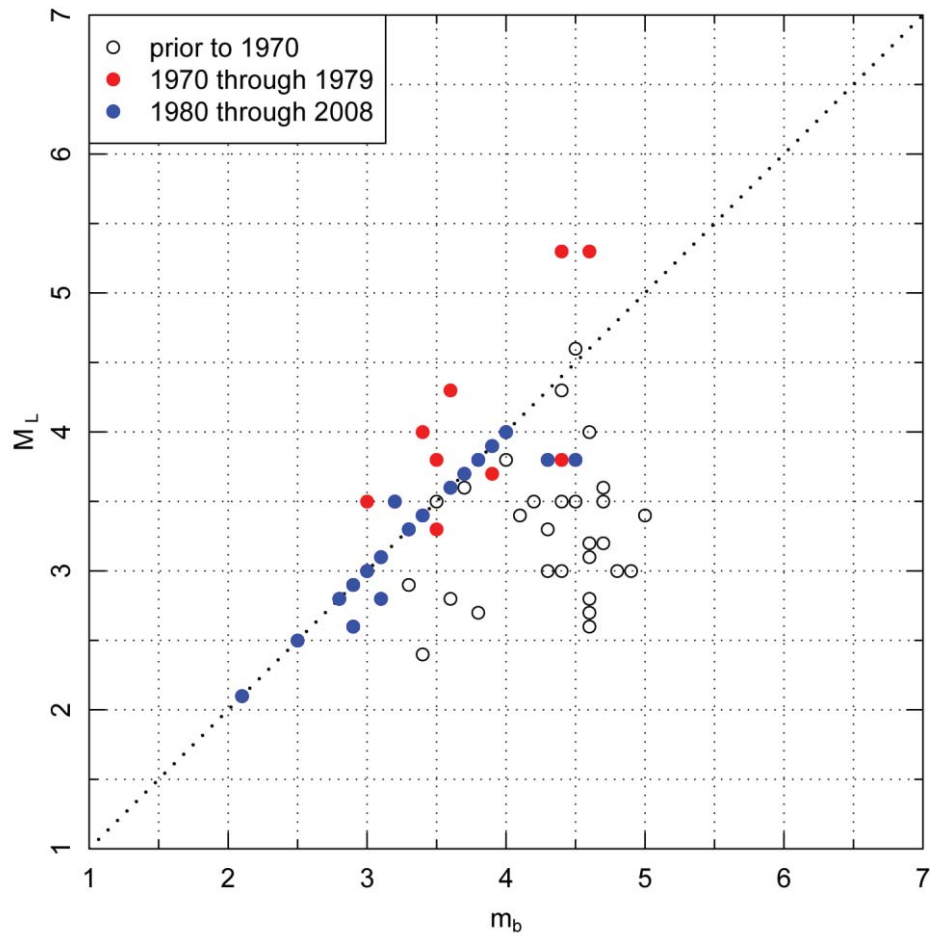


Figure 3.3-40  
Comparison of  $M_C$  and  $M_D$  magnitudes with  $M_L$  magnitudes for the region between longitudes  $105^\circ\text{W}$  and  $100^\circ\text{W}$



**Figure 3.3-41**  
Comparison of  $m_b$  magnitudes with  $M_L$  magnitudes for the region between longitudes 105°W and 100°W

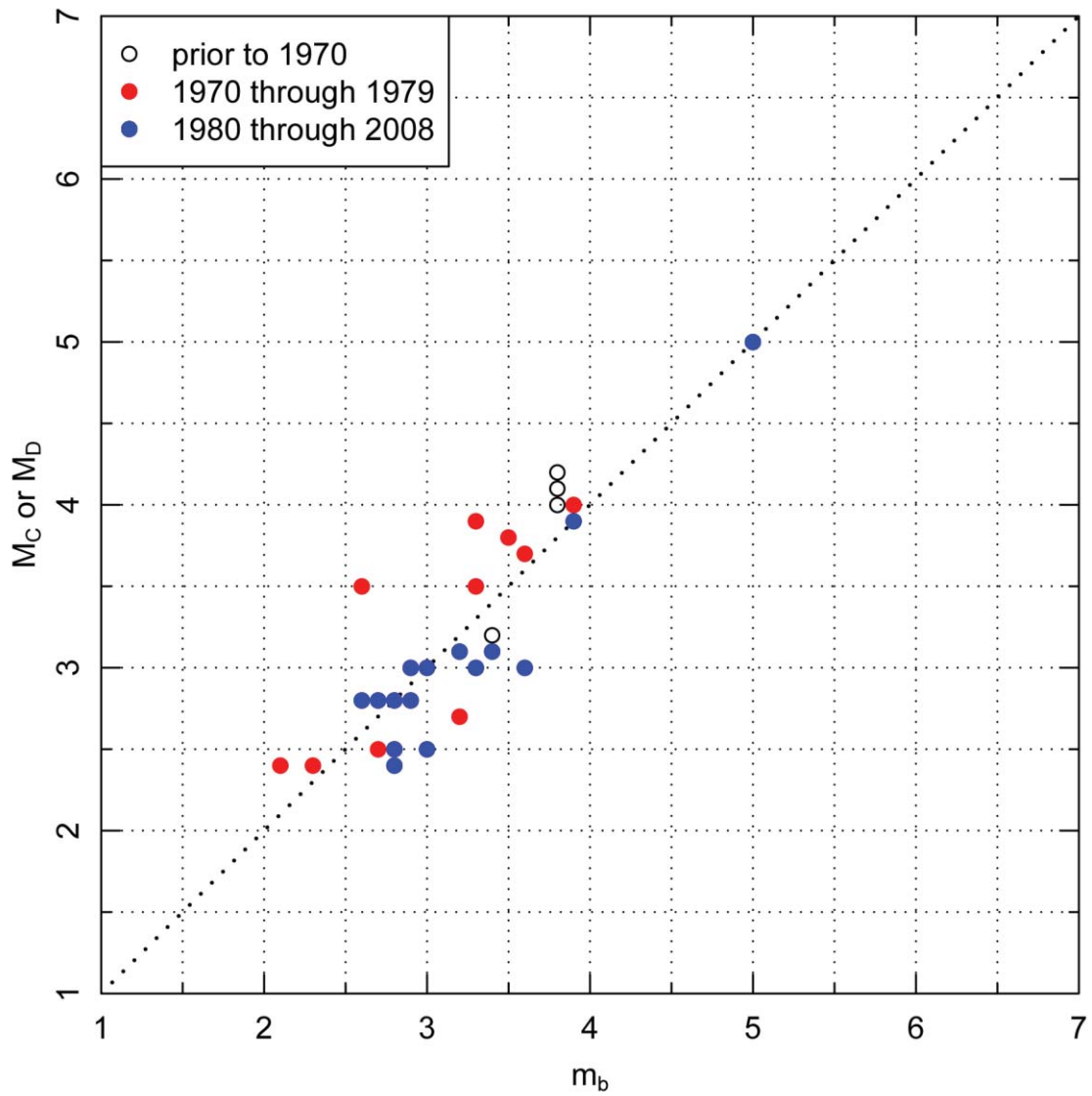
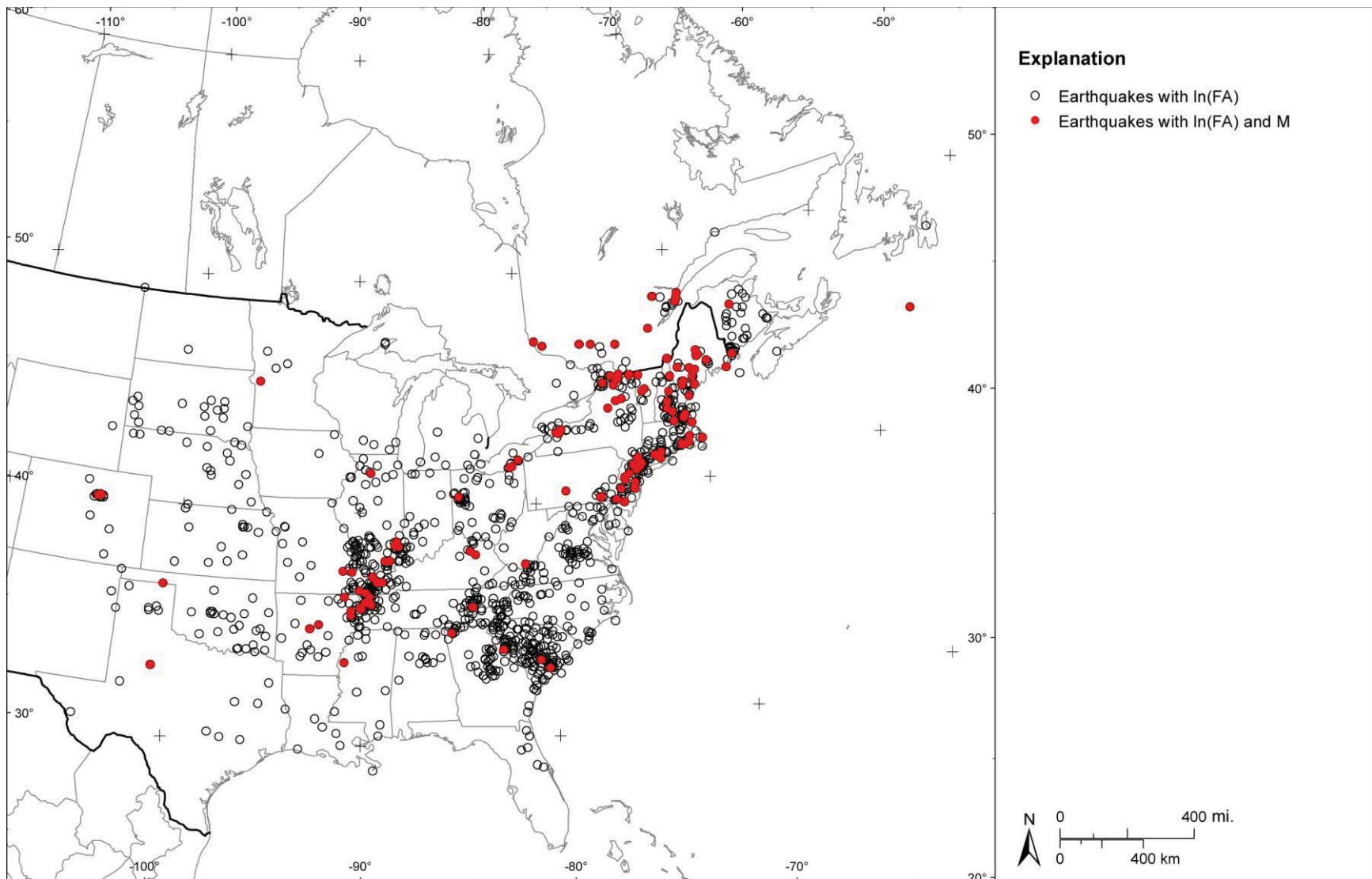


Figure 3.3-42  
Comparison of  $m_b$  magnitudes with  $M_c$  and  $M_D$  magnitudes for the region between longitudes 105°W and 100°W



**Figure 3.3-43**  
Spatial distribution of earthquake with In(FA) in the CEUS SSC Project catalog

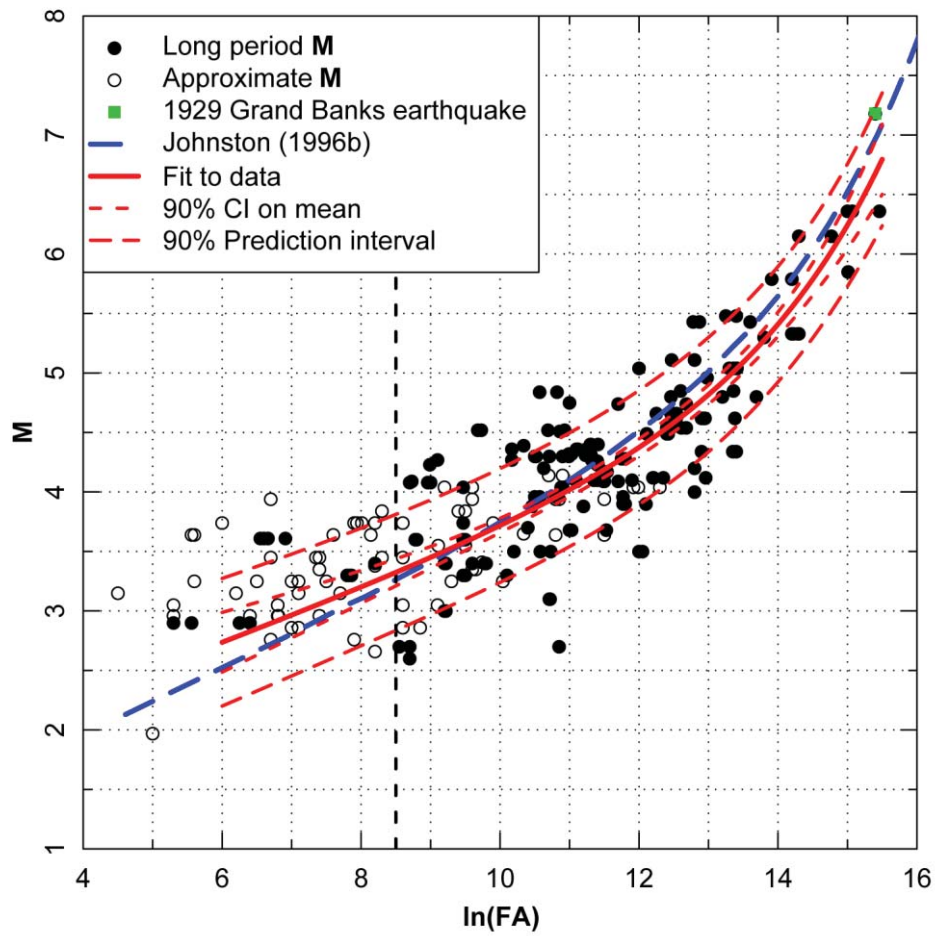
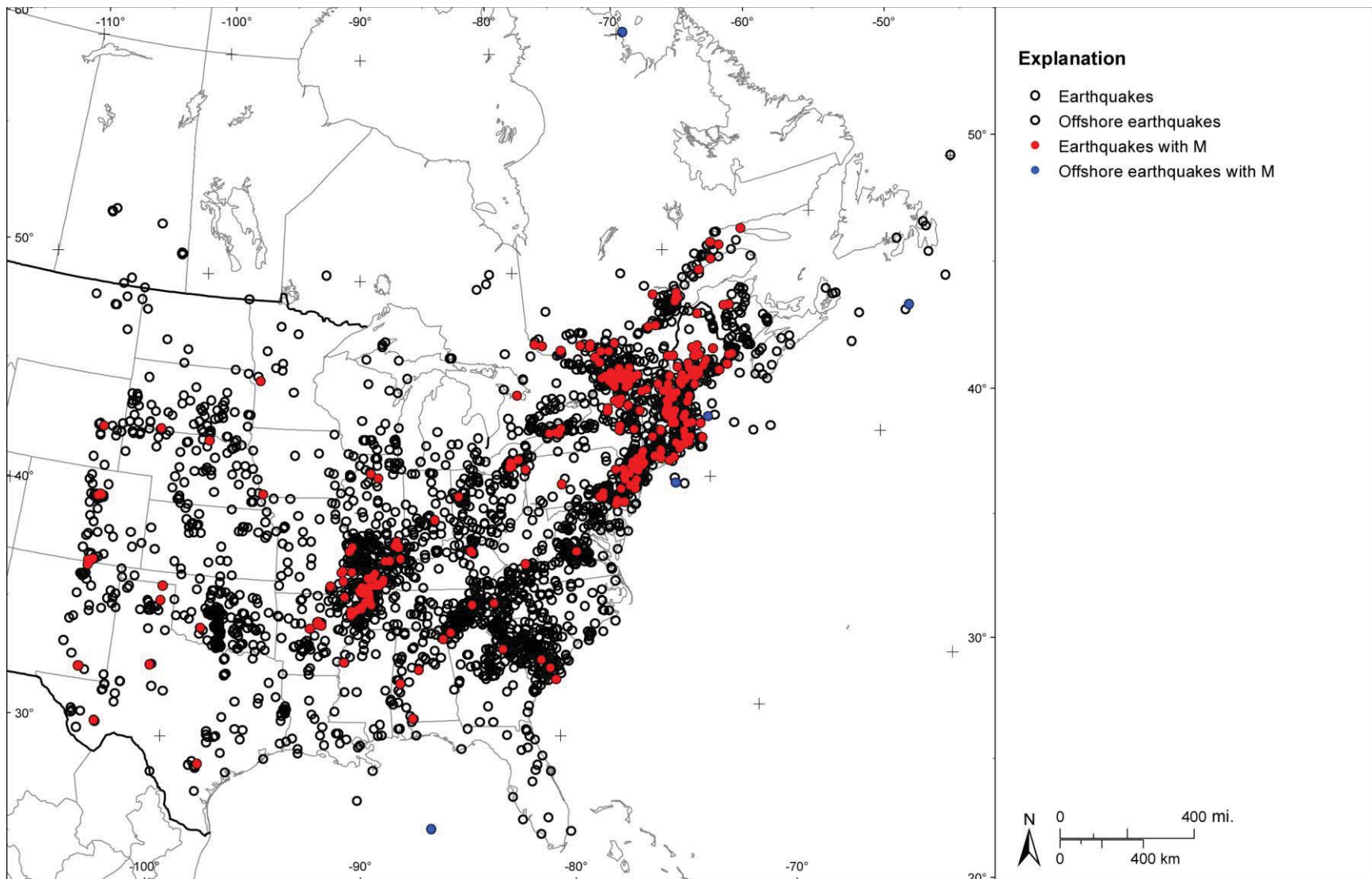
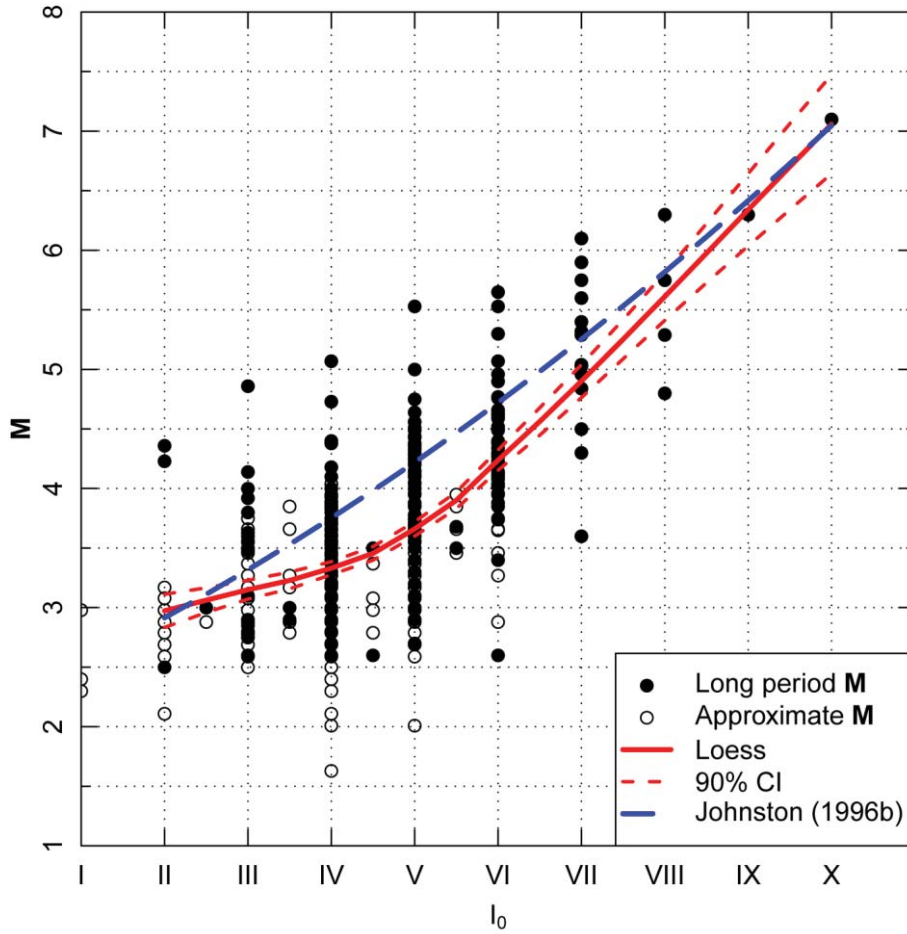


Figure 3.3-44  
Catalog  $\ln(FA)$ - $M$  data and fitted model



**Figure 3.3-45**  
Spatial distribution of earthquakes in the CEUS SSC Project catalog with reported values of  $I_0$



**Figure 3.3-46**  
**I<sub>0</sub> and M data for earthquakes in the CEUS SSC Project catalog. Curves show locally weighted least-squares fit (Loess) to the data and the relationship published by Johnston (1996b).**

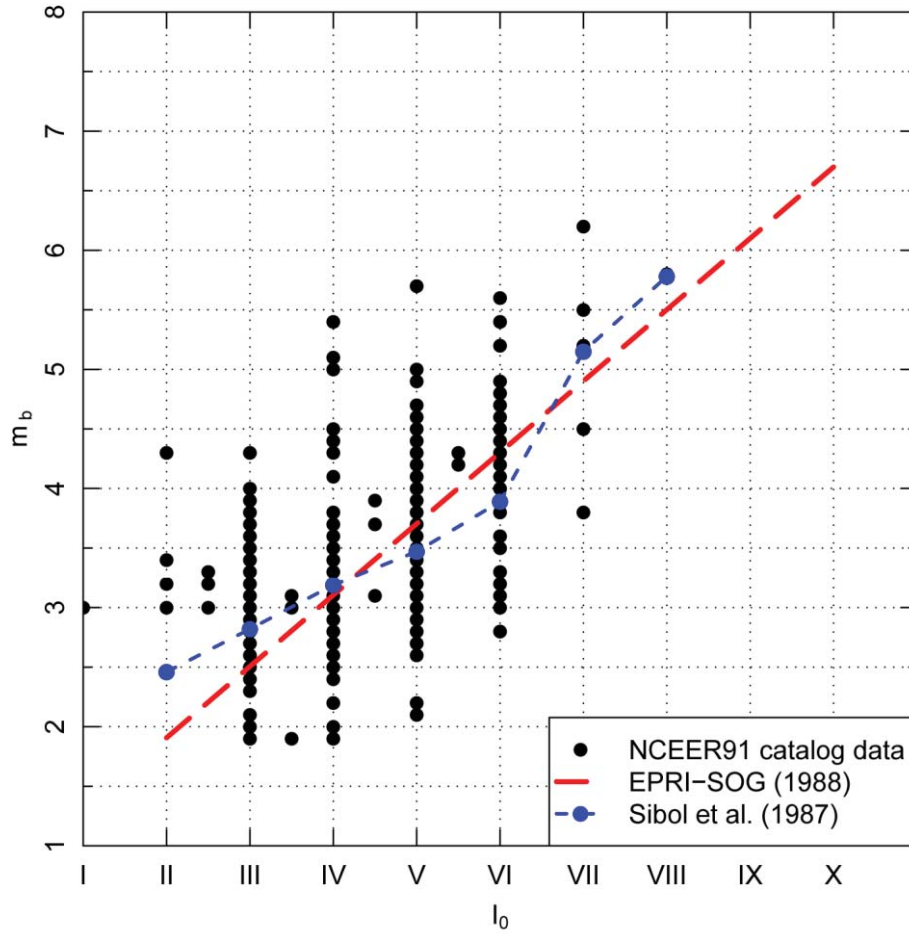


**Figure 3.3-47**  
 $I_0$  and  $m_b$  data from the NCEER91 catalog. Plotted are the relationships between  $I_0$  and  $m_b$  developed by EPRI (1988) (EPRI-SOG) and Sibol et al. (1987).

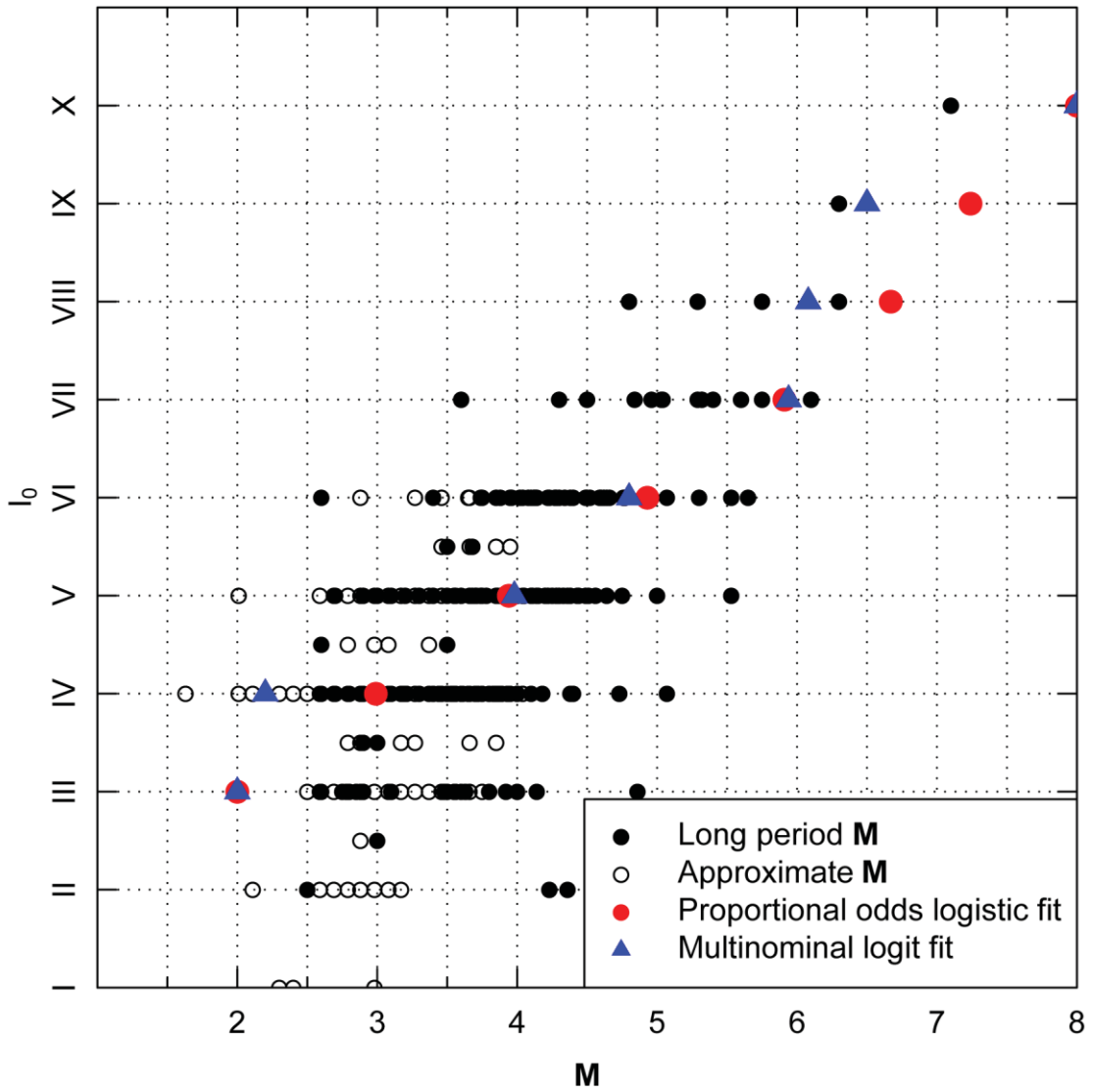
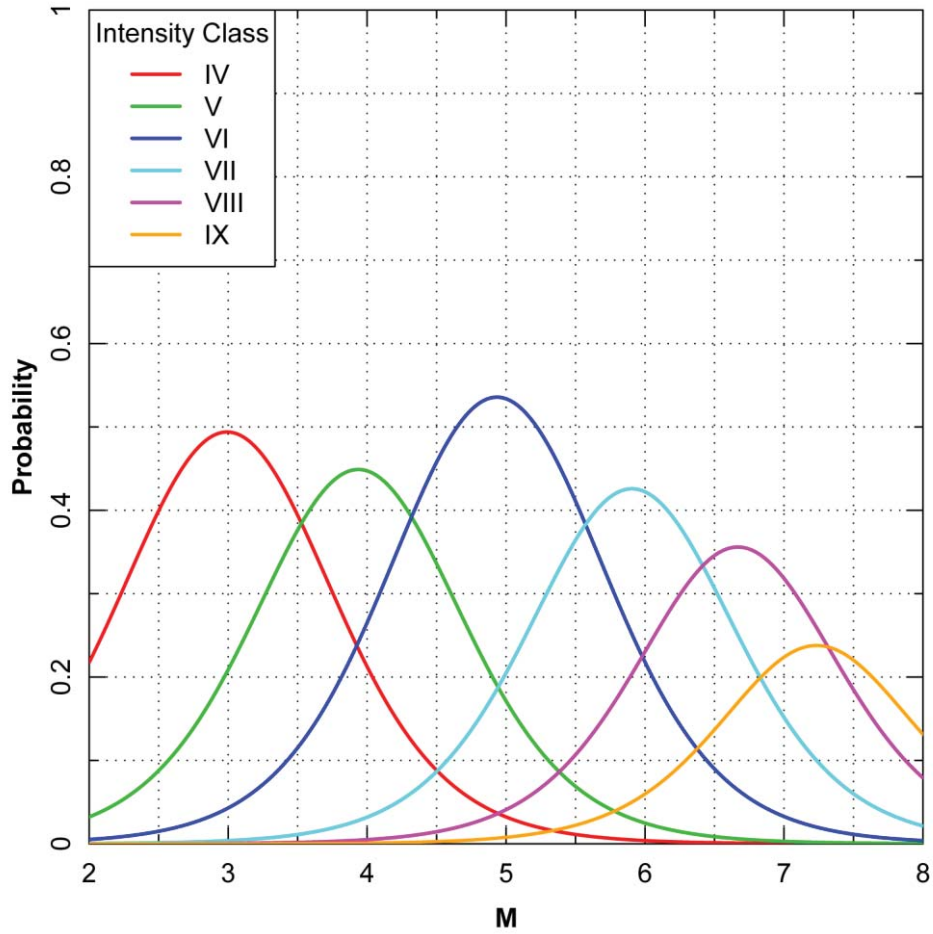
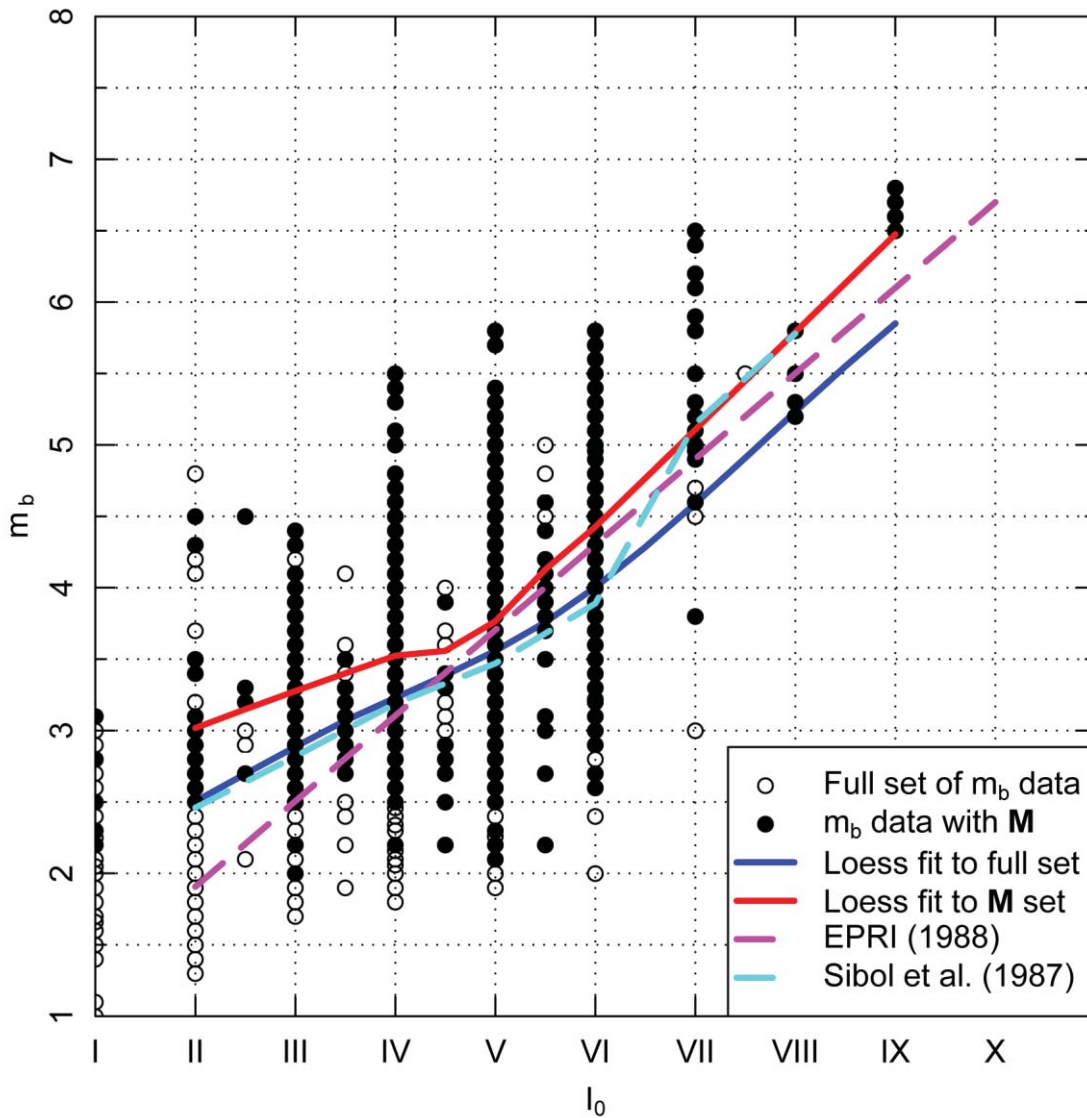


Figure 3.3-48  
Categorical model fits of  $I_0$  as a function and  $M$  for earthquakes in the CEUS SSC Project catalog



**Figure 3.3-49**  
Results from proportional odds logistic model showing the probability of individual intensity classes as a function of M



**Figure 3.3-50**  
Comparison of  $I_0$  and  $m_b$  data from the CEUS SSC Project catalog for those earthquakes with reported values of  $M$  ( $M$  set) and the full catalog (full set). Locally weighted least-squares fits to the two data sets are shown along with the relationship use to develop the EPRI (1988) catalog and the Sibol et al. (1987) relationship used in the NCEER91 catalog.

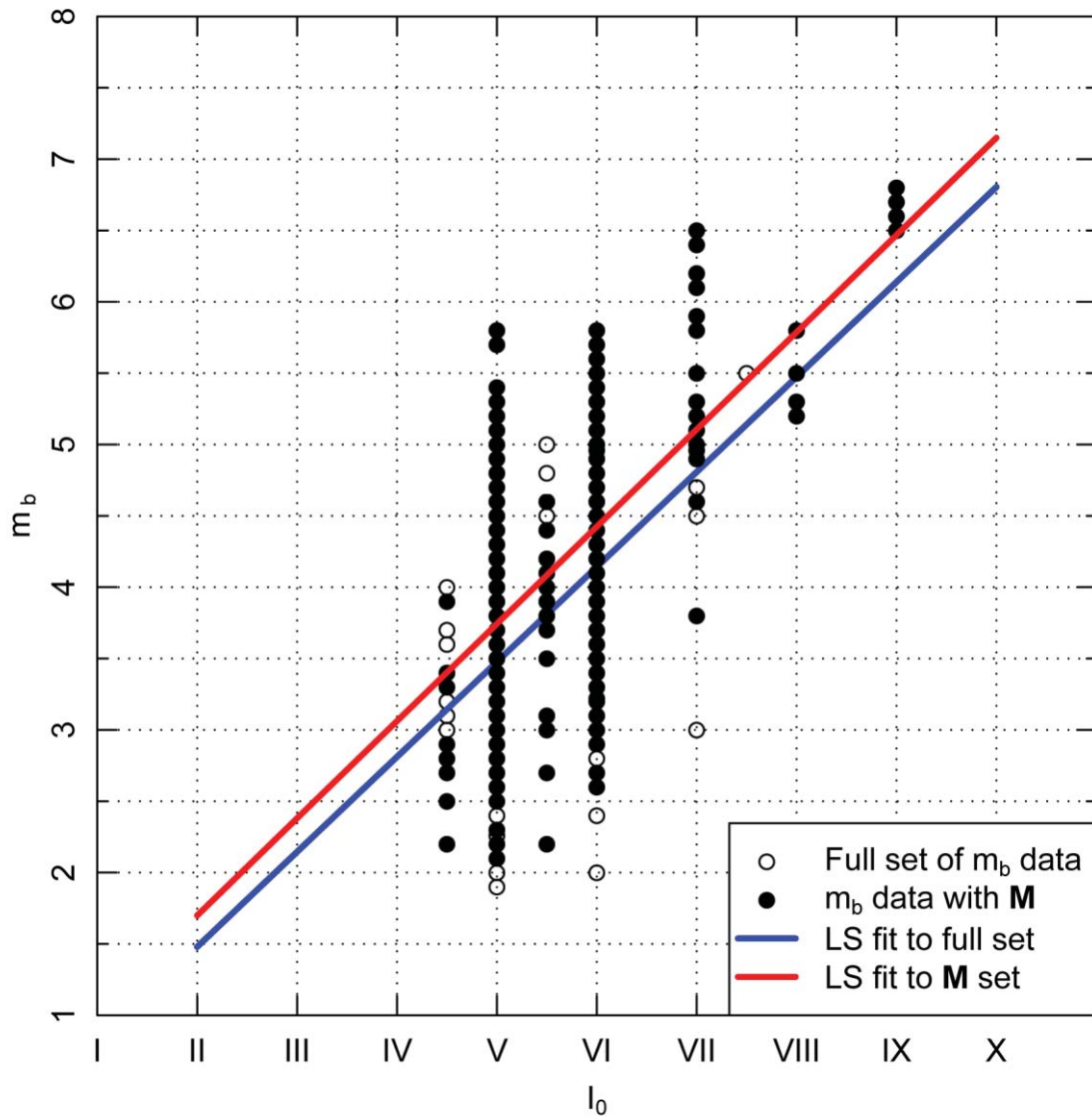


Figure 3.3-51  
Linear fits to the data from Figure 3.3-50 for  $I_0 \geq V$

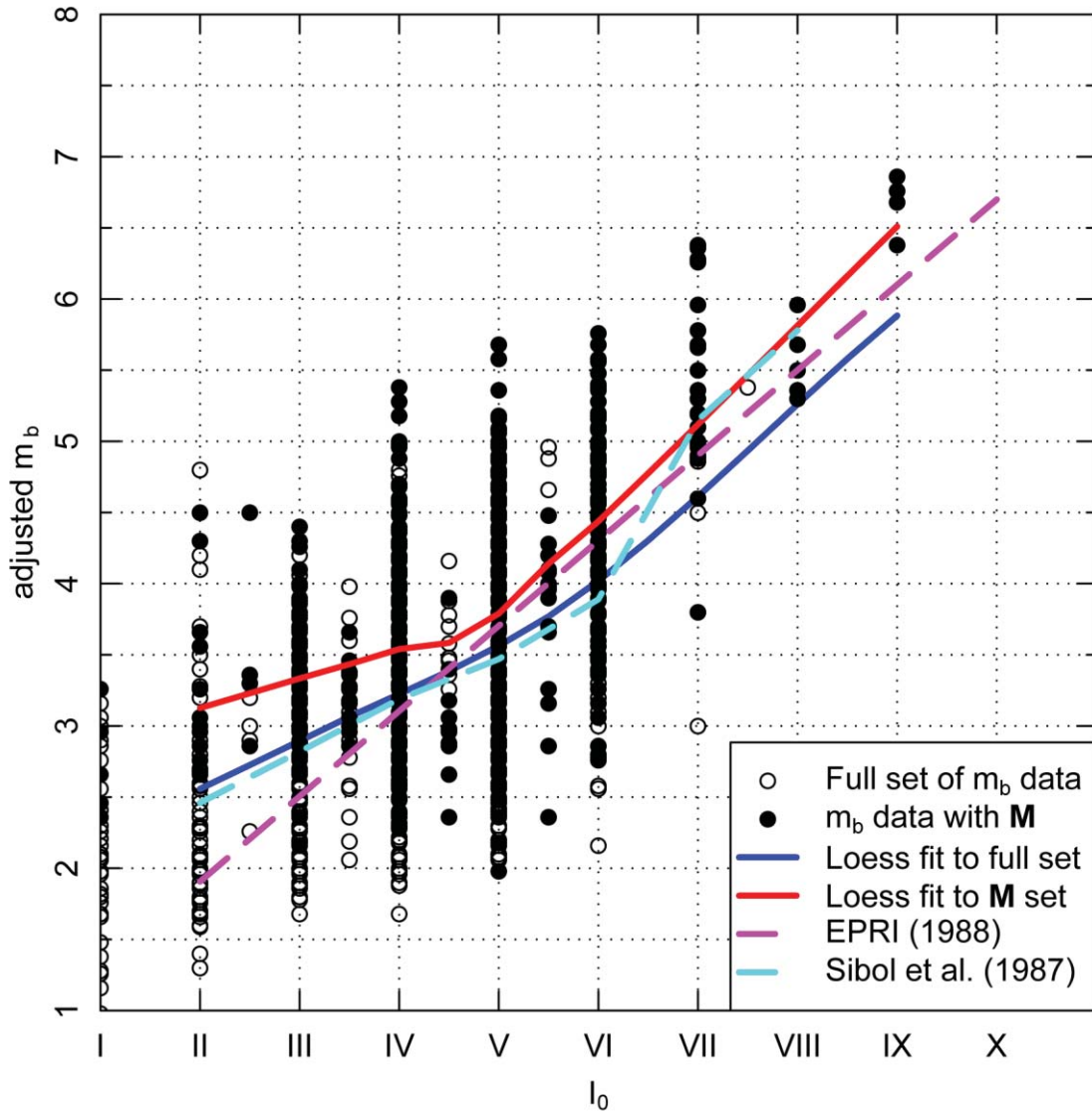


Figure 3.3-52  
Comparison of  $I_0$  and  $m_b$  data from the project, with  $m_b$  adjusted for the difference in  $m_b$  to  $M$  scaling

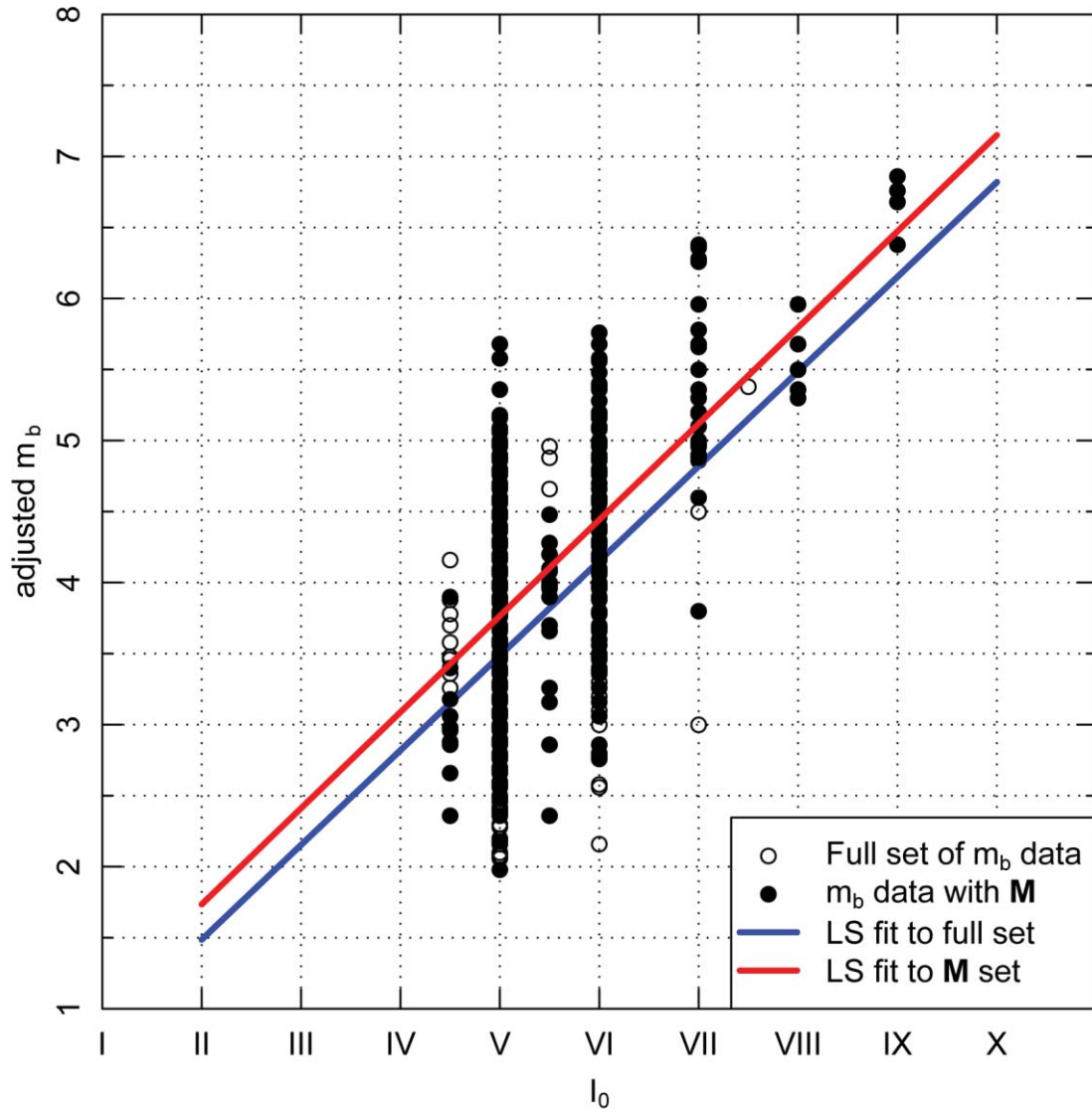


Figure 3.3-53  
Linear fits to the data from Figure 3.3-52 for  $I_0 \geq V$

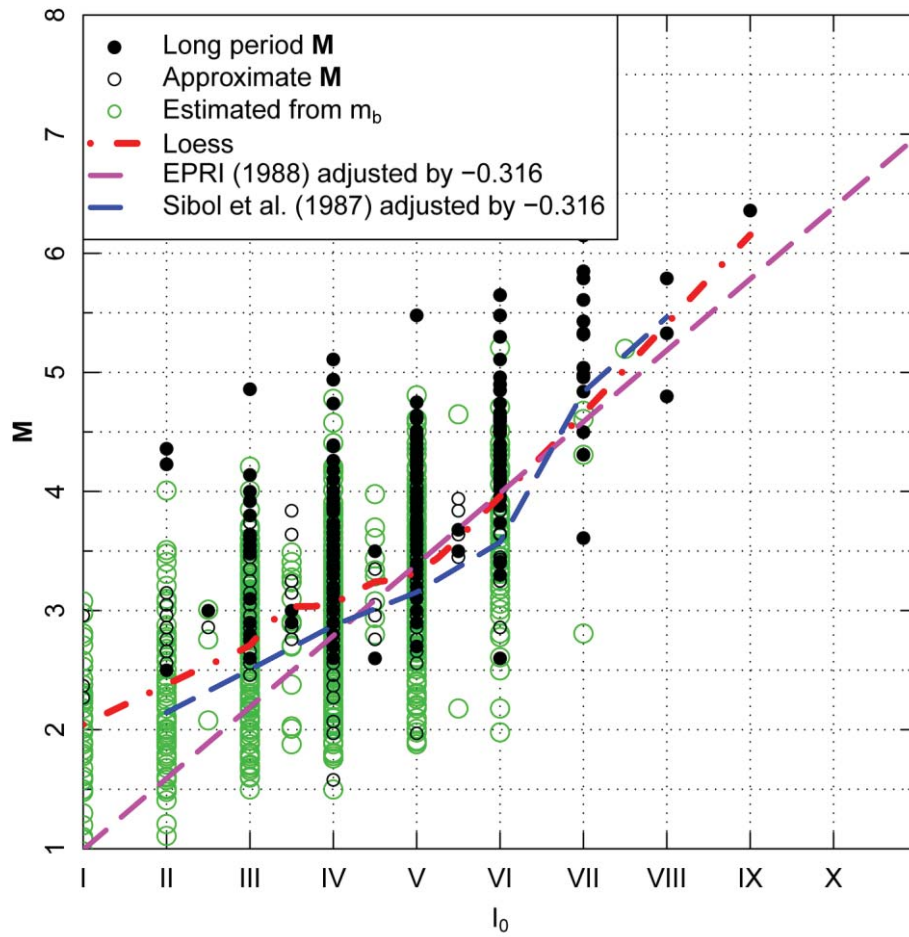
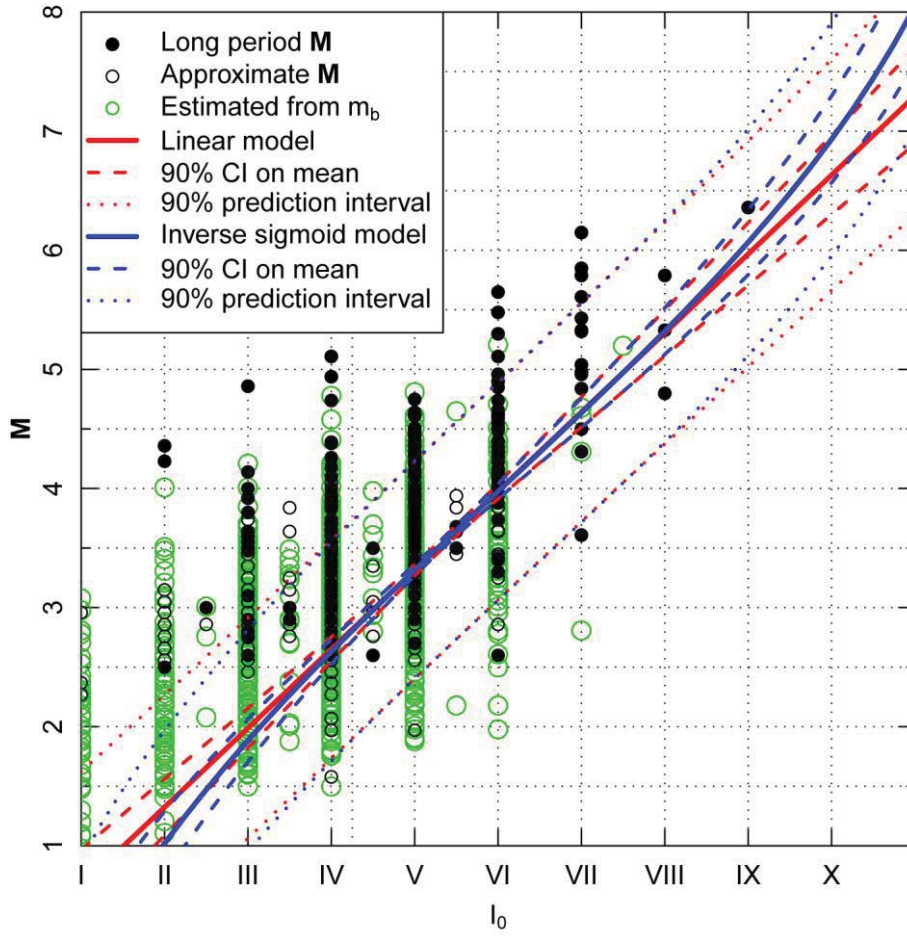
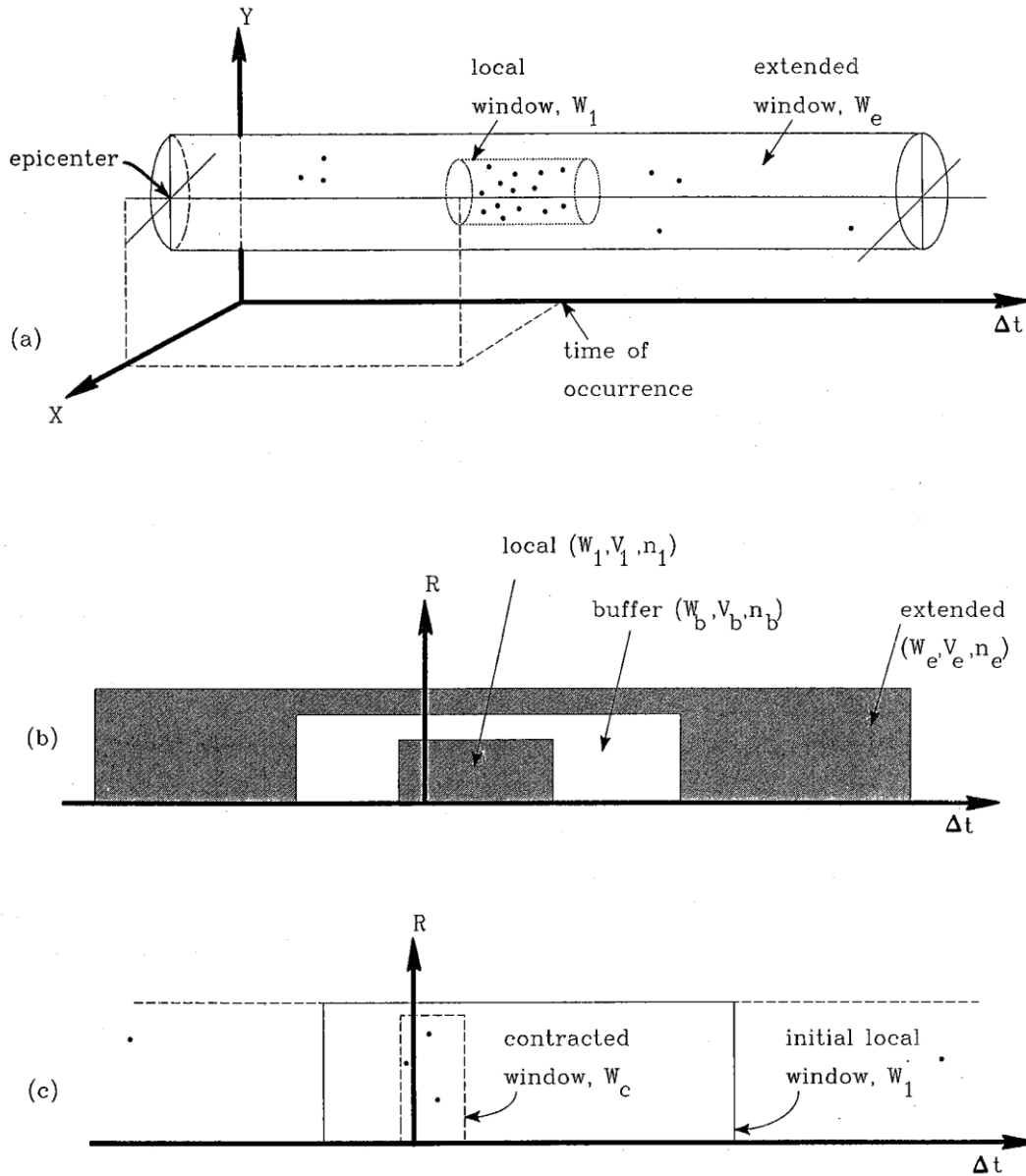


Figure 3.3-54  
Composite I<sub>0</sub>-M data set used for assessment of I<sub>0</sub> scaling relationship



**Figure 3.3-55**  
Linear and inverse sigmoid models fit to the project data for  $I_0 > IV$



**Figure 3.4-1**  
Illustration of process used to identify clusters of earthquakes (from EPRI, 1988, Vol. 1):  
(a) local and extended time and distance windows, (b) buffer window, and (c) contracted window

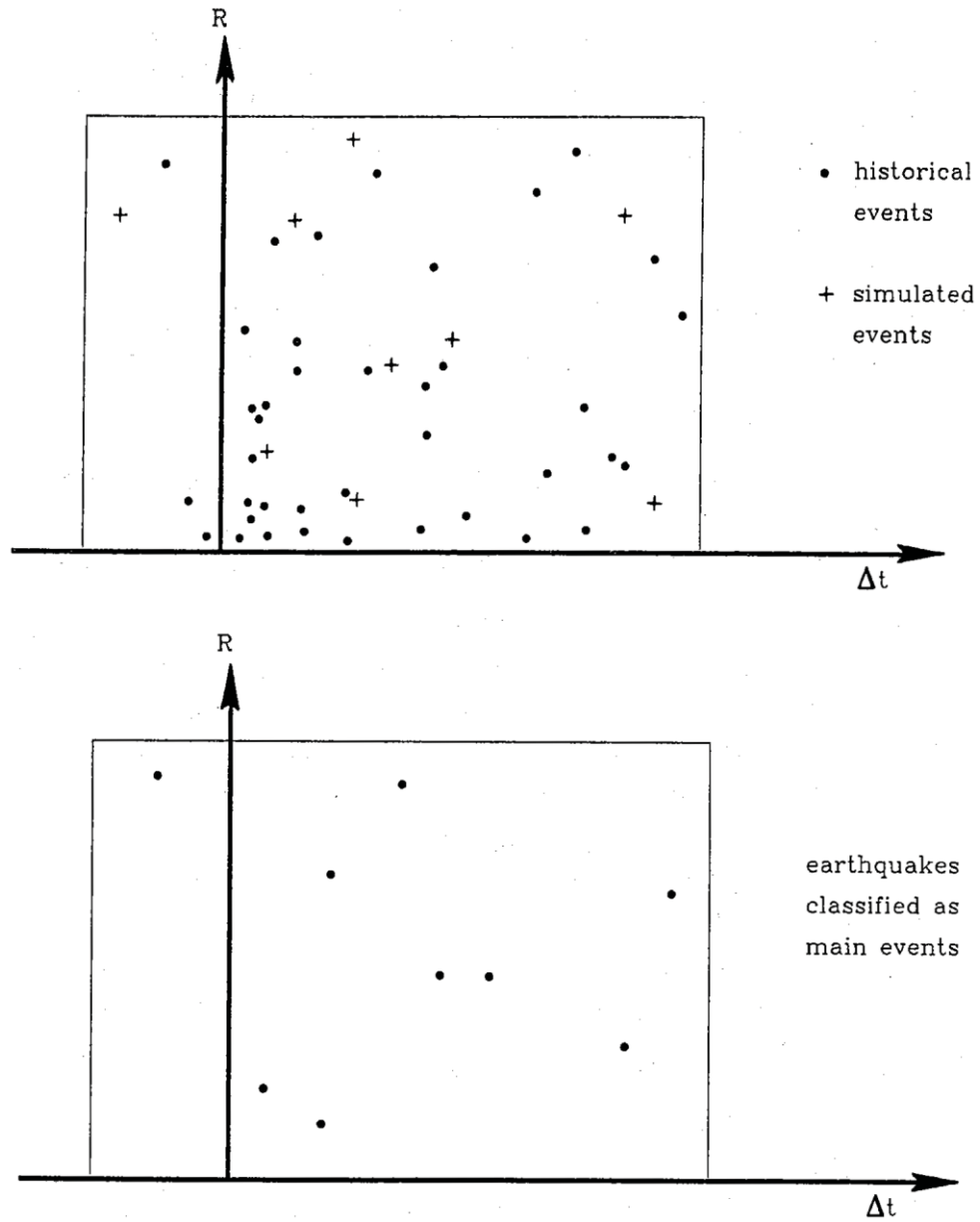


**Figure 3.4-2**  
Identification of secondary (dependent) earthquakes inside the cluster region through Poisson thinning (from EPRI, 1988, Vol. 1)

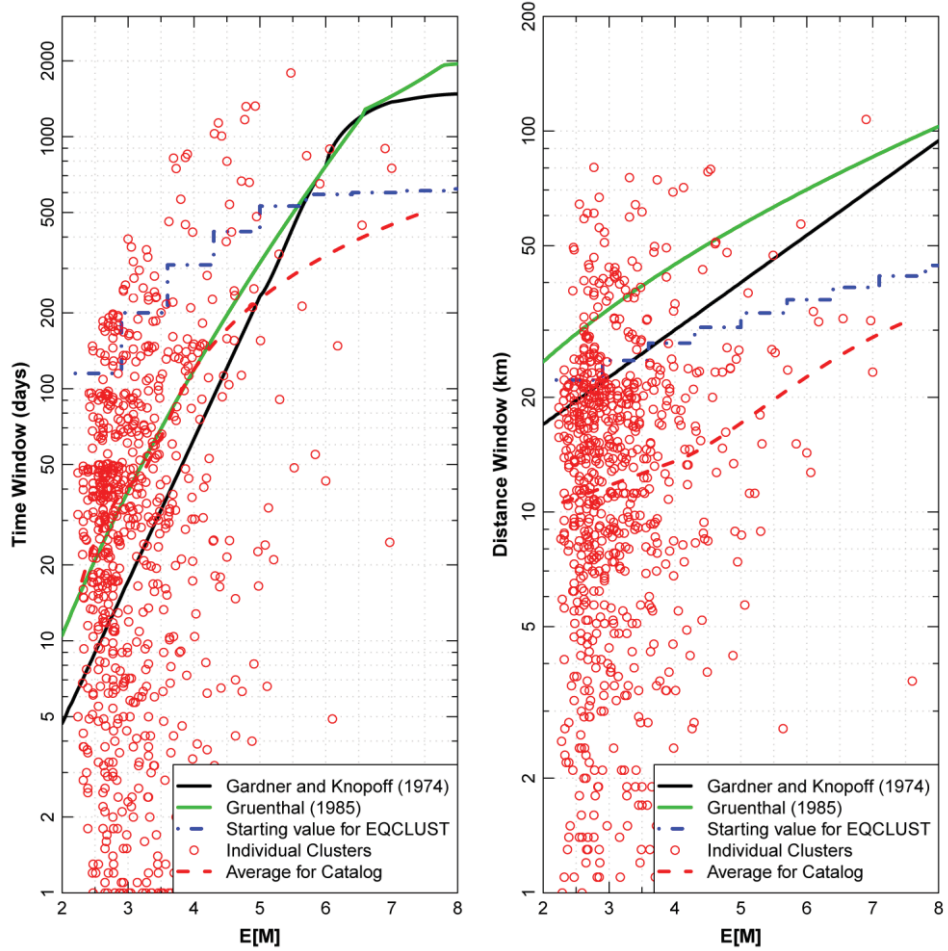


**Figure 3.4-3**  
**Comparison of dependent event time and distance windows with results for individual clusters in the project catalog**

Note: Time windows represent the sum of the foreshock and aftershock windows for Grünthal (1985) and 1.5 times the aftershock window for Gardner and Knopoff (1974).

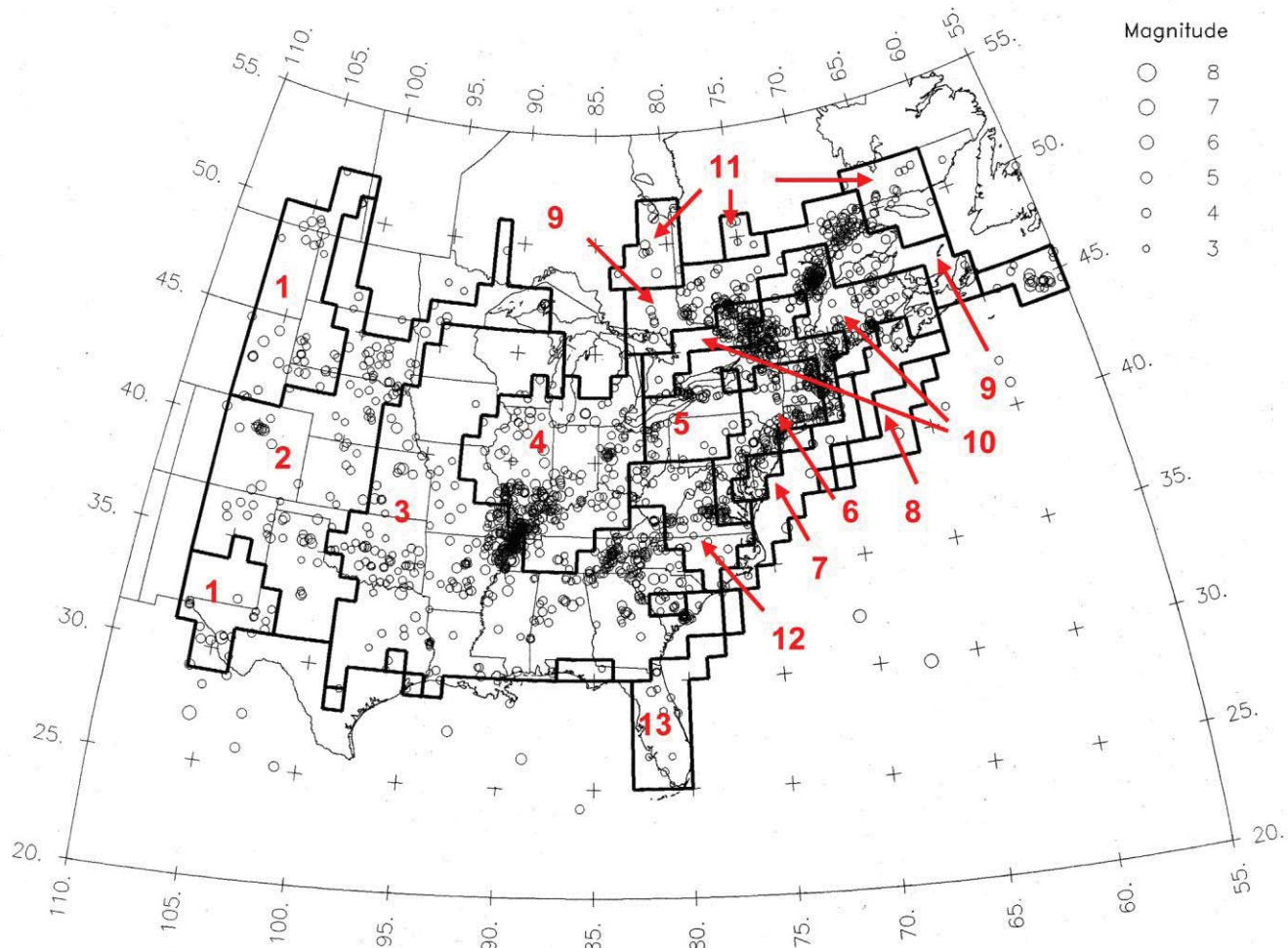


**Figure 3.5-1**  
Earthquake catalog and catalog completeness regions used in EPRI-SOG (EPRI, 1988)

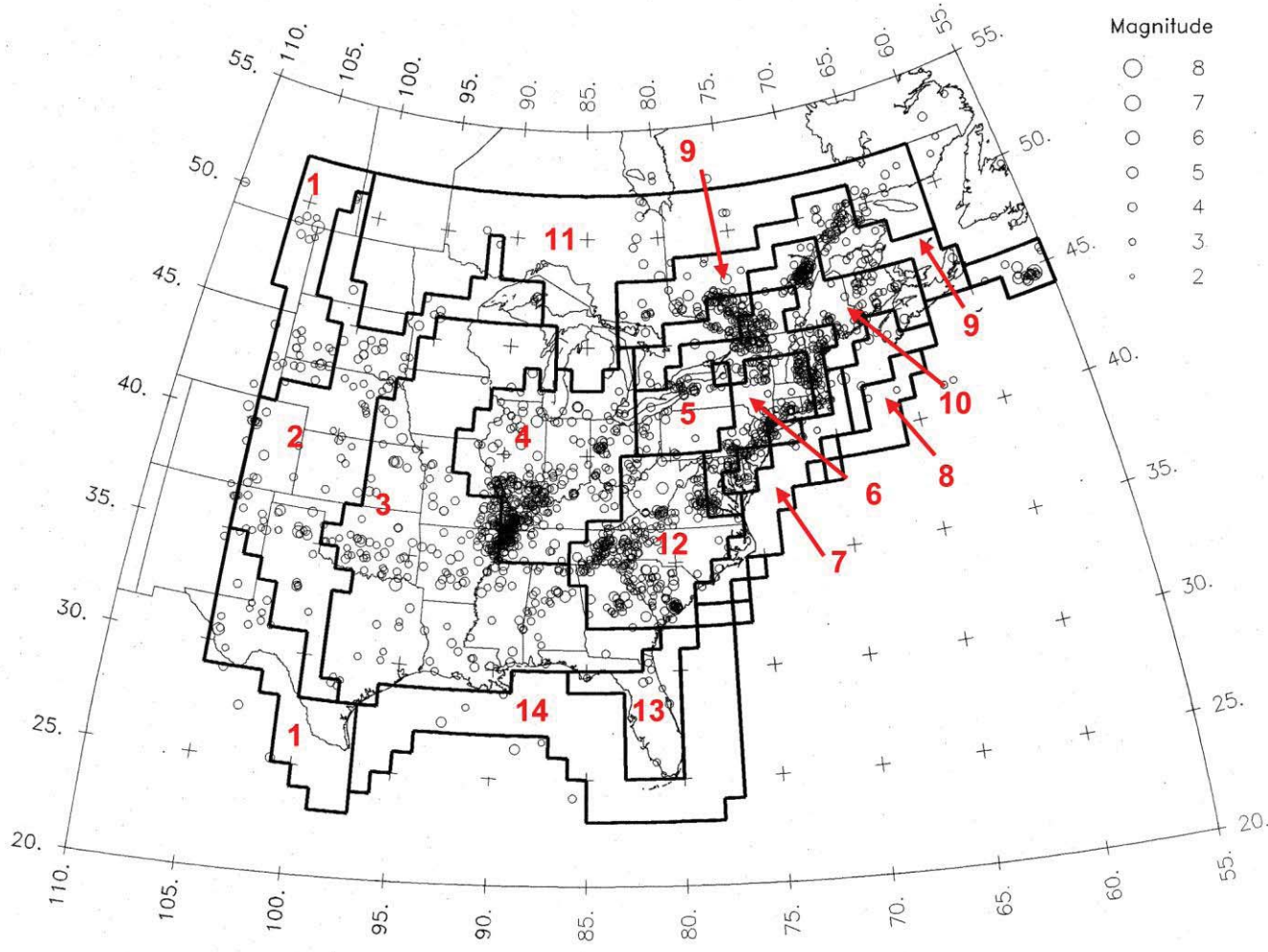
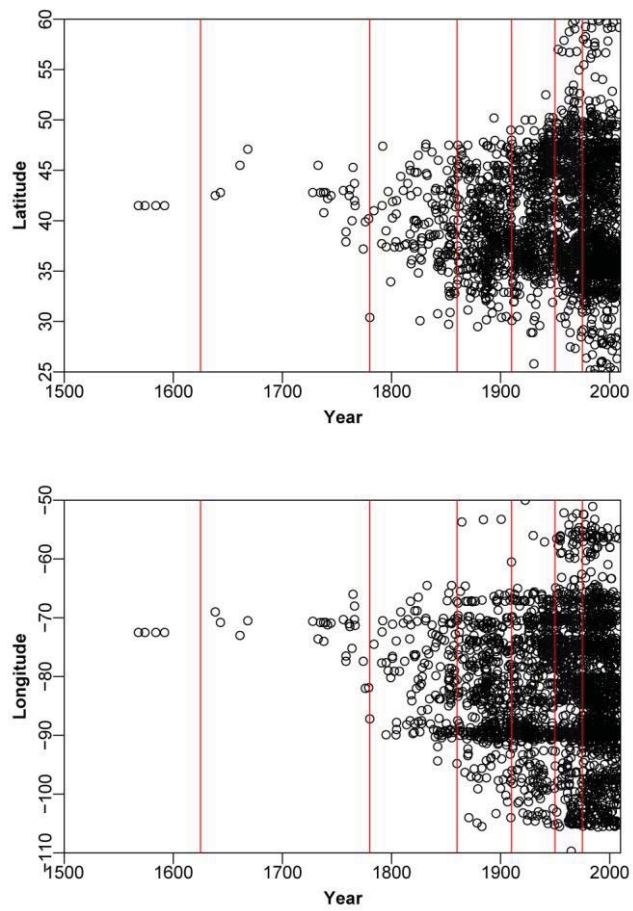


Figure 3.5-2  
CEUS SSC Project earthquake catalog and modified catalog completeness regions



**Figure 3.5-3**  
Plot of year versus location for the CEUS SSC Project earthquake catalog. Red lines indicate the boundaries of the catalog completeness time periods.

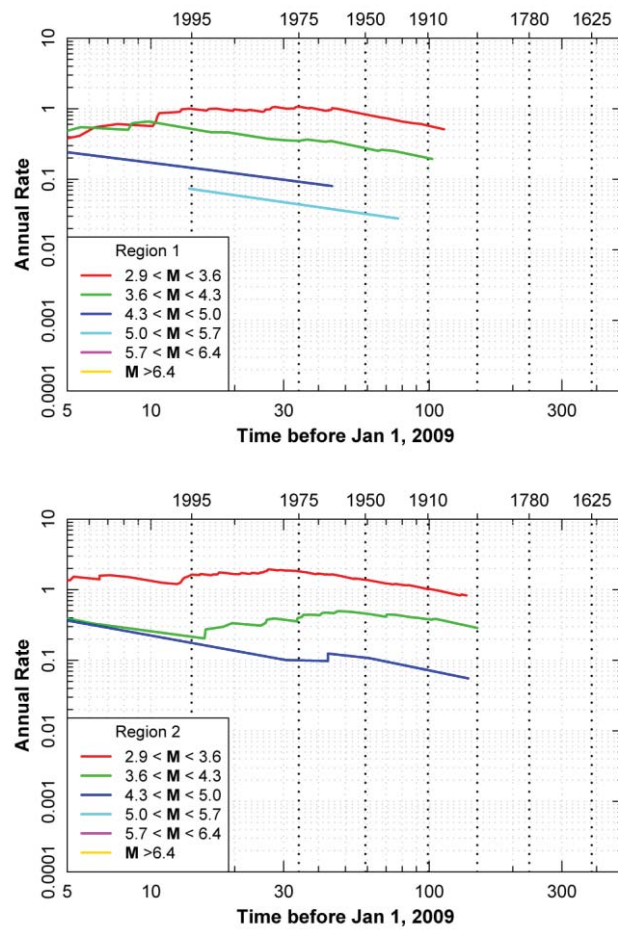


Figure 3.5-4 (1 of 7)  
“Stepp” plots of earthquake recurrence rate as a function of time for the individual catalog completeness regions shown on Figure 3.5-2

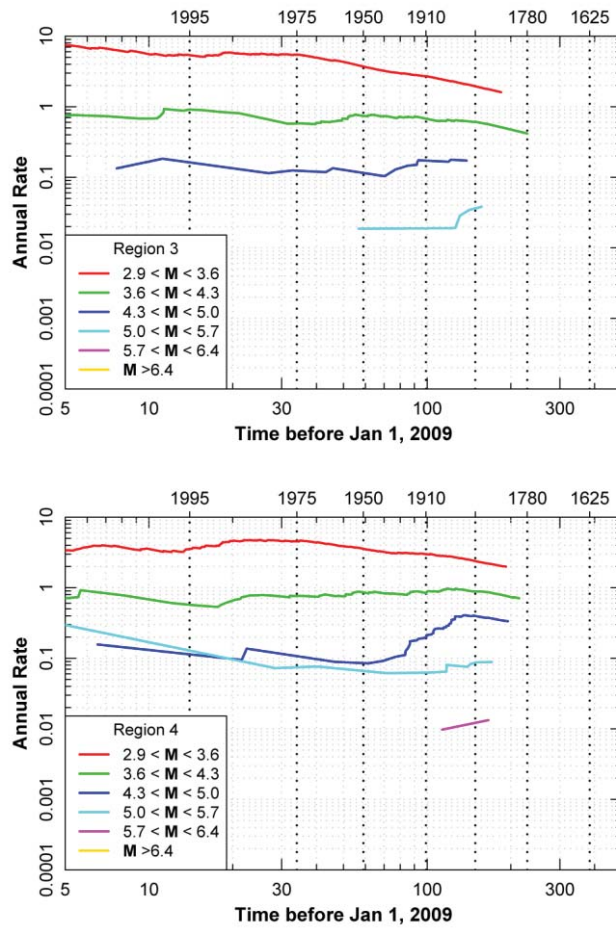


Figure 3.5-4 (2 of 7)  
“Stepp” plots of earthquake recurrence rate as a function of time for the individual catalog completeness regions shown on Figure 3.5-2

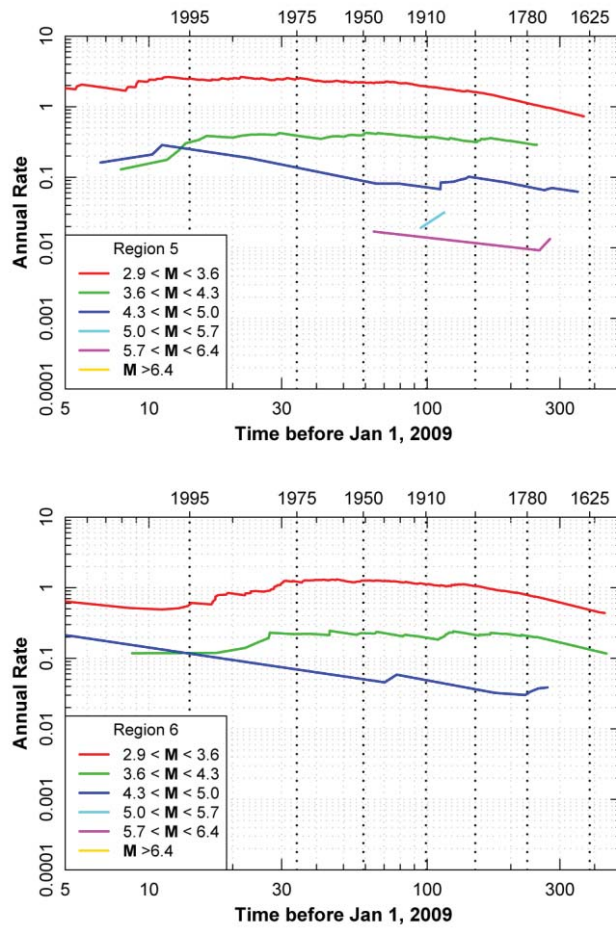


Figure 3.5-4 (3 of 7)  
“Stepp” plots of earthquake recurrence rate as a function of time for the individual catalog completeness regions shown on Figure 3.5-2

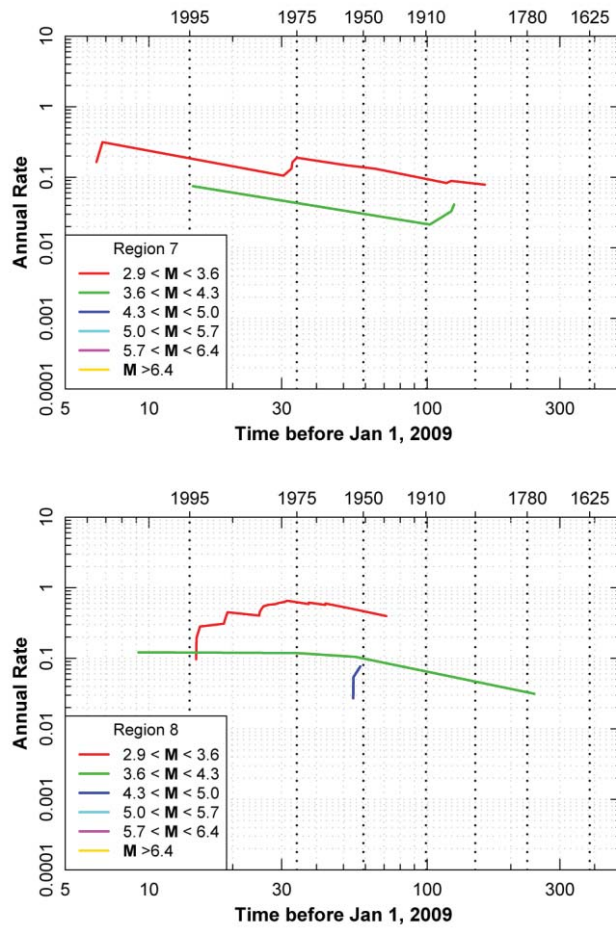


Figure 3.5-4 (4 of 7)  
“Stepp” plots of earthquake recurrence rate as a function of time for the individual catalog completeness regions shown on Figure 3.5-2

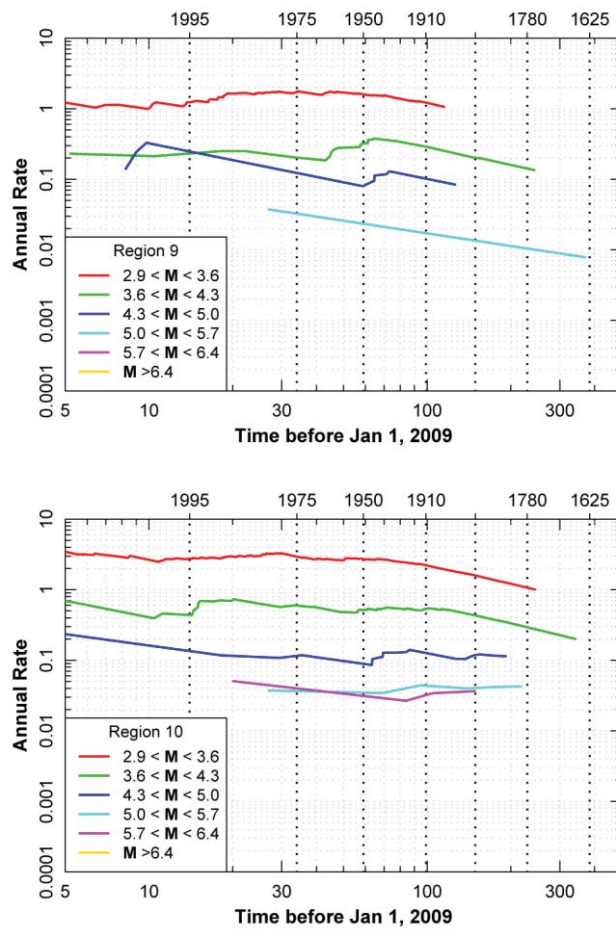


Figure 3.5-4 (5 of 7)  
“Stepp” plots of earthquake recurrence rate as a function of time for the individual catalog completeness regions shown on Figure 3.5-2

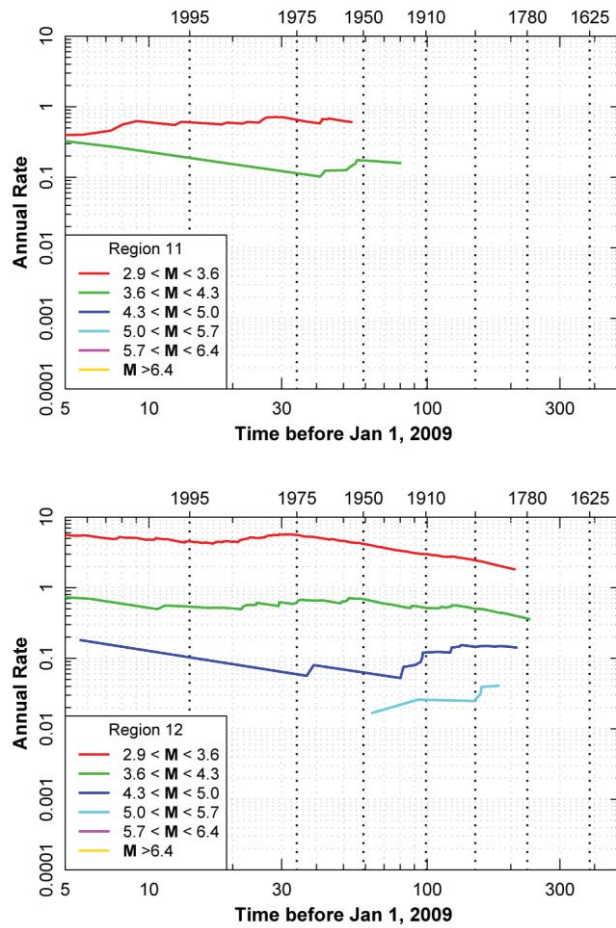


Figure 3.5-4 (6 of 7)  
“Stepp” plots of earthquake recurrence rate as a function of time for the individual catalog completeness regions shown on Figure 3.5-2

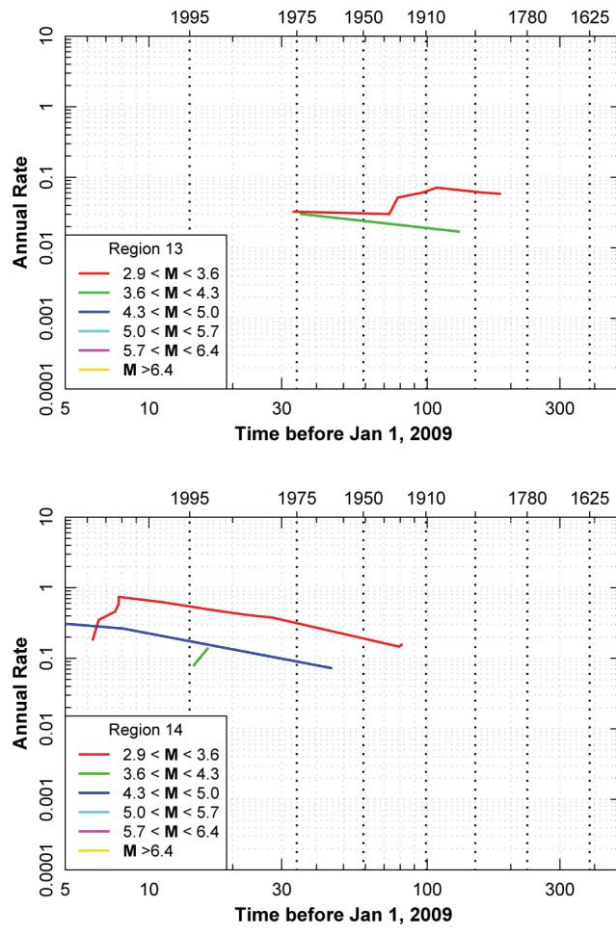


Figure 3.5-4 (7 of 7)  
“Stepp” plots of earthquake recurrence rate as a function of time for the individual catalog completeness regions shown on Figure 3.5-2